NSTX Upgrade

DISRUPTION ANALYSIS OF PASSIVE PLATES, VACUUM VESSEL AND COMPONENTS

NSTXU-CALC-12-01-01

Rev 1

February , 2012

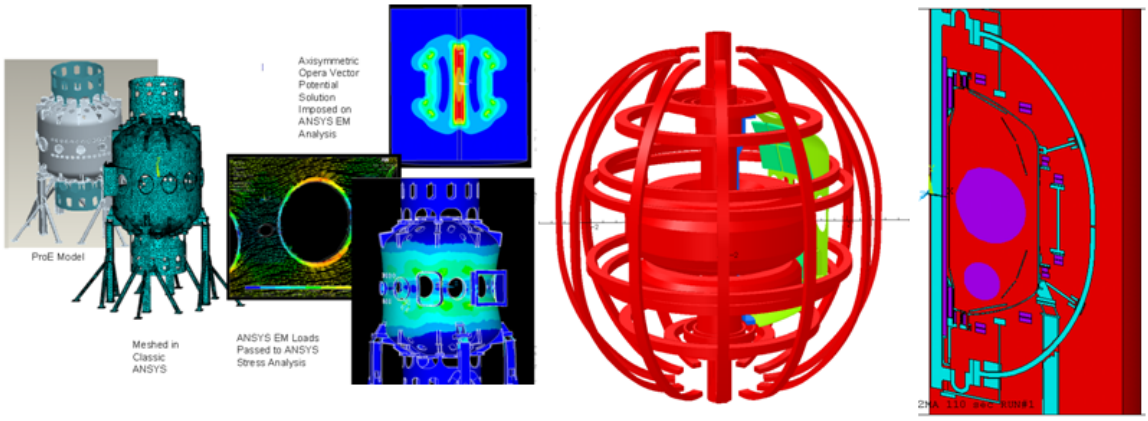

Prepared By:

Peter Titus,
Contributing Authors: A.Brooks, Srinivas Avasarala, J. Boales, PPPL Mechanical Engineering

Reviewed By:

Yuhu Zhai

Reviewed By:

Phil Heitzenroeder, Head, Mechanical Engineering

PPPL Calculation Form

Calculation # **NSTXU-CALC-12-01-01** Revision # **01** ____ WP #, **1672**
(ENG-032)

Purpose of Calculation: (Define why the calculation is being performed.)

To provide guidance on passive plate and divertor hardware upgrades needed to survive upgrade disruption loads. In addition, the vessel, and a number of other vessel internal components are analyzed for disruption loads.

References (List any source of design information including computer program titles and revision levels.)

These are included in the body of the calculation, in section 6.3

Assumptions (Identify all assumptions made as part of this calculation.)

This calculation is based on transfer of Vector Potential (VP) data from an OPERA disruption simulation. The OPERA simulation is axisymmetric and relatively simple with respect to it's modeling of conducting structures near the plasma. An assumption is made that the complicated hardware of the passive plates, antennae. diagnostics tiles etc do not substantially alter the electromagnetic environment of the disruption, beyond what is represented in the 2D OPERA model. This assumption was found inadequate for the specific case of the modeling of the CuCrZr passive plate modeling because the OPERA 2D analysis substantially adjusted the resistivity to model toroidally discontinuous plates. Attachment H was added by the calculation reviewer, Yuhu Zhai to properly calculate the 3D effects and Yuhu Zhai's analyses were checked by P.Titus in Section I

Calculation (Calculation is either documented here or attached)

These are included in the body of the following document

Conclusion (Specify whether or not the purpose of the calculation was accomplished.)

The existing 1/2 inch passive platees are adequate for the upgrade disruption loads. Attachments need modest improvements in the form of 718 washers that improve shear capacity of the slotted counterbores.

For all other components aside from the passive plates, the method of vector potential transfer is appropriate for calculating loads and stresses. This method has been applied to a number of sections of the vessel, Stresses for these components, like the area around the vessel leg, are qualified in other calculations with normal operating stresses included. The passive plate results of record are included in Attachment H and cross checked in Section I

Cognizant Engineer's printed name, signature, and date

Phil Heitzenroeder _____

I have reviewed this calculation and, to my professional satisfaction, it is properly performed and correct.

Checker's printed name, signature, and date

_____

2.0 Table of Contents

Title Page	1.0
ENG-33 Forms	
Table Of Contents	2.0
Revision Status Table	3.0
Executive Summary	4.0
Input to Digital Coil Protection System	5.0
Design Input,	
Criteria	6.1
References	6.2
Photos and Drawing Excerpts	6.3
Materials and Allowables	6.4
Disruption Specifications from the GRD	6.5
Analysis Procedure and Test Runs	7.0
Reading the Vector Potentials from OPERA	7.1
Addition of Halo Loads	7.5
Disruption Simulation…	7.6
Comparison of Bdots with Disruption Analysis on the RF Antenna	7.6.1
Structural Test Runs	7.7
Damping	7.7.1
Test Run Static Analysis	7.7.2
Test Run Dynamic Analysis	7.7.3
Comparison of Dynamic and Static Analysis	7.7.4
Global Vacuum Vessel	8.0
Mid-Plane Disruption	8.1
Mid Plane Disruption Currents and Stresses Near Bay L	8.1.2
Vessel Response to a Plasma 4 Quench	8.3
Estimate of Disruption Accelerations at the Lower Head Nozzles	8.4
Vessel Support Leg Analyses	8.5
Vessel Leg Drawing Excerpts and Photos	8.5.1
Vessel Stresses Near the Column Supports	8.5.2
Passive Plate Analyses	9.0
Drawing Excerpts and Photos	9.1
Mid-Plane Disruption	9.2
Mid-Plane Disruption With and Without Halo Currents	9.2.1
Currents Flowing in the Passive Plates, Mid-Plane Disruption, Plasma 1	9.2.2
Slow VDE's	9.3
P1-P2 Radial Slow Motion	9.3.1
P1-P3 Slow	9.3.2
P1-P4 Slow	9.3.3
P1P5Slow	9.3.4
VDE to Plasma 4 Then Quench	9.4
With Halo	
Bolting Analysis	9.5
Bracket Welds	9.6
Frequency Analysis of the Passive Plate Model	9.7
Centerstack Casing Analysis	11.0

Drawing Excerpts 11.1
Bellows Analysis 12.0
NB Backing Plate Analysis 13.0
TAE Antenna Moly Shield 14.0
Liquid Lithium Divertor 15.0

Appendix A Macro to Generate Eddy currents.....
Appendix B Macro for Static Structural Analysis……
Appendix C Macro for Dynamic Structural Analysis……
Appendix D Macro for Imposing a 1/r Toroidal Field ……
Appendix E Background Poloidal Fields…(By J. Boales)……
Appendix F Passive Plate Bracket Weld QA Report
Appendix G Email from Michael Bell quantifying the loads on the TAE antenna shield.
Appendix H Yuhu Zhai Report on OPERA analysis of the Passive Plates.
Appendix I P. Titus Report on 3D ANSYS analysis of the Passive Plates.

4.0 Executive Summary

The objective of this analysis is to estimate and assess the stresses in the vacuum vessel, selected internal components, and passive plates caused by the plasma disruption. Bake-out stresses on the passive plates have been considered in the original design and are addressed in calculation #NSTX-CALC-11-6. [1]

Mid-plane disruptions and quenches are manageable. For these events, the loads required some modest upgrades of the mounting hardware. The slow VDE's may be more severe for the secondary passive plate. These appear to be generating large counter currents in the plate as the plasma approaches it. - as would be expected from passive plates.

Development of the vector potential transfer procedure began in Summer 2009 and was worked on by Srinivas Avasarala, Ron Hatcher.\, Art Brooks, Larry Bryant, and Joseph Boales. Early test runs are included in Section 7 as illustrations of the procedure

The Vector Potential solution for a 2D axisymmetric simulation of disruption in OPERA is imposed on the 3-D model in ANSYS to obtain the eddy currents and Lorentz forces. A static and dynamic stress pass is then run and the stresses are computed. A number of other calculations address components not covered in this calculation. Some components like the vessel port region, and the bellows, are considered in this calculation, and in greater depth in other calculations. The divertor tiles, diagnostic shutters are some of the components addressed in other calculations. The primary purpose of this calculations was to address the passive plates. Other components have been added because the procedures developed for the passive plates are useful for many components.Problems were identified with the vector potential transfer procedure for the passive plates because of the large difference in the treatment of discontinuous copper components in the OPERA 2D and the 3D ANSYS model that uses the axisymmetric vector potential data. For the non-copper and axisymmetric structures like the centerstack casing, the vector potential transfer method is satisfactory.

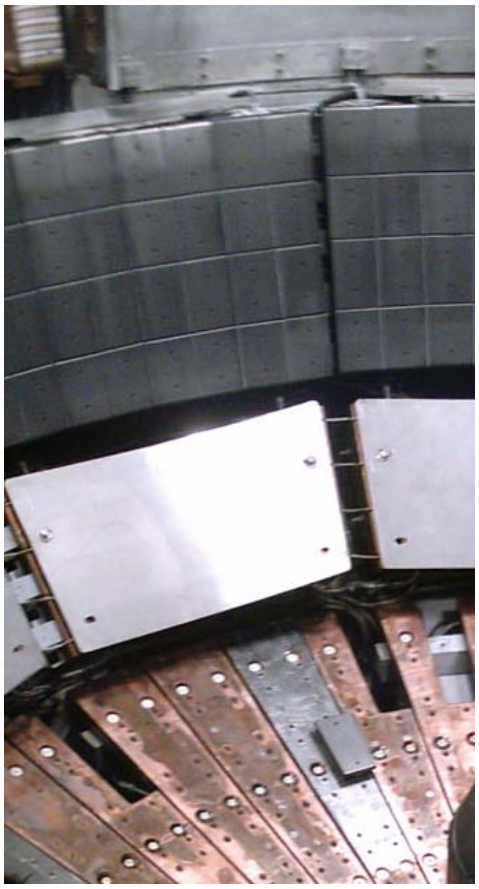

Figure 4.0-1 View of Passive Plates and Lower Divertor During an Outage. Divertor Tiles have been removed an a protective cover is on the secondary passive plate

Vector potentials obtained from OPERA are arranged in 80x80 tabular form so that they can be fed into ANSYS. The first 11 tables are considered for the study and these tables are spaced 0.5 ms apart. Macros are developed that read these values into ANSYS. The meshes in OPERA and ANSYS are dissimilar, but since ANSYS interpolates the tables between two adjacent indices, proper indexing of the coordinates yields a reasonable approximation of the Vector Potentials. The element type used was SOLID 97 and the material properties used are that of Stainless Steel except for the passive plates which are made up of Copper. This model is then solved for eddy currents and Lorentz forces..

The model is then converted into a structural model by switching the SOLID 97s into SOLID 45s. For the test cases, eleven load steps, 5ms apart are written for the stress pass. Later analyses use up to 45 steps. Forces are read from the earlier E-mag results by using LDREAD command and both the static and dynamic analyses are performed. A 0.5% damping factor is used in the dynamic run.

The procedure has been checked. In section 7 of this calculation the consistency with the OPERA analysis was checked. Poloidal and toroidal field plots were checked. In section 7.6.1, results were compared with disruption simulations done only in ANSYS for the HHFW antenna. Results for the mid plane disruption were similar. In section 9.2.2 the total currents in the major components of the toroidal elements that would inductively pick up the plasma current, were summed. These included the vessel, the passive plates and the centerstack casing. They approximately add to the plasma current. This should be the case for inductively coupled closely nested current loops.

Stress Summary (Dynamic Unless Otherwise Noted)

Component	Section	Damp	Disruption	Stress	Allowable
Vessel At Port Ligaments Near Bay L NB and Thom Scattering Ports		.5%	Mid Plane Disruption	40 MPa	40 MPa*
Vessel Support Column Intersection with Vessel		.5%	Mid Plane Disruption	40 MPa	40 MPa*
Secondary Passive Plate		.5%	Mid Plane Disruption	90 MPa	253 MPa**
Secondary Passive Plate			Fast Quench Plasma 4	180 MPa	253 MPa
Secondary Passive Plate	Attach H, I	.5%, and 1%	P1-P5 Slow	230 MPa	
Tresca from Shear Stress in Passive Plate Counter-bore	9.5 Attach H,I	.5%	P1-P5 10ms VDE and Fast Quench at P5	13.3ksi	24 ksi
Centerstack Casing (No Halo)	11.2	.5%	Mid Plane Disruption	1 MPa	1 MPa*
TAE Antenna Moly Shield	14.0	.5%	Mid-Plane Disruption	200MPa	600 MPaYield

* These are values passed on to other calculations to be added to normal operational loads. Comparison with the allowable needs to be performed in these calculations.
** Bending Allowable from Section 6.4

Review comments by Y. Zhai for Peter's calculation **NSTXU-CALC-12-01-01** titled "**Disruption Analysis of Passive Plates, Vacuum Vessel and Components**"

This FE based disruption analysis is to calculate the static and dynamic stress response of passive plates, vacuum vessel and its components during plasma disruption and VDEs. The vector potentials from OPERA 2D simulation are transferred to classical ANSYS APDL for stress analysis. The 2D OPERA model is an axisymmetric model assuming copper and bracket average material electrical conductivity based on the available measurement data. The output disruption forces on the center stack, the vessel and its

components from this analysis will be used as input for a number of other calculations for NSTX upgrade. Therefore, it is important to validate methodology used in this analysis and cross check magnetic field distribution and eddy current forces during plasma disruption.
In working closely with Pete and Ron Hatcher, we found a mistake in the disruption analysis of Passive Plates reported in this documentation, mainly due to the fact that important skin effect of Passive Plates during disruption cannot be captured using the approach reported in this calculation. My solution is to create a complete 3D EM model using OPERA with not only the plates, but also supporting bracket and the vessel. Center stack casing is also included in my 3D model. Various plasma shapes from square, trapezoid to octagon (close to circular) are studied to understand its impact on the disruption loads for passive plates.

Following is a summary of my review comments after numerous discussions with Pete.

1) To obtain eddy current and Lorentz force on passive structure components during plasma disruption, the approach of transferring Vector Potential data from an OPERA disruption simulation to ANSYS structural model is valid in general. However, the passive plates are made of CuCrlZr and Chromium Zirconium Copper C18150 is a copper alloy with high electrical conductivity, if averaged conductivity is used as in Ron Hatcher's OPERA 2D model, the skin depth effect during plasma disruption will not be captured. The skin depth for copper is ~2 mm for 1 ms fast plasma disruption and ~6 mm (~half of PP thickness) for 10 ms slow VDEs. The skin effect is important for getting the right magnetic field in the passive plates during plasma disruption or VDEs.

   A new OPERA 3D model is created and including not only passive plates but also supporting bracket and VV. The procedure of mapping OPERA 3D disruption loads onto ANSYS workbench is also established. The new modeling procedure is benchmarked against Ron's 2D model and Bob Woolley's Design Sheet – using Green's function approach for magnetic field calculation.
2) Transient magnetic field during plasma disruption is taken from OPERA 2D simulation but the background field from NSTX coils is assumed with uniform disruption in 3D space. This is not quite accurate.

3) Intuitively, P1-P4 VDE should give larger force and stress on secondary plate due to plasma center at P4 is closer to secondary plate, however, Figure 9.3.4-2 Tresca Stress from Dynamic Analysis, P1-P5 Slow shows larger stress than in Figure 9.3.3.-2 Tresca Stress from the Dynamic Solution, P1-P5 Slow.

5.0 Digital Coil Protection System.

There is no input to the DCPS planned for disruption loading of components. The loading calculated for the vessel, passive plates and other components in this calculation is based on the maximum toroidal field for the upgrade, and the maximum poloidal fields for the 96 scenarios specified in the design point spreadsheet.

6.0 Design Input

6.1 Criteria

Stress Criteria are found in the NSTX Structural Criteria Document. Disruption specifications are outlined in the GRD -Ref [7] and are discussed in more detail in section 6.5

6.2 References

[1] Structural Analysis of NSTX Passive Plates and Support Structures, NSTX CALC 11-06, Brad Nelson, B. Gorenson, June 8 1998

[2] Disruption specification J. Menard spreadsheet: disruption_scenario_currents_v2.xls, July 2010. NSTX Project correspondence, input to Reference [1]

[3] "Characterization of the Plasma Current quench during Disruptions in the National Spherical Torus Experiment" S.P. Gerhardt, J.E. Menard and the NSTX Team Princeton Plasma Physics Laboratory, Plainsboro, NJ, USA Nucl. Fusion 49 (2009) 025005 (12pp) doi:10.1088/0029-5515/49/2/025005

[4] ITER material properties handbook, ITER document No. G 74 MA 15, file code: ITER-AK02-22401.

[5] Disruption Analysis Of Vacuum Vessel and Passive Plates NSTX-CALC-12-001-00, S. Avasarala

[6] NSTX Disruption Simulations of Detailed Divertor and Passive Plate Models by Vector Potential Transfer from OPERA Global Analysis Results P. H. Titus[a], S. Avasaralla, A.Brooks, R. Hatcher 2010 SOFT Conference, Porto Portugal October 20110

[7] NSTX Upgrade General Requirements Document, NSTX_CSU-RQMTS-GRD Revision 0, C. Neumeyer, March 30, 2009

[8] Inductive and Resistive Halo Current s in the NSTX Centerstack, A.Brooks, Calc # NSTX-103-05-00

[9] OPERA 2D Disruption Analyses, R. Hatcher, NSTX upgrade calculation #NSTXU-CALC- NSTXU-CALC-12-03-00

[10] NSTX HHFW (High Harmonic Fast Wave) Eddy Current Analysis for Antenna NSTX-CALC-24-03-00 Jan 10, 2011, Han Zhang, PPPL

[11] email from Michael Bell estimating loads on the TAE antenna, Appendix G.

[12] Modeling of the Toroidal Asymmetry of Poloidal Halo Currents in Conducting Structures N. Pomphrey, J.M. Bialek_, W. Park Princeton Plasma Physics Laboratory,

[13] NSTX Halo Current Analysis of Center Stack NSTX-133-05-00-April 13, 2010Art Brooks

[14] Center Stack Casing Bellows, NSTXU-CALC-133-10-0 by Peter Rogoff.

[15] Neutral Beam Armor Backing Plate NSTXU-CALC-24-02-00, Larry Bryant

[16] Diagnostics Review and Database NSTXU-CALC-40-01-00, Joseph Boales

[17]Vessel Port Re-work for NB and Thompson Scattering Port, Calculation number NSTXU-CALC-24-01-00

[18] Damping in ANSYS/LS-Dyna Prepared by: Steven Hale, M.S.M.E Senior Engineering Manager CAE Associates (Web Search Results)

[19] Disruption Load Calculations Using ANSYS Transient Electromagnetic Simulations for the ALCATOR C-MOD Antennas, P Titus Plasma Sci. & Fusion Center, MIT, Cambridge, MA; Fusion Engineering, 2002. 19th Symposium on Fusion Engineering 02/2002; DOI: 10.1109/FUSION.2002.1027634 ISBN: 0-7803-7073-2

6.3 Photos and Drawing Excerpts

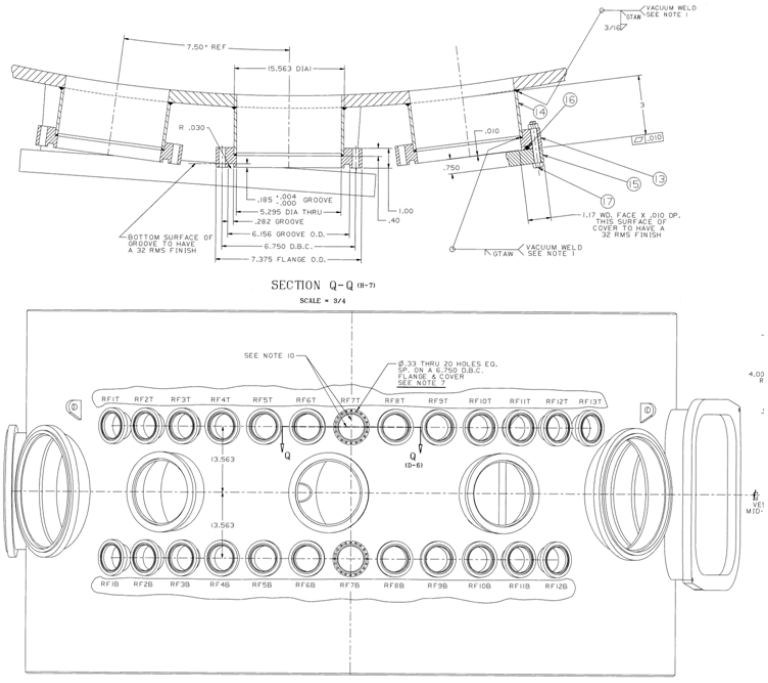

Figure 6.4-1 Vessel Cylindrical Shell Elevation

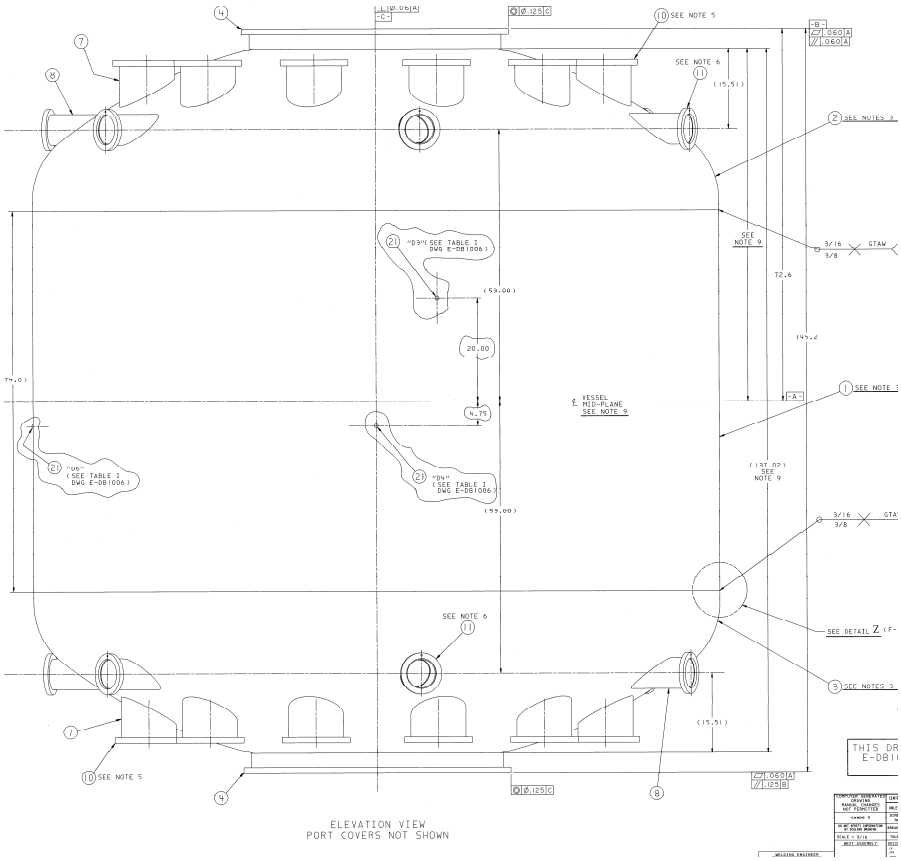

Figure 6.4-2 Vessel Elevation

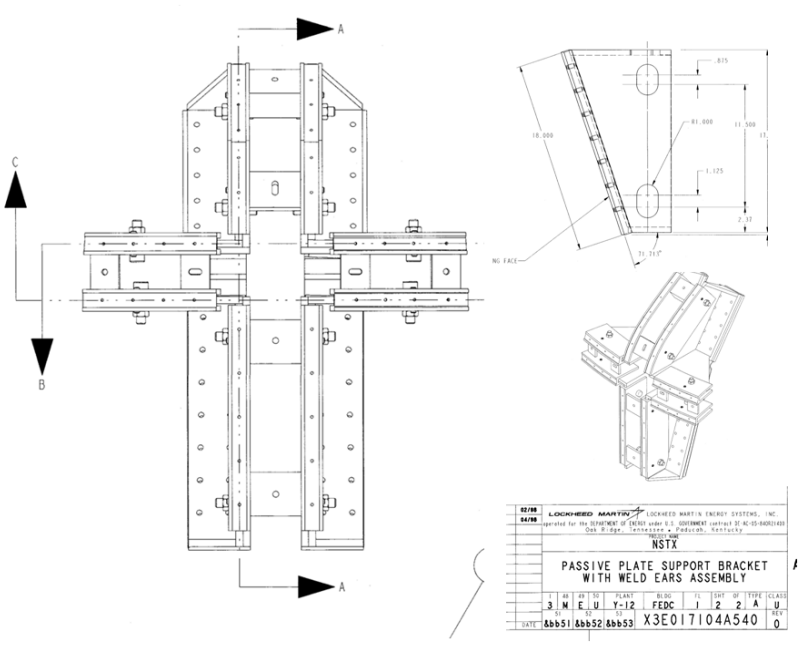

Figure 6.4-3 Passive Plate Bracket

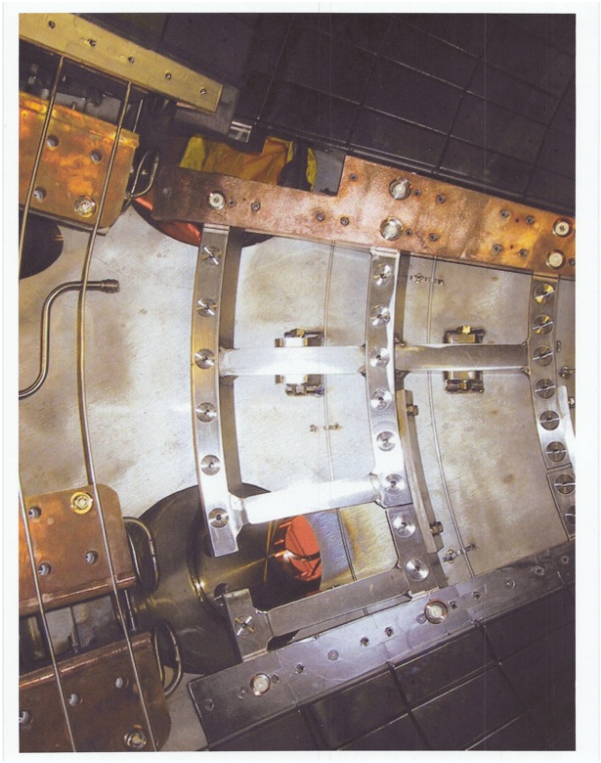

Figure 6.4-4 Lower Outer Divertor "Barbeque" Rails

6.4 Materials and Allowables

Vessel Shell – 304 Stainless 45 ksi Yield, 30 ksi Near Welds

05/19/1998 13:53 6174728409 NEWENGLANDSTEELTANK PAGE 03

Avesta Sheffield

Avesta Sheffield Plate Inc.

Certificate of Analysis and Tests

OUR ORDER 106101 - 01 HEAT & PIECE 87893-3B 5/13/98

SOLD TO: PROCESS SYSTEMS INTERNATIONAL
20 WALKUP DRIVE
WESTBOROUGH MA 01581

SHIP TO: NEW ENGLAND STEEL TANK
111 BROCK ROAD
SOUTH QUINCY MA 02169
737001-06

PSI MIC NO. PSI2

YOUR ORDER & DATE

558635 3/18/98 TAG# PART #V077P001

ITEM DESCRIPTION

HEAT & PIECE 87893 - 3B 3A
WEIGHT 3092
FINISH 1
GRADE 304 UNS-S30400
DIMENSIONS .625 X 76.000 X 212.000 EXACT

SPECIFICATIONS

THE PRODUCTS LISTED ON THIS MILL TEST REPORT SATISFY PREFERENCE CRITERION B AS DEFINED IN ARTICLE 401 OF THE NORTH AMERICAN FREE TRADE AGREEMENT. COUNTRY OF ORIGIN IS USA

ASTM A240-96A ASMESA240-96AD
NO WELD REPAIR ON MATERIAL
ASTM A262-93A PRAC A

ASTM A480-96,ASMESA480-96AD
MAG PERM <1.05 ASTM A342 (6)
ASTM A262-93A PRAC E

PLATES & TEST PCS SOLUTION ANNEALED @ 1950 DEGREES FARENHEIT MINIMUM. THEN WATER COOLED OR RAPIDLY COOLED BY AIR
/FREE OF MERCURY CONTAMINATION
HOT ROLLED, ANNEALED & PICKLED (HRAP)

MECHANICAL & OTHER TESTS

HARDNESS RB	81	
GRAIN SIZE	5	
YIELD STRENGTH (PSI)	45254	✓
TENSILE STRENGTH (PSI)	91368	✓
BEND	OK	✓
INTERGRANULAR CORROSION	OK	✓
ELONGATION % IN 2"	63.6	✓
REDUCTION OF AREA %	72.5	

Centerstack Casing

INCONEL 625

Test Temperature, °F(°C)	Ultimate Tensile Strength, ksi (MPa)	Yield Strength at 0.2% offset,ksi (MPa)	Elongation in 2" percent
Room	138.8 (957)	72.0 (496)	38
200	133.3 (919)	67.3 (464)	41
400	129.4 (892)	62.2 (429)	44
600	125.6 (866)	59.5 (410)	45
800	122.2 (843)	59.2 (408)	45

The passive Plates are made of CuCr1Zr UNS.C18150. Chromium Zirconium Copper C18150 is a copper alloy with high electrical conductivity, hardness, and ductility, moderate strength, and excellent resistance to softening at elevated temperatures. The addition of 0.1% zirconium (Zr) and 1.0% chromium (Cr) to copper results in a heat treatable alloy which may be solution treated and subsequently aged to produce these desirable properties. NSTX Bake-out temperature is 350 degrees C. The softening temperature of properly heat treated C18150 rod exceeds 500°C as compared to unalloyed pure copper which softens at 200°C, and silver bearing coppers which soften at 350°C.

From Ref [1] **Table 4 Material properties assumed for analysis**

Property	units	304L sst [7]		Cu-Cr-Zr, (18150) Solution annealed and aged [6]	
		150 C (302 F)	350 C (662 F)	150 C (302 F)	350 C (662 F)
Young's modulus (temp effect < 5%)	psi	28 E6	28 E6	17 E6	17 E6
Min Tensile strength	psi	70,000 (RT)	--	49,000	38,000
Min. Yield Strength	psi	25,000 (RT)	--	40,000 276 MPa	34,000 234 MPa
Sm		15, 300	13,700	16,500 114 MPa	13,000
1.5Sm				171 MPa	
3Sm				341 MPa	
Coeff of therm expansion	in/in-F	0.96 E-5	0.96 E-5	0.98 E-5	0.98 E-5
Thermal Conductivity	BTU/ hr-ft-F	9.4	9.4	208	202

According to the NSTXU criteria as currently written, the Sm for CuCrZr should be the lesser of 2/3 yield or 26.6ksi/184 MPa at 150C, or 24.5ksi,or 169 MPa - or Sm = 24.5ksi/169 MPa. The Bending allowable would then be 169*1.5 = 253 MPa. The shear allowable is .6*Yield = .6*276 = 165.6 MPa or 24 ksi

Tensile Property (average) [4]

Material	Yield strength (MPa)	UTS (MPa)	Average over
Low strength (L)	78	248	3
Intermediate strength (I)	199.4	318.6	3
High strength (H)	297	405.3	5

This is from the ITER Materials Database and the NSTX allowable would be the lesser of 202 or 198 MPa.

6.5 Disruption Specs:

The requirements for disruption analysis are outlined in the NSTX Upgrade General Requirements Document [7]. The latest (August 2010) disruption specification were provided by Jon Menard as a spreadsheet: disruption_scenario_currents_v2.xls.[2] This reference includes a suggested tile phasing of the inductively driven currents and the halo currents.

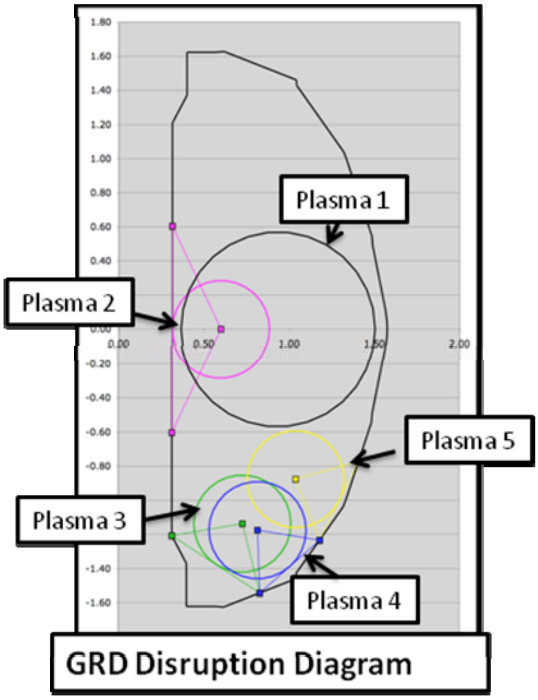

New High Priority Disruption Analyses

Centered disruption, fast quench
Initiated shifted to CS, fast quench, no halo
Inward drift to CS, very slow quench, halo
Initiated shifted down to inboard, fast quench, no halo
Vertical drift to inboard, very slow quench, halo
Initiated shifted down to middle, fast quench, no halo
Vertical drift to middle, very slow quench, halo
Initiated shifted down to outboard, fast quench, no halo
Vertical drift to outboard, very slow quench, halo

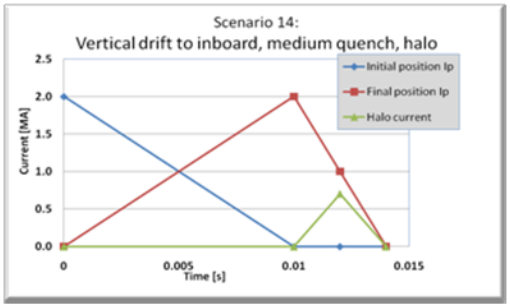

	Plasma 1	Plasma 2	Plasma 3	Plasma 4	Plasma 5
	Centered	Offset, Midplane	Offset, Inboard	Offset, Central	Offset, Outboard
Center of plasma (r,z) [m]	0.9344	0.5996	0.7280	0.8174	1.0406
	0.0000	0.0000	-1.1376	-1.1758	-0.8768
Minor radius of plasma [m]	0.5696	0.2848	0.2848	0.2848	0.2848

Criteria from the GRD:

Current and field directions (referring to Figure 2.2-2) shall be as follows; Plasma current Ip into the page (counter-clockwise in the toroidal direction, viewed from above) Halo current exits plasma and enters the structure at the entry point, exits the structure and re-enters the plasma at the exit point (counter-clockwise poloidal current, in the view of the figure) Toroidal field into the page (clockwise in the toroidal direction, viewed from above)

For the halo currents a toroidal peaking factor of 2:1 shall be assumed in all cases. Thus the toroidal dependence of the halo current is $[1 + \cos(\phi - \phi_0)]$, for $\phi = 0$ to 360° where ϕ is the toroidal angle.

Table 2-2 - Plasma Disruption Specifications

	Centered	Offset, Midplane	Offset, Inboard	Offset, Central	Offset, Outboard
Center of plasma (r,z) [m]	0.9344	0.5996	0.7280	0.8174	1.0406
	0.0000	0.0000	-1.1376	-1.1758	-0.8768
Minor radius of plasma [m]	0.5696	0.2848	0.2848	0.2848	0.2848
Current Quench					
Initial plasma current [MA]	2	2	2	2	2
Linear current derivative [MA/s]	-1000	-1000	-1000	-1000	-1000
VDE/Halo					
Initial plasma current	2	0	0	0	0
Final plasma current [MA]	0	2	2	2	2
Linear current derivative [MA/s]	-200	200	200	200	200
Halo current [MA]	n.a	20%=	35%=	35%=	35%=
		400kA	700kA	700kA	700kA
Halo current entry point (r,z) [m]	n.a	0.3148	0.3148	0.8302	1.1813
		0.6041	-1.2081	-1.5441	-1.2348
Halo current exit point (r,z) [m]	n.a	0.3148	0.8302	1.1813	1.4105
		-0.6041	-1.5441	-1.2348	-0.7713

7.0 Analysis Procedure and Test Runs

The analysis procedure is discussed in a more concise fashion in a SOFT paper, ref. [6]. Ron Hatcher's disruption analyses [9] were used to provide a vector potential "environment" for a model of all the components affected by the disruption. Sri Avasarala developed a procedure which starts with Ron Hatcher's OPERA disruption simulation, and transfers the axisymmetric vector potential results into a 3 D electromagnetic (EM) model of the vessel and passive plates. Background toroidal and poloidal fields are applied by superimposing appropriate vector potential distributions. The macros used to impose the background fields were supplied by Art Brooks. With modest changes, any of the vessel internal components can be evaluated with this procedure. Originally the OPERA analyses included poloidal fields that were selected to be worst case loading for a specific component - initially for the passive plates, but to be able to used the OPREA data more generically for other components, the opera analysis was revised to use no added background fields, but simply to develop the poloidal field changes from the disruption. Background fields are added in the ANSYS analysis.

7.1 Opera Analyses

OPERA axisymmetric analyses utilize a specialized formulation of the VP degree of freedom. Computations are done with r*A theta as the solution degree of freedom. The resulting VP solution must be divided by the radius of the coordinate point before passing this to the 3D ANSYS EM analysis. Figure 7.3-1 shows an ANSYS reconstruction of the NSTX poloidal fields from the OPERA to ANSYS VP data transfer.

An email from Bob Pillsbury:

```
The 2D OPERA default potential is r*A-theta - they call it "modified
potential".It is definitley an axisymmetric formulation.  Are you
thinking of converting to cartesian components and applying to 3D
structures? It's a kludge, but if that's the only way to get close...
Not sure if it helps, but I think it's not a real problem to do the
math in OPERA and output Ax and Ay. BTW - you can ask for a potential
of A-theta, but VF recommends the other.
Regards
Bob:
```

The VDE specified by the CDR GRD did not include a final quench – This was a reasonable assumption for a fast VDE (a flux conserved solution would attempt to preserve the original flux state of the centered mid-plane plasma). In later analyses a final quench was added.

7.2 Preparation and Use of the Table Data

Vector potentials obtained from OPERA are arranged in 81x81 tabular form so that they can be mapped into ANSYS as table data. Data transfer is done in a cylindrical coordinate system with only r-z coordinate results from the 2D analysis mapped to the 3D model.

*dim,vect%inum%,table,81,81,1,x,z,,5 ! Specifies a 81X 81 parameter table

*tread,vect%inum%,'VecPot_case_%inum%','txt' ! Reads the table text file into the table

A typical number of time points extracted from the OPERA analysis produced 44 tables The time points represented by the tables are input with a parameter set. . Macros are developed that read these table values into ANSYS. The meshes in OPERA and ANSYS are dissimilar, but since ANSYS interpolates the tables between two adjacent indices, proper indexing of the

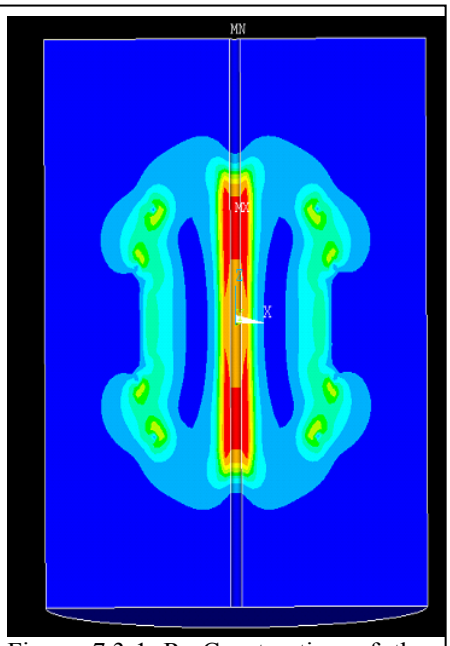

Figure 7.3-1 Re-Construction of the OPERA Poloidal Field in ANSYS using a wedge of elements after reading in an OPERA vector Potential Result.

coordinates yields a reasonable approximation of the VP. The ANSYS EM element type used was SOLID 97 which is converted to SOLID 45 for the structural analyses. The lower order elements are needed to support the EM ANSYS vector potential analysis. Higher order elements use boundary element formulations and are not consistent with the OPERA vector potential results.

7.3 Application of the Background Fields.

The poloidal background fields are extracted from separate analyses of the scenarios, or operating experience. Figure 7.3-2 shows maps of enveloped poloidal fields from all (96) design equilibria for the planned upgrade of NSTX. The poloidal and toroidal background fields are converted to VP gradients. The resulting VP values are superimposed on the VP values from the OPERA analysis.

$$\mathbf{B} = \nabla \times \mathbf{A} = \frac{1}{r}\begin{vmatrix} u_r & u_\theta & u_z \\ \frac{\partial}{\partial r} & \frac{\partial}{\partial \theta} & \frac{\partial}{\partial z} \\ A_r & rA_\theta & A_z \end{vmatrix}$$

The above equation can be solved for the VP for a constant field in any one of the directions. An expression of the total field in terms of VP is obtained by superposition. While the expressions are linear in A and B, they are coupled in the coordinate directions, so that the presence of a radial field induces a non uniform vertical field. The specified field can be obtained only over a limited range from the field point chosen.

```
!       ANSYS Commands

!d,i,ay,vect%inum%(x,z) ! Interpolates and applies the Vector Potential on the node

d,i,ay,BackBz*x/2-BackBr*(z-z0)+vect%inum%(x,z) ! Intrepolates and applies the Vector Potential on the node

!       Applying the Toroidal Field

d,i,az,-0.5*BR*log(x*x) ! applies vector potential for toroidal magnetic field
```

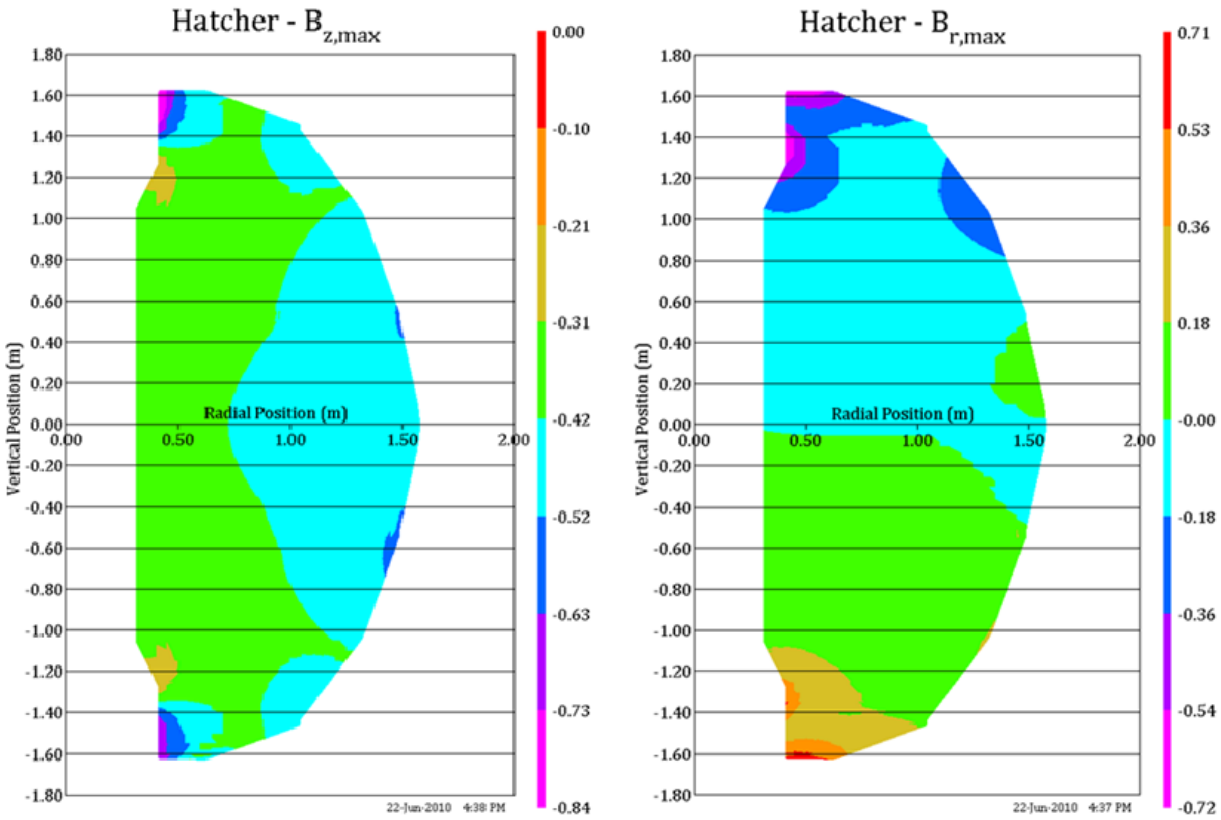

Fig.7.3-2 Maximum Poloidal Field Magnitudes for All NSTX Upgrade Planned Scenarios (R. Hatcher Data, J Boales Plot). More included in Appendix E. This is used to select the worst poloidal field for the component being considered.

7.4 ANSYS 3D Model

The ANSYS EM analysis is transient analysis that must track the time points and VP from the OPERA transient analysis

In order to obtain tractable models of the components, yet still capture the effect of shared currents with the vessel, symmetry and cyclic symmetry can be used. On poloidal cuts of the system, the volt degree of freedom is coupled across cyclic symmetry faces using the ANSYS CPCYL command. Where current transfer is small for example across the equatorial plane of the vessel, volt degrees of freedom are allowed to "float"..

Concurrently with the addition of halo currents, the EM model is solved for eddy currents and Lorentz forces, which are saved in the results file for input to the structural analysis.

7.5 Addition of Halo Loads

Halo currents are applied at the appropriate entry and exit points specified in the GRD by a nodal amp "force" ANSYS command. Entry is modeled with positive nodal currents and exit is modeled as negative nodal currents. Halo current flow needs to be considered in choosing the symmetry boundary conditions In the passive plate model presented in section 9, the symmetry sector is 60 degrees/lower half, and the halo current specified in the GRD is multiplied by the peaking factor, then divided by 6. The symmetry conditions imposed in the passive plate model actually model identical halo currents in the top and bottom of the vessel, and a toroidal distribution of currents uniformly multiplied by the peaking factor.

Halo currents are added in the transient ANSYS analysis. The halo current distribution between the entry and exit points will have resistive and inductive components. The inductive vs. resistive distribution of Halo currents has been studied by A. Brooks for the NSTX center stack casing[4]. Halo currents were

modeled initially as poloidal. currents in the plasma Then interrupted with entry and exit points on the casing and peaking factors in accordance with the GRD. Early analyses of the current distributions in the NSTX centerstack casing claimed a resistive re-distribution that improved the peaking factor[12]. The A.Brooks analysis showed that an initial inductive distribution that maintained the peaking factor throughout the height of the centerstack and then produced a resistive re-distribution. The decision is to retain the peaking factor in the halo current distribution, but with an appropriate time duration. In the procedure outlined here, the distribution of entry and exit nodes are chosen to retain the peaking factor.

There is also the question of timing of the inductive currents from the plasma quench and the halo current peak. Some guidance in the time phasing of these current peaks is provided in [2] and figure 7.5-1. Time duration of the loading is important in properly simulating the dynamic response.

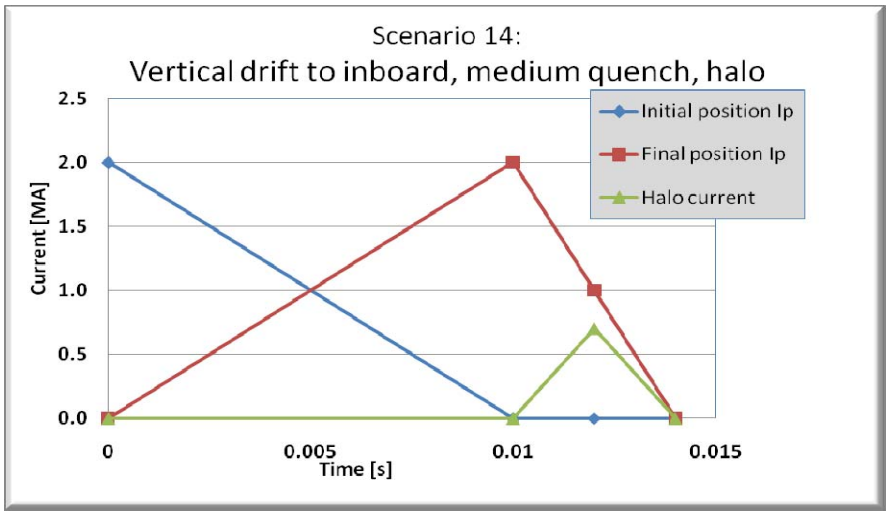

Figure 7.5-1Time phasing of the plasma current changes that induce currents in the vessel and vessel components, and the halo currents. From J. Menard

7.6 Procedure Test Run

7.6.1 The Solid Model:

The solid model of the Vessel, Port Extensions legs and umbrella structure are processed in both Pro-E and ANSYS to merge components, to yield a simpler model for FEA. The umbrella structure is modeled as a separate solid to incorporate the sliding joint at a later stage in analysis. At the time the test runs were made, the solid model of the passive plates had not been prepared. A simple representation of the passive plates was added for the test runs.

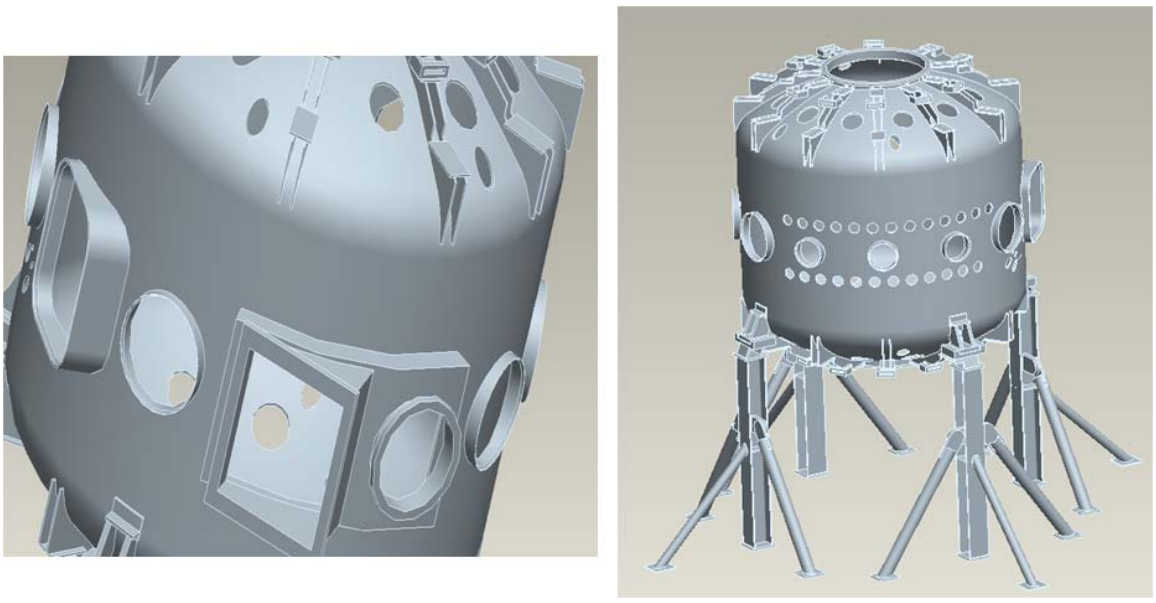

Figure 7.6.1-1 Neutral Beam Ports (left) Vessel and Supports (Right)

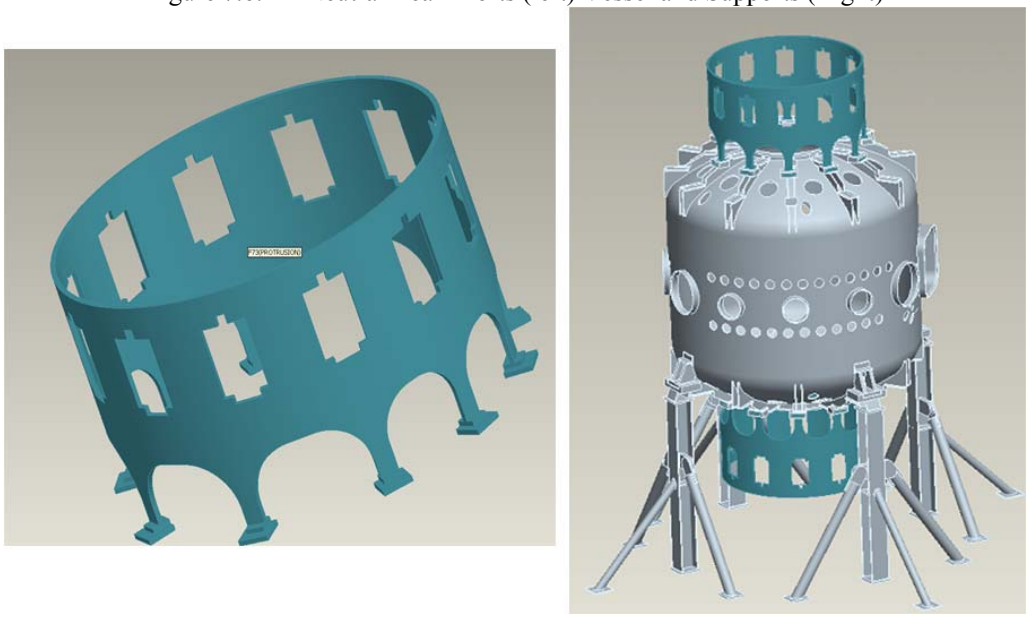

Figure 7.6.1-2 Umbrella Structure (Left) Vessel With Umbrella Structure (Right)

7.6.2 Finite Element Model

The solid models of the vessel, umbrella structure, port extensions and support legs are imported from Pro-E. The model retains all the complex 3-D geometry but the port extensions, legs and the vessel are merged together to form one solid. The umbrella structure is a separate solid. This model is meshed with 8 node bricks in workbench and the mesh is carried into ANSYS classic. To get around the DOF compatibility issues, the mesh is rebuilt in ANSYS classic, retaining the number of nodes and elements and the connectivity.

The model is meshed in ANSYS- Workbench with an 8-node brick element and the mesh is transferred to ANSYS-Classic. The preferred element type is SOLID 97 because of its capability to handle Vector Potentials. However, there were some DOF compatibility issues when the mesh is transferred to ANSYS-

Classic. Several methods to circumvent this obstacle, like using the CDWRITE and CDREAD commands failed. The mesh was reconstructed in ANSYS retaining the same nodes, elements and the connectivity. The Model has 216112 elements and 76436 nodes.

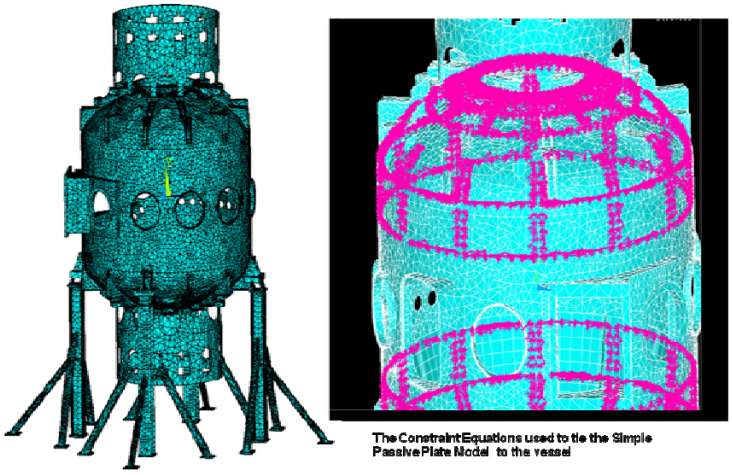

Figure 7.6.2-1 Finite Element Model

An approximate FE model of the passive plates is built based on the 2-D OPERA model and an earlier axisymmetric model of the vessel. This model could not be glued to the vessel because of the difference in dimensions. Hence, the CEINTF command was used to tie the passive plates to the vessel both electrically and structurally.

Table 7.6.2-1 Passive Plate and Outboard Divertor Coordinates

Primary Passive Plate Coordinates	Secondary Passive Plate Coordinates	Outboard Divertor Coordinates
X=1.3600 Y=1.0056	X=1.0640 Y=1.4447	x=0.6208 y=1.6390
X=1.5092 Y=0.5530	X=1.3399 Y=1.0543	x=1.2056 y=1.4092
X=1.5213 Y=0.5569	X=1.3503 Y=1.0617	x=1.2149 y=1.4185
X=1.3720 Y=1.0095	X=1.0744 Y=1.4520	X=1.0744 Y=1.4520

Registration of the OPERA passive plates and ANSYS passive plates is important. Effects of the currents flowing in the passive plates need to be captured consistently in the OPERA and ANSYS EM analysis. If the change in vector potential due to the passive plates in the OPERA model is not positioned directly on the ANSYS passive plates, the eddy currents may not be driven in a consistent manner.

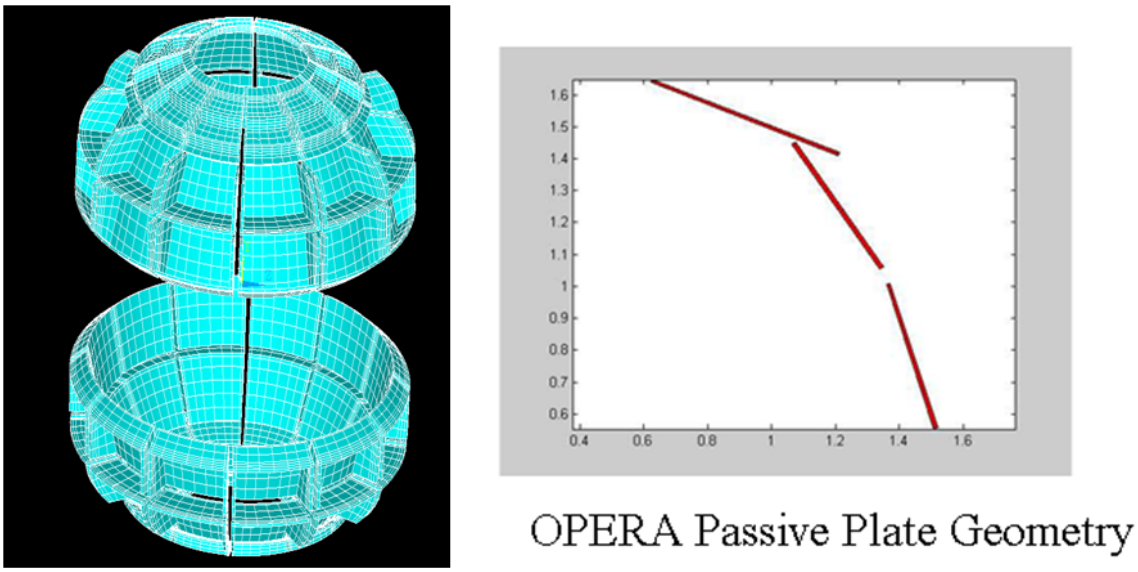

Figure 7.6.2-2: The Simple FEA Model of the passive plates.

A vector potential gradient was then applied on this model to see if the model works. Eddy currents and Lorentz forces obtained agreed qualitatively with what would be expected from a mid-plane quench.. An approximate model of the passive plates, in agreement with the 2-D model used in OPERA, was modeled in ANSYS. This is tied to the vessel using constraint equations. The degree of freedom coupled is Volt during the E-mag run and Displacement during the structural run.

7.6.3 Application of the Vector Potential and Reading the Vector Potential Data From the OPERA Results

Charlie Neumeyers group, and Ron Hatcher have the responsibility to run the NSTX disruption simulations, but the Analysis Branch has to qualify all the nuts and bolts and welds and brackets, so the OPERA vector potential solution is transferred to an ANSYS model with all the detail and then the EM transient is run with the proscribed A's. They are converted to cylindrical coordinates and A's are superimposed for the toroidal field (Rons analysis doesn't have it) then get Lorentz Forces and stresses. -

Before taking the analysis further the model is tested—a Vector Potential gradient is applied to see if it yielded eddy currents and Lorentz forces as expected. The model worked as expected.

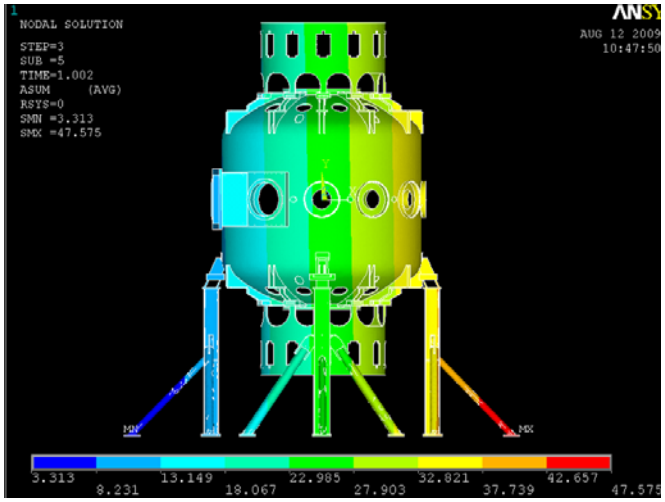

Figure 7.6.3-1 Vector Potential gradient.

For the MIT C-Mod Divertor Upgrade, the PPPL Engineering Analysis Branch is doing a similar analysis. An ANSYS coarse disruption model is used to pass A's to a detailed model of the divertor hardware. For C-Mod, both analyses are 3D, so the 1/r correction is not needed here. The correction to Ron's OPERA result in ANSYS by dividing the A's by r. In later analyses, Ron Hatcher includes the r correction in the data.

The vector potentials from OPERA, which are generated in cylindrical coordinate system, are arranged in a matrix format to be compatible with ANSYS requirements. MATLAB is used to achieve this in the test runs by S. Avasarala. In later analyses Ron Hatcher used the output formatting features of OPERA to create the needed tables. . These values are imposed on the nodes using TREAD command. ANSYS uses linear interpolation and will use an approximated vector potential on nodes that are not coincident with the nodes is OPERA. A toroidal field is also applied along with the values from OPERA. Before running the disruption simulation on the vessel, the vector potentials are applied on a hollow cylinder and the poloidal and toroidal fields are plotted.

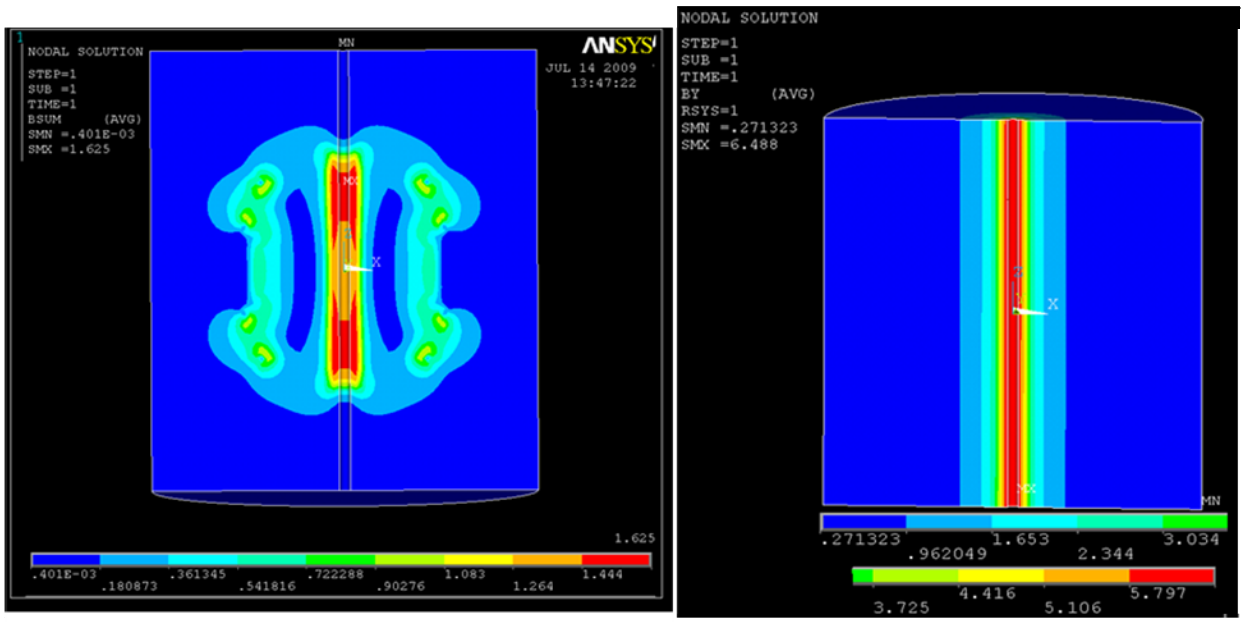

Figure 7.6.3-2 Field plots - Poloidal Created by an ANSYS Interpretation of OPERA input, and Toroidal from A.Brooks Macro

7.6.4 Test Case Disruption Simulation

OPERA results in this first test case, are spaced 0.5 ms apart and hence the load steps in ANSYS are written 0.5 ms apart too. Only the first load step was written at 10 sec to allow for the model to settle and not produce any currents due to the steep change in vector potentials over a short period. A total of 11 load steps are written for the plasma quench. The vector potential boundary conditions are then applied to the model in an ANSYS E-mag analysis.

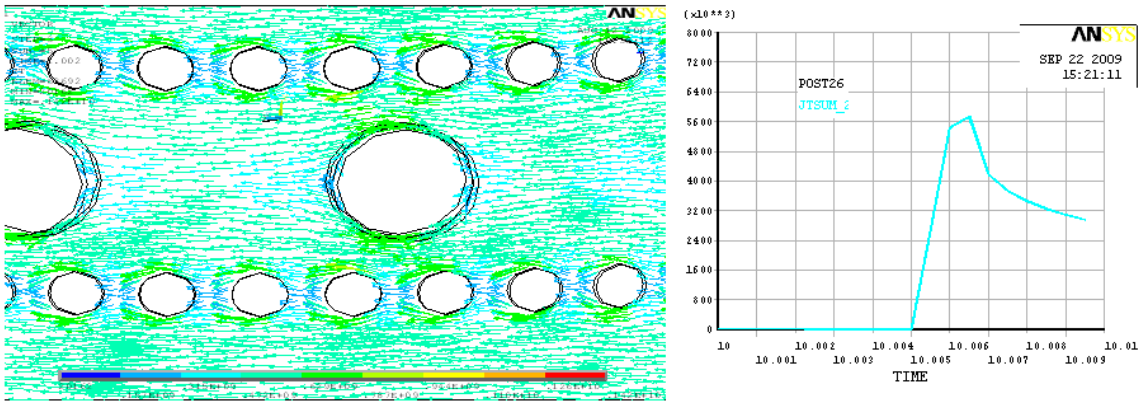

Figure 7.6.4-1 Current Densities

The above figure shows that the currents are maximum at time =10.0065 seconds.It also shows expected "Bunching" above ports

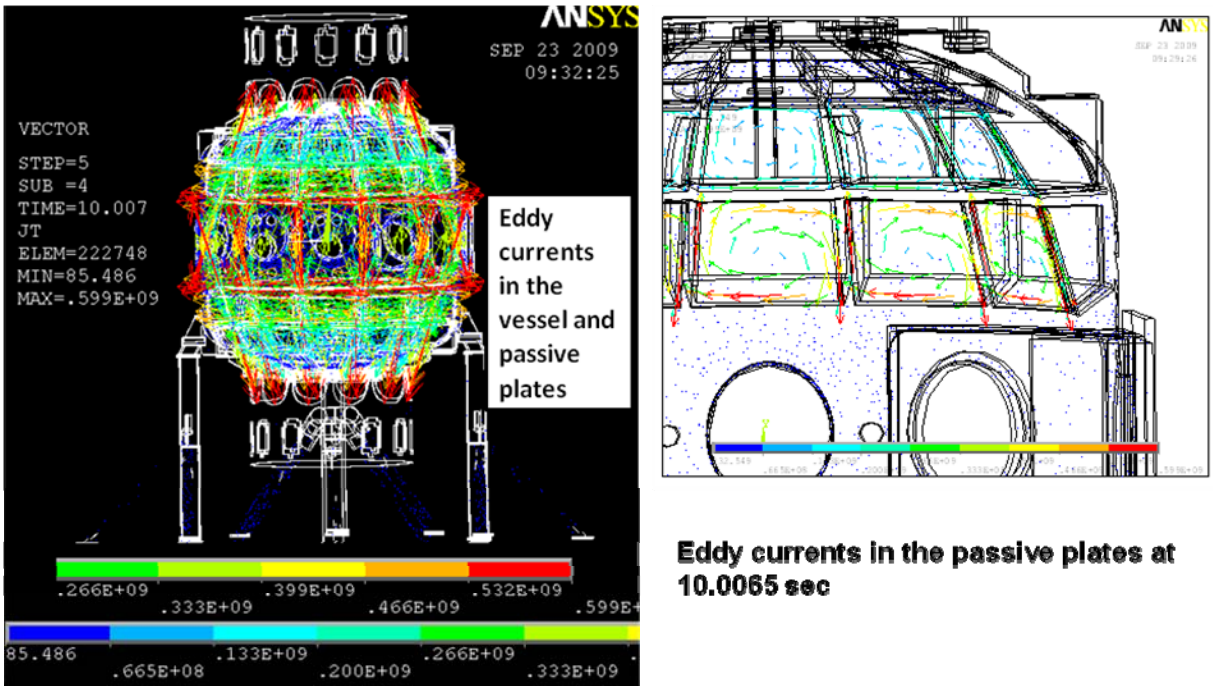

Figure 7.6.4-2 Passive Plate Eddy Currents

The above figure shows that the eddy currents in Cu are larger compared to those in the stainless steel. Also the eddies in the plates are evident. The analysis procedure produces appropriate poloidal currents that the axisymmetric OPERA model does not include.

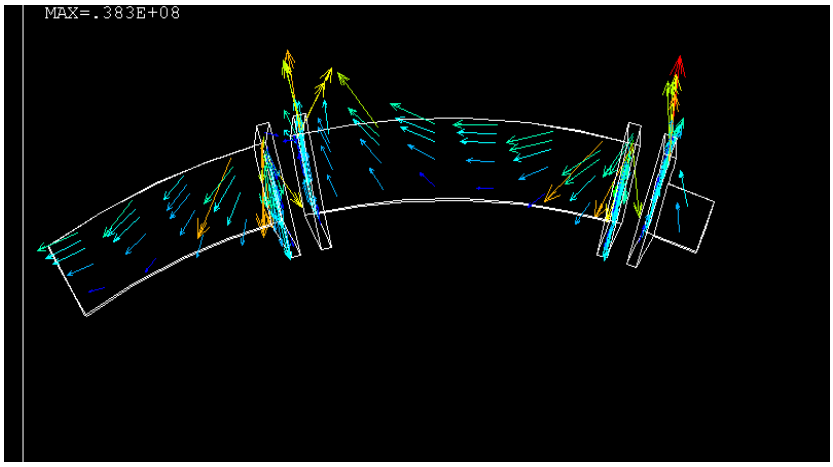

Figure 7.6.4-3Eddy currents flowing in and out of the passive plates

The above figure shows the eddy currents making a loop from the vessel into the passive plates and then back into the vacuum vessel. This indicates that the constraint equations have tied the plates to the vessel as expected. Also, this confirms that the analysis procedure develops realistic three dimensional currents in the toroidally discontinuous structures. The OPERA model that serves as the source of the disruption electromagnetic "environment" is axisymmetric and does not have three dimensional current distributions. The OPERA model must adjust the toroidal resistance of the corresponding complex structures to simulate the toroidal currents that develop during the disruption.

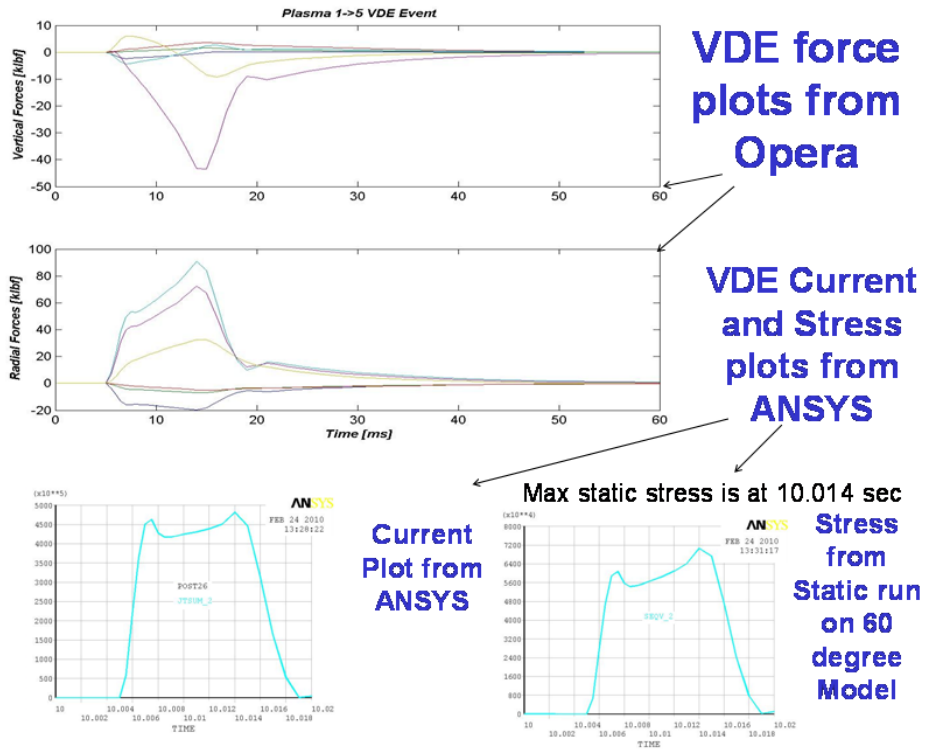

Figure 7.6.3-4 VDE Comparison Between OPERA and ANSYS Results

S. Avasarala ann R. Hatcher ran a VDE case and compared results, in Feb 2009. Current and force profiles are similarly shaped. This was an attempt at doing a "sanity check" on whether data was being successfully transferred from OPERA to ANSYS

7.6.5 Comparison of Bdots with Disruption analysis of the HHFW Antenna

Three nodes on the vessel are picked to compare the rate of change of Vertical Bs with the values obtained from the disruption analysis on the RF antenna. The disruption in both the cases is 2 MA in 1ms.

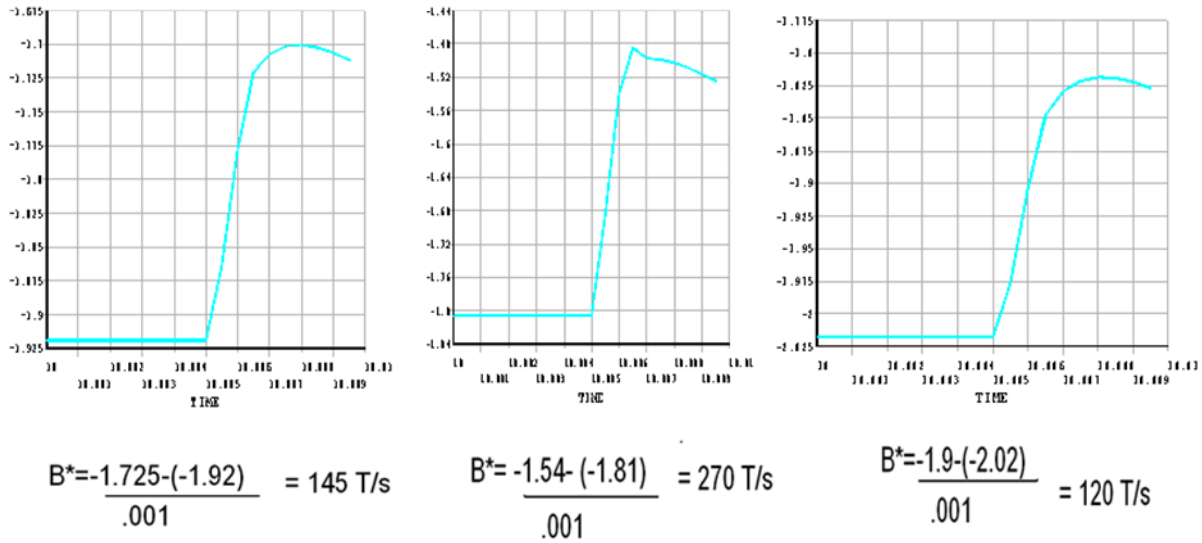

Figure 7.6.5-1 Vertical B values on three nodes on the vessel surface

From Han Zhang's HHFW Antenna Analysis

	above antenna			inside antenna			below antenna		
time (s)	BZ_2	BZ_3	BZ_4	BZ_5	BZ_6	BZ_7	BZ_8	BZ_9	BZ_10
1.00E-03	-6.43E-02	-4.53E-02	-5.10E-02	-0.153989	-0.18615	-0.158143	-5.65E-02	-6.59E-02	-5.47E-02
1.09E-03	-4.03E-02	-2.75E-02	-3.30E-02	-0.151737	-0.183004	-0.15682	-3.33E-02	-4.72E-02	-3.76E-02
1.18E-03	-1.66E-02	-9.03E-03	-1.41E-02	-0.145861	-0.175897	-0.15132	-1.04E-02	-2.74E-02	-1.94E-02
1.27E-03	7.06E-03	9.86E-03	5.22E-03	-0.135675	-0.165017	-0.1415	1.26E-02	-7.03E-03	-6.26E-04
1.36E-03	3.08E-02	2.92E-02	2.50E-02	-0.121633	-0.150762	-0.127905	3.56E-02	1.39E-02	1.87E-02
1.45E-03	5.46E-02	4.87E-02	4.51E-02	-0.104215	-0.134021	-0.111012	5.87E-02	3.53E-02	3.84E-02
1.55E-03	7.84E-02	6.86E-02	6.55E-02	-8.39E-02	-0.115067	-9.13E-02	8.17E-02	5.71E-02	5.85E-02
1.64E-03	0.102127	8.86E-02	8.61E-02	-6.11E-02	-9.44E-02	-6.92E-02	0.10475	7.91E-02	7.89E-02
1.73E-03	0.12588	0.108719	0.106917	-3.63E-02	-7.21E-02	-4.50E-02	0.12777	0.101344	9.95E-02
1.82E-03	0.149592	0.128977	0.127823	-9.53E-03	-4.86E-02	-1.90E-02	0.150742	0.123768	0.120255
1.91E-03	0.173284	0.14935	0.148872	1.87E-02	-2.40E-02	8.49E-03	0.1737	0.146364	0.141214
2.00E-03	0.196926	0.169782	0.169984	4.83E-02	1.57E-03	3.73E-02	0.196604	0.169059	0.162282
	Bz_dot (T/s) in cylindrical coordinate								
	263.90	195.77	198.37	24.77	34.61	14.55	255.14	205.85	187.70
	260.65	203.44	207.71	64.64	78.18	60.51	252.53	217.48	200.33
	260.88	207.86	212.75	112.06	119.69	108.03	252.81	224.26	206.59
	261.37	212.39	217.85	154.48	156.82	149.56	253.34	230.77	213.04
	261.45	215.31	221.25	191.62	184.17	185.84	253.38	235.16	216.57
	261.36	217.91	224.24	223.19	208.29	216.62	253.30	239.01	220.76
	261.32	219.90	226.52	250.63	226.87	243.39	253.23	242.19	224.03
	261.31	221.81	228.68	273.54	245.70	266.31	253.25	244.85	226.50
	260.86	222.86	229.99	294.02	258.68	285.85	252.72	246.69	228.69
	260.64	224.13	231.56	311.09	270.91	302.23	252.56	248.58	230.57
	260.09	224.77	232.26	325.13	280.99	316.41	251.97	249.67	231.77

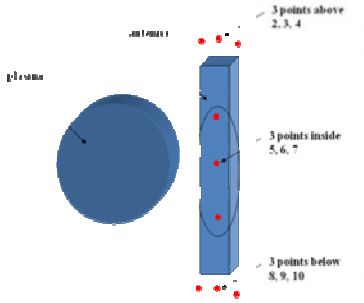

Figure 7.6.4-2: Vertical Bdots from the Disruption analysis on RF antenna, Ref [10]

Han Zhang's HHFW analysis is a mid-plane disruption similar to the Plasma 1 quench simulated by R. Hatcher. In the comparison above, only the equatorial plane Bdot is at the same coordinate, and the results agree. for that point.

7.7 Structural Test Runs

7.7.1 Damping

The damping value used in the structural dynamic analysis has a significant impact on the results. In these NSTX calculations, a conservative 0.5% damping is used. The figure below is a collection of some other damping value guidance from fission and fusion reactor sources. Larger damping values than 0.5% could be justified for the worst of the disruptions in NSTX, but if the response is fully elastic, and the vessel velocities remain small, 0.5% is approriate

Fission Reactor Experience

Regulatory Guide 1.61 - Damping Values for Seismic Design of Nuclear Power Plants

Table 1 Damping Values[1] (Percent of Critical Damping)

[1] Table 1 is derived from the recommendations given in Reference 1.
[2] In the dynamic analysis of active components as defined in Regulatory Guide 1.48, these values should also be used for SSE.
[3] Includes both material and structural damping. If the piping system consists of only one or two spans with little structural damping, use values for small meter piping.

Structure or Component	Operating Basis Earthquake or 1/2 Safe Shutdown Earthquake[2]	Safe Shutdown Earthquake
Equipment and large-diameter piping systems[3], pipe diameter greater than 12 in	2	3
Small-diameter piping systems, diameter equal to or less than 12 in.	1	2
Welded steel structures	2	4
Bolted steel structures	4	7
Prestressed concrete structures	2	5
Reinforced concrete structures	4	7

Fusion Reactor Experience (ITER) Vessel Loads Spec

Magnetic Damping is important in the ITER vessel dynamic analyses. Magnetic damping is conservatively neglected in the NSTX analyses

Horizontal Support due to Magnetic Coupling

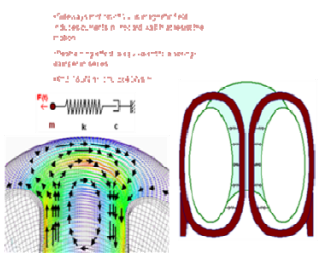

Damping Discussion from Ref [18]:

Rayleigh damping constants α and β As Used in ANSYS
These are applied as multipliers of [M] and [K] to calculate [C]:

$$[C] = \alpha[M] + \beta[K]$$
$$\alpha/2\omega + \beta\omega/2 = \xi$$

Where ω is the frequency, and ξ is the damping ratio. These are input in ANSYS in situations where damping ratio ξ cannot be specified. Alpha is the viscous damping component, and Beta is the hysteresis or solid or *stiffness* damping component.

Beta Damping As Used in ANSYS

Good for damping out high-frequency component-level oscillations (typically low amplitude).
From Section 9.7 the first four modes of oscillation of the passive plates are : 191.9, 194.97, 205.33, 206.3 cps. Considering beta damping alone, and ξ = .5%:

$$\beta = 2\xi/\omega$$
$$\beta = 2\xi/\omega = 2*.005/(200*2*3.1416) = 7.96E\text{-}06$$

Alpha Damping As Used in ANSYS
Alpha damping is also known as *mass damping.* It is Good for damping out low-frequency system-level oscillations (typically high amplitude).
 If beta damping is ignored, α can be calculated from a known value of ξ (damping ratio) and a known frequency ω:

$$\alpha = 2\xi\omega$$

Only one value of alpha is allowed, the most dominant response frequency should be used to calculate α.

Considering Alpha damping alone, and ξ = .5%:

$$\alpha = 2\xi\omega = 2*.005*200*2*3.1416 = 12.57$$

7.7.2 Static Analysis Results for the Test Case:

The EM model is used for the structural model after conversion of element type from 97 to 45 and addition of appropriate displacement constraints. Material properties used are that of Stainless Steel except for the passive plates which are made up of a high strength copper. If only static analysis results were used, the conclusion would be that the passive plates are significantly overstressed. A dynamic analysis is needed to properly simulate the response of the passive plates.

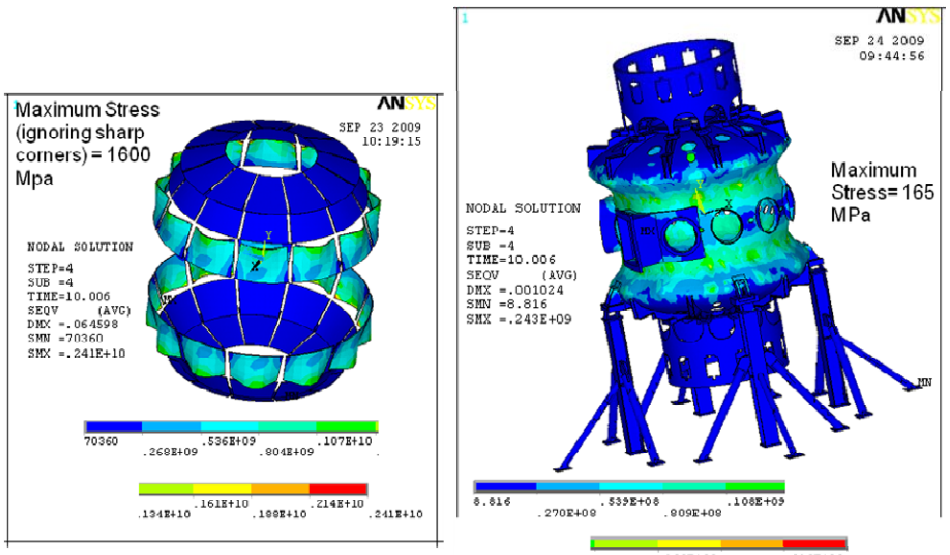

Von-Mises Stress on Passive Plates from Static Analysis

Von-Mises Stress on Vacuum Vessel from Static Analysis

Figure 7.7.2-1 Von-Mises Stress on Passive Plates from Static Analysis

7.7.3 Dynamic Analysis Results for the Test Case:

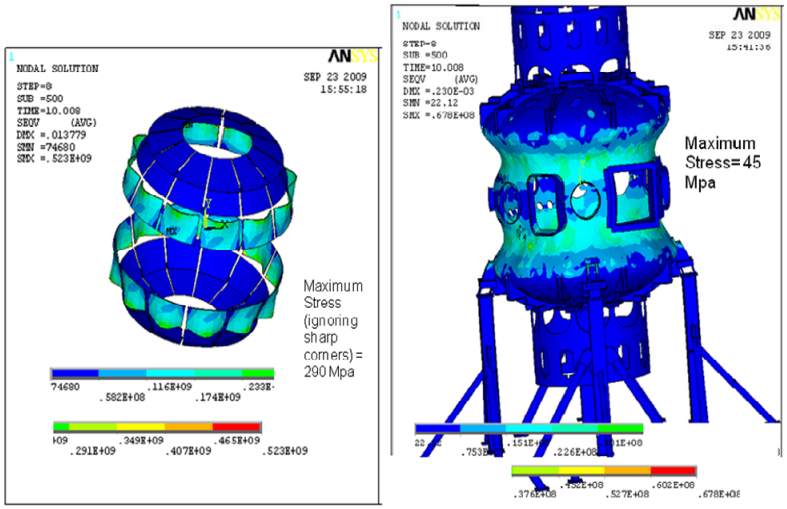

Von-Mises Stress on Passive Plates from Dynamic Analysis

Von-Mises Stress on Vacuum Vessel from Dynamic Analysis

Figure 7.7.3-1 Von-Mises Stress on Passive Plates from Dynamic Analysis

The dynamic response is substantially below that for the static analysis. This is relied on to qualify the passive plates and bolting. It also raised the issue as to whether the fastest quench in fact caused the worst loading. As a result some of the slow VDE/quench cases were run.

7.7.4 Comparison of Dynamic and Static Analyses

Four regions are selected on the vacuum vessel and the passive plates to compare displacements and stresses.

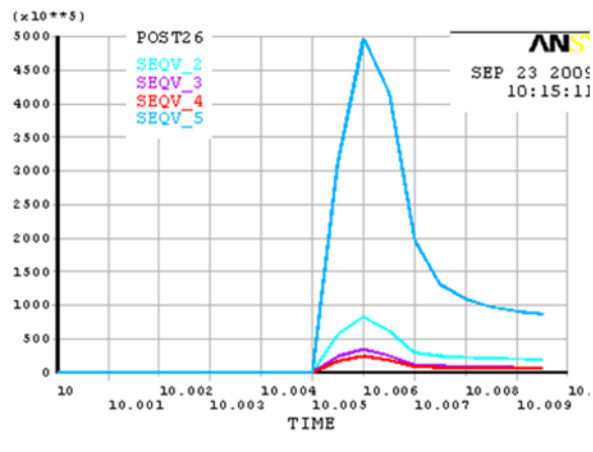

Stress from static analysis on nodes 47059,29593,19132 and 76456

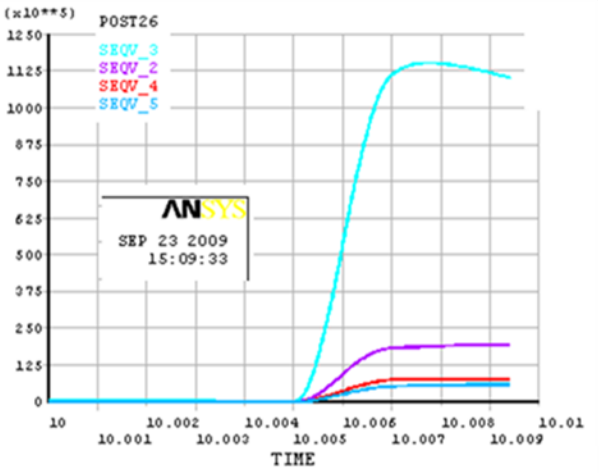

Stress from dynamic analysis on nodes 47059,29593,19132 and 76456

Figure 7.7.4-1 Stress from Static and Dynamic Analysis on nodes 47059,29593,19132 and 76456

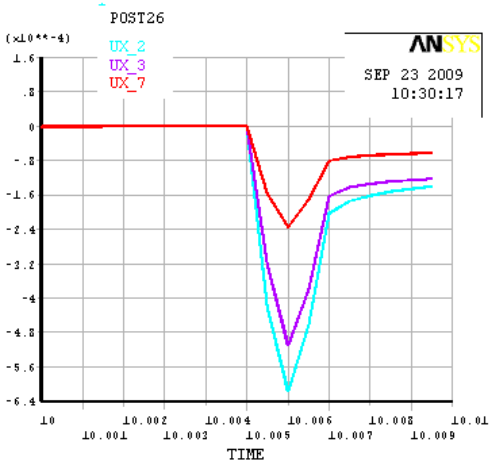

Displacements from static analysis on nodes 47059,29593 & 19132.

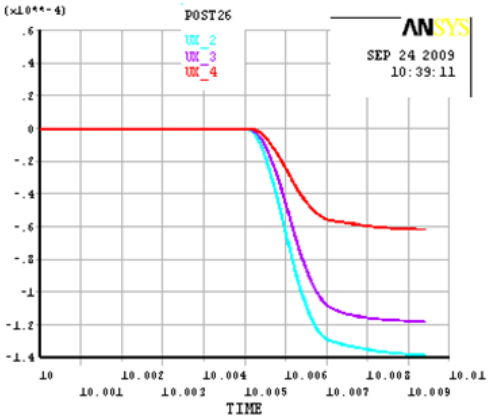

Displacements from Dynamic analysis on nodes 47059,29593 & 19132

Figure 7.7.4-2 Displacements from Static and Dynamic Analysis on nodes 47059,29593,19132 and 76456

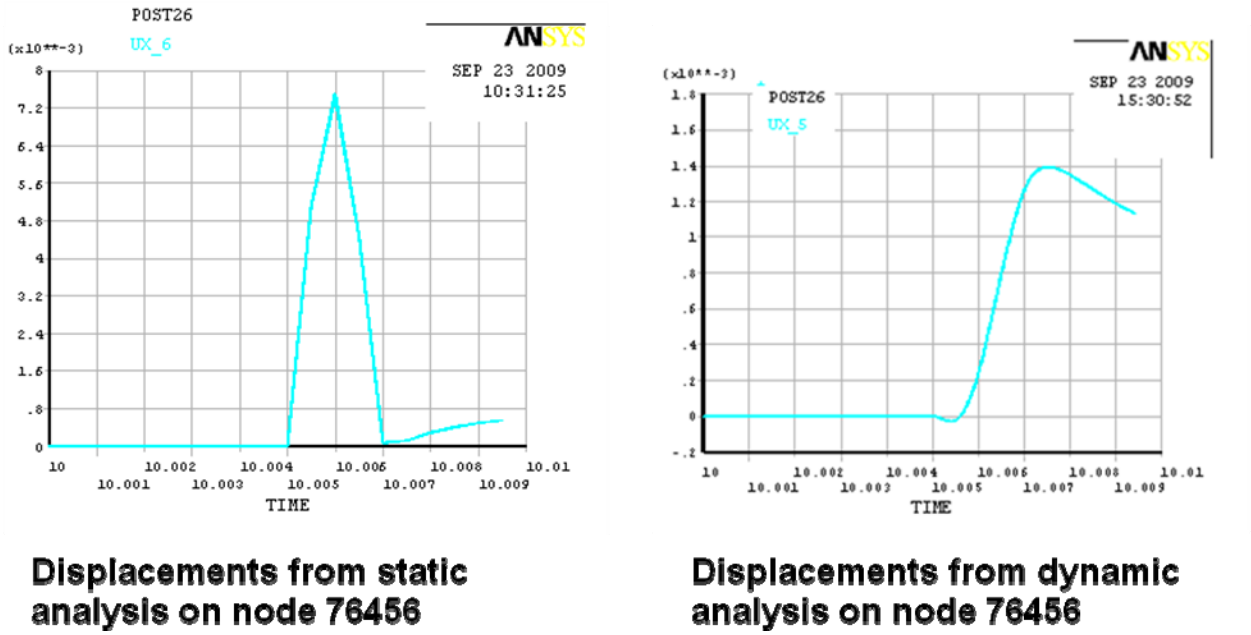

Figure 7.7.4-3 Displacements from Static and Dynamic Analysis on node 76456

8.0 Global Vacuum Vessel

8.1 Mid-Plane Disruption

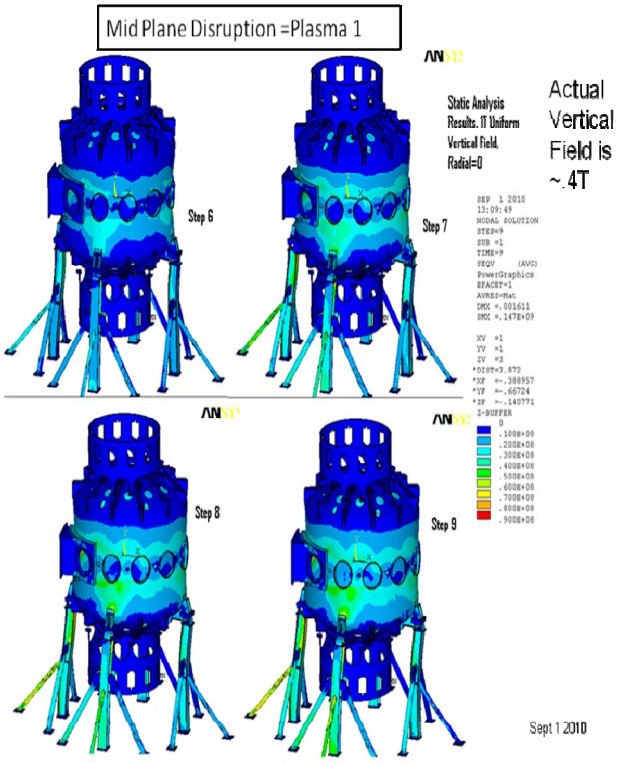

8.1.2 Mid Plane Disruption Currents and Stresses Near Bay L,

The primary responsibility for qualifying this area of the vessel is found in reference [17], "Vessel Port Rework for NB and Thompson Scattering Port". Results are included here for comparison.

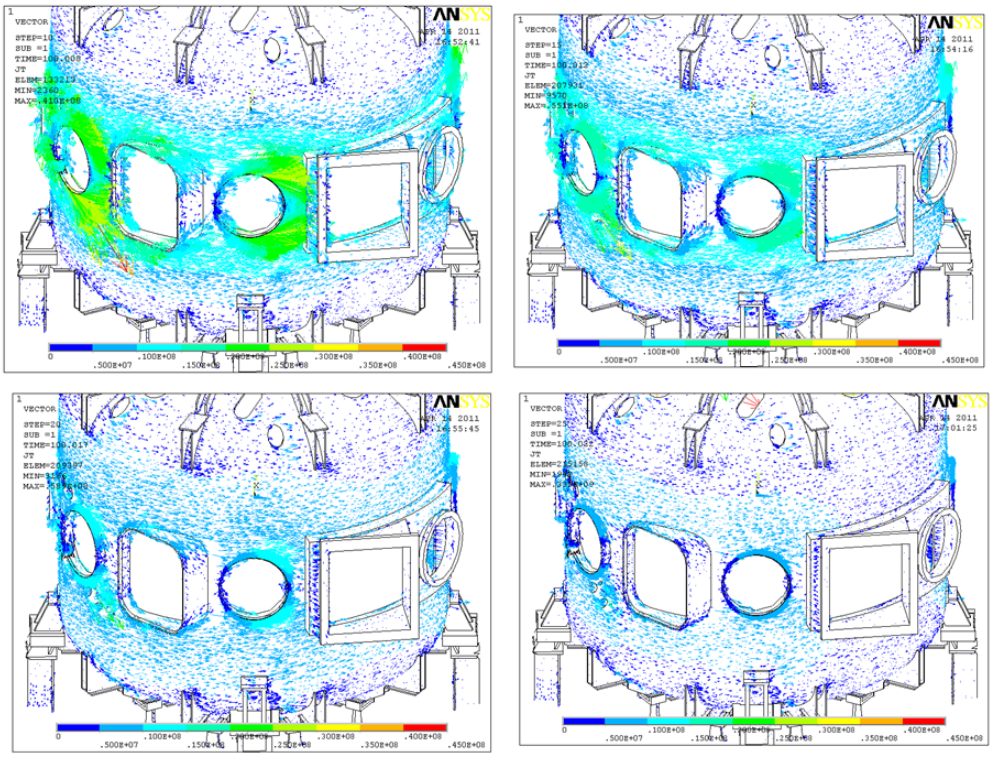

Figure 8.1.2-1 Current Densities in the NB/Thompson Scattering Port Area

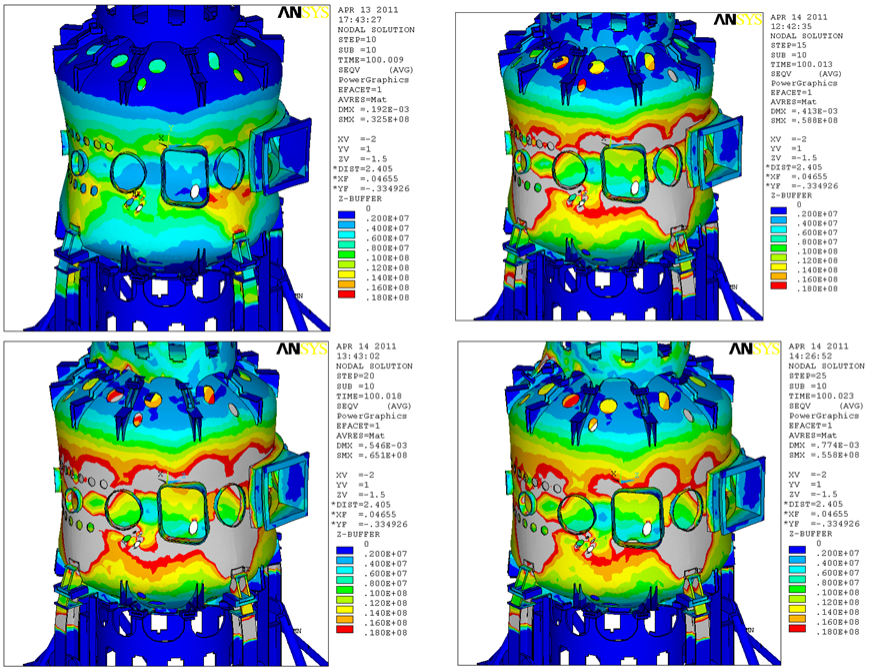

Figure 8.1.2-2 Von Mises Stresses (Contoured for a Max=18 MPa) in the NB/Thompson Scattering Port Area

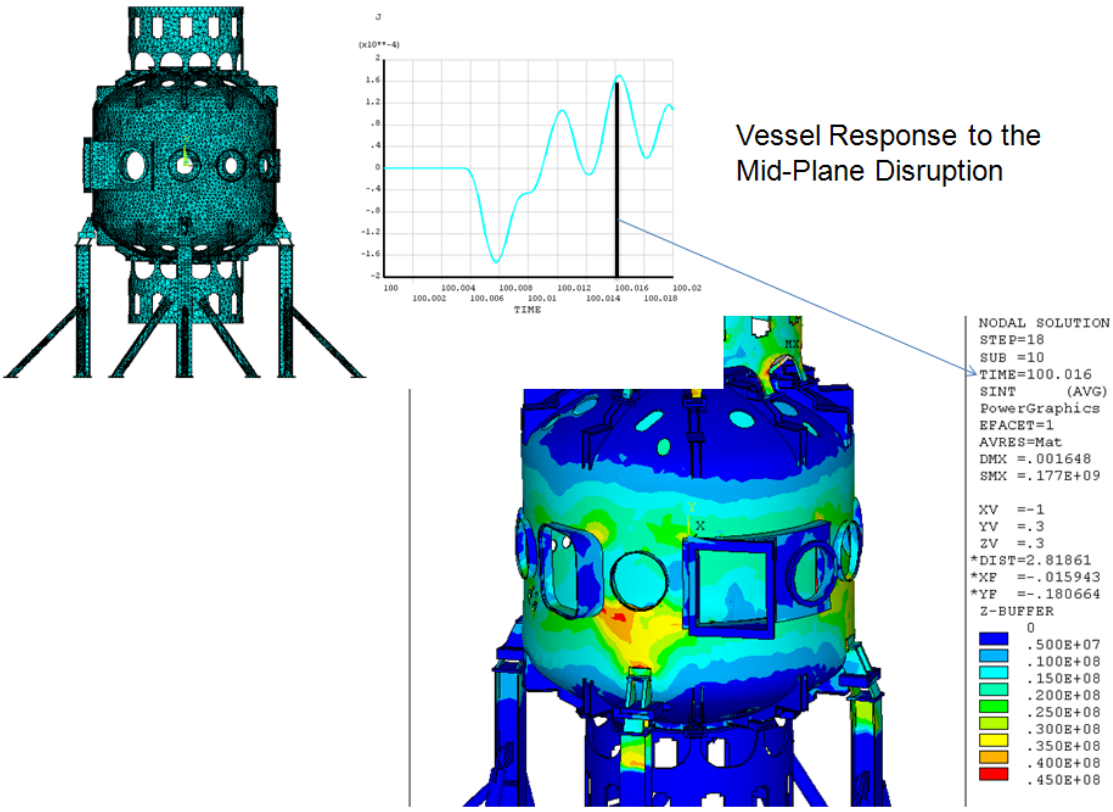

Figure 8.1.2-3 Tresca Dynamic Analysis Results - Stress in the NB/Thompson Scattering Port Area

8.3 Vessel Response to a Plasma 4 Quench

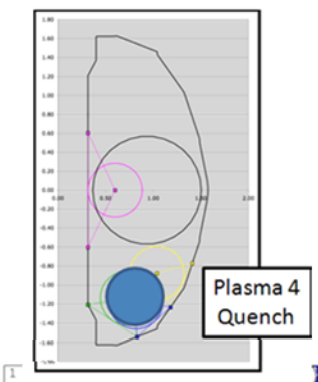

Plasma4 Quench Analysis of the Vessel

PP and Full Vessel Have not Been Integrated, But the Shielding Effect of the PP is included in the OPERA Analysis

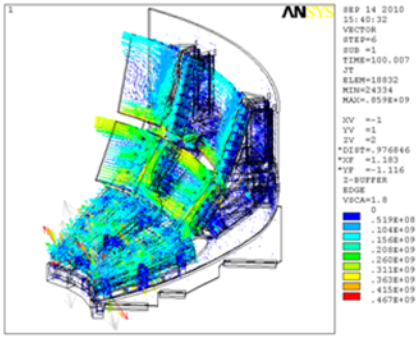

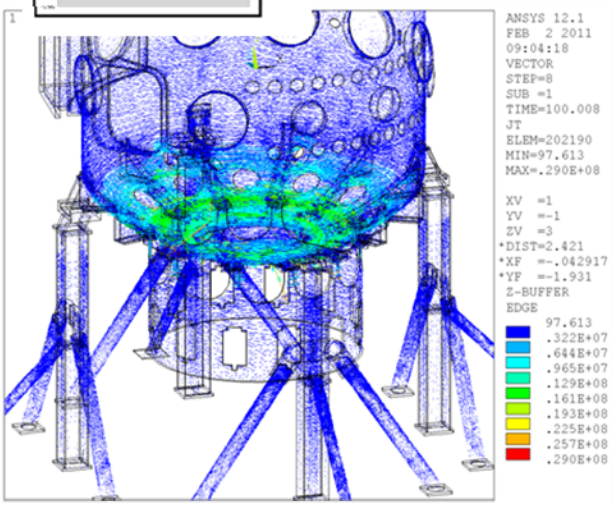

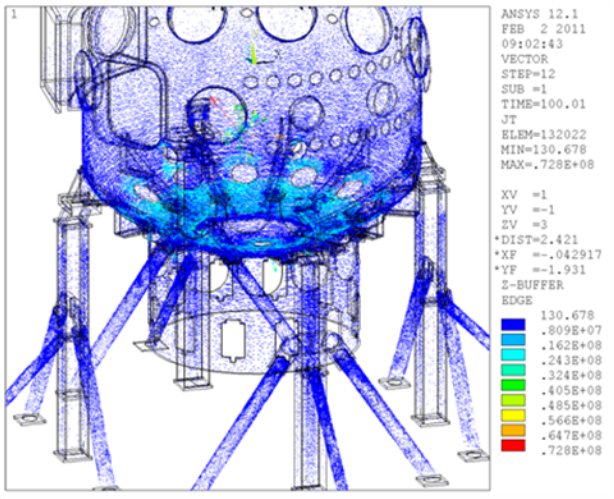

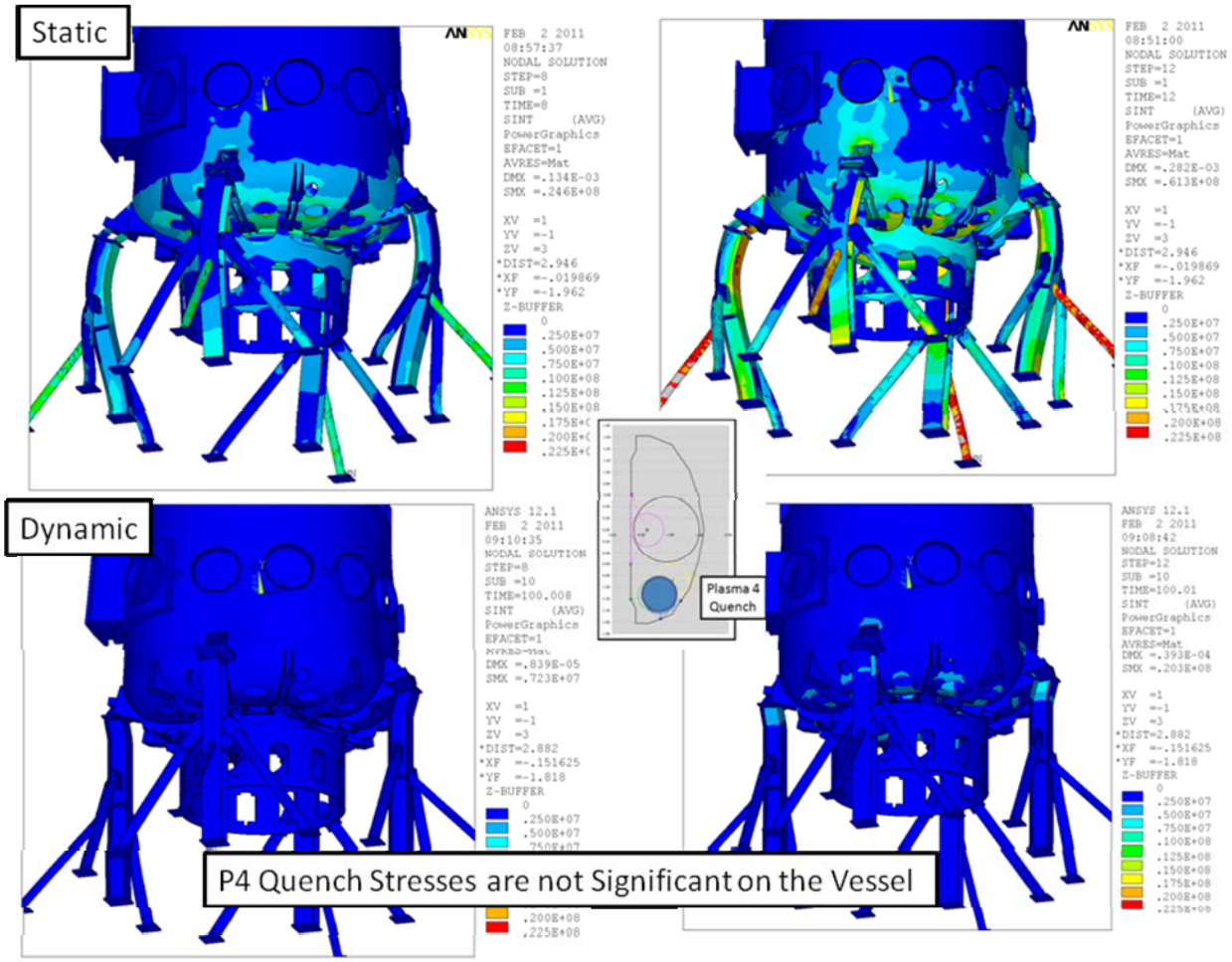

8.4 Estimate of Disruption Accelerations at the Lowe Head Nozzles

Diagnostics mounted on the heads of the vacuum vessel will experience some dynamic excitation at their mounting location. The Plasma 4 Quench results were post processes in the area near the lower vertical nozzles. Vertical displacement plots from the dynamic analysis were obtained, and the peak velocity estimated from the slope. The velocity divided by the time needed to develop the velocity yielded an estimate of the acceleration. Only .05 g's was obtained, which is modest compared with gravity loads, and has no structural consequence. It may have some impact on the resolving power of the diagnostic if data is needed during the disruption.

Dynamic Disruption Displacements at Lower Nozzle

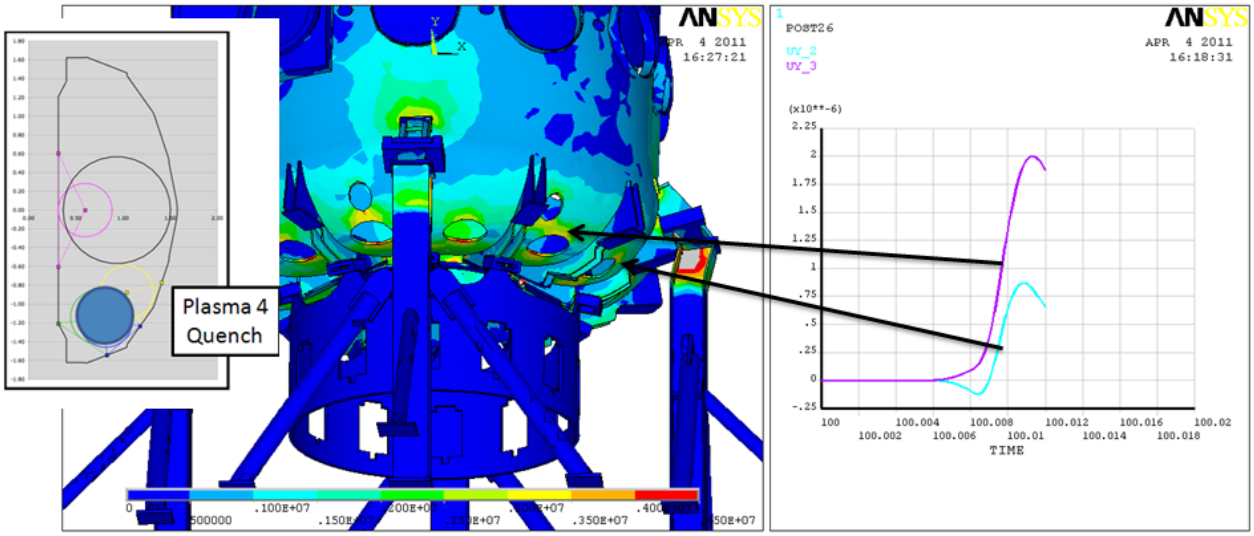

Peak Velocity is Approx 1e-6/.001= 1e-3 m/sec
This develops over About 2 milli-sec. The acceleration
= .5 m/sec^2 = .5/9.8 = .05 g

8.5 Vessel Support Leg Analyses

8.5.1 Drawing Excerpts and Photos

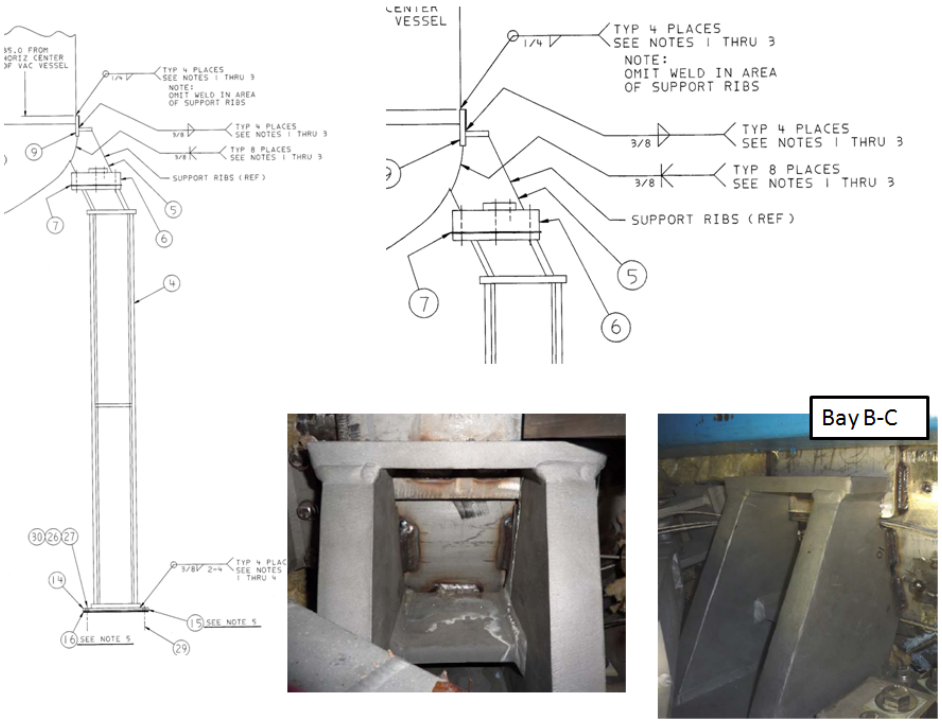

8.5.2Vessel Stresses Near the Column Supports

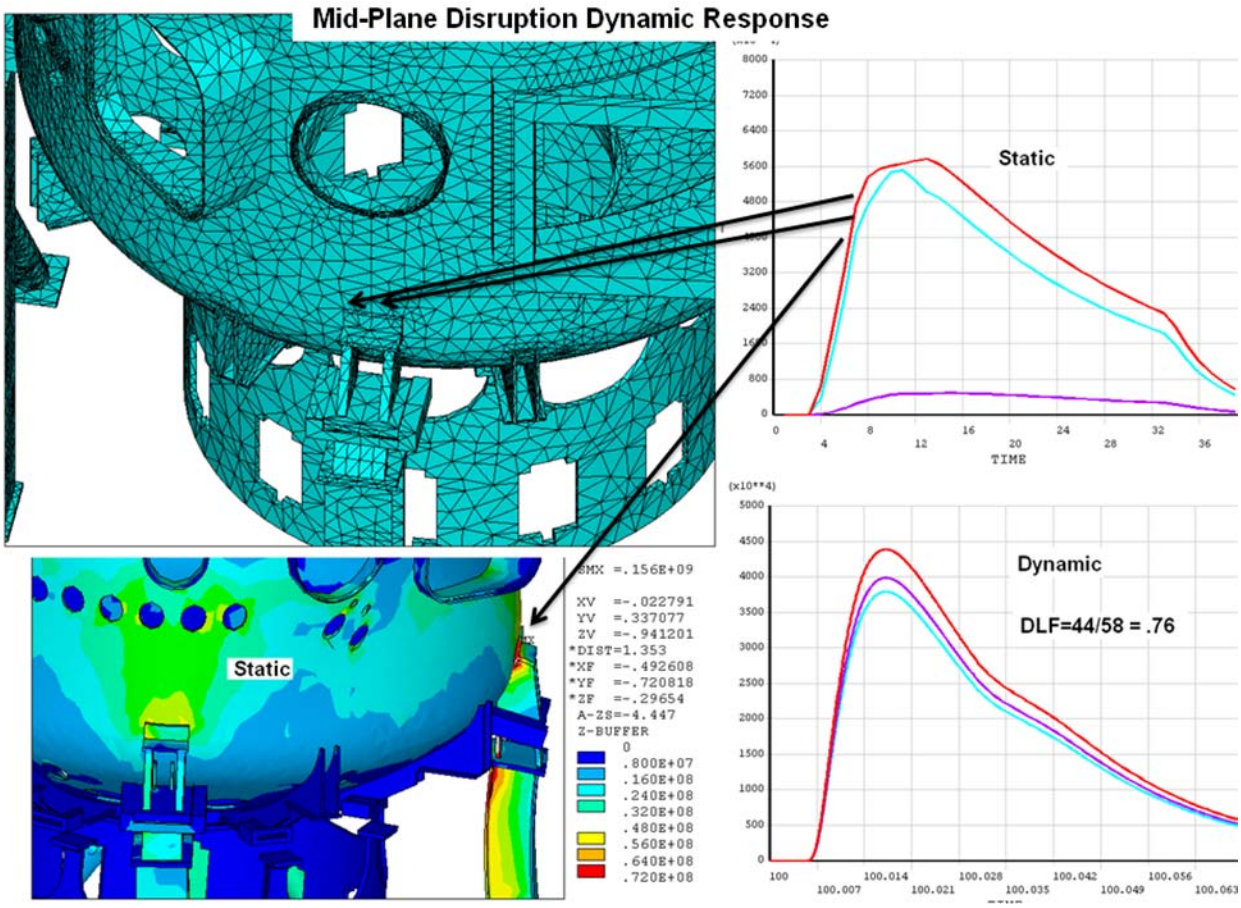

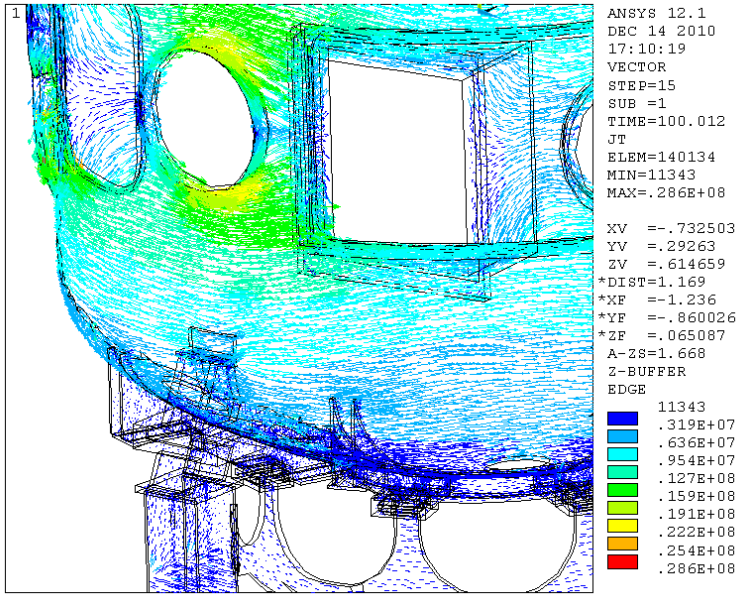

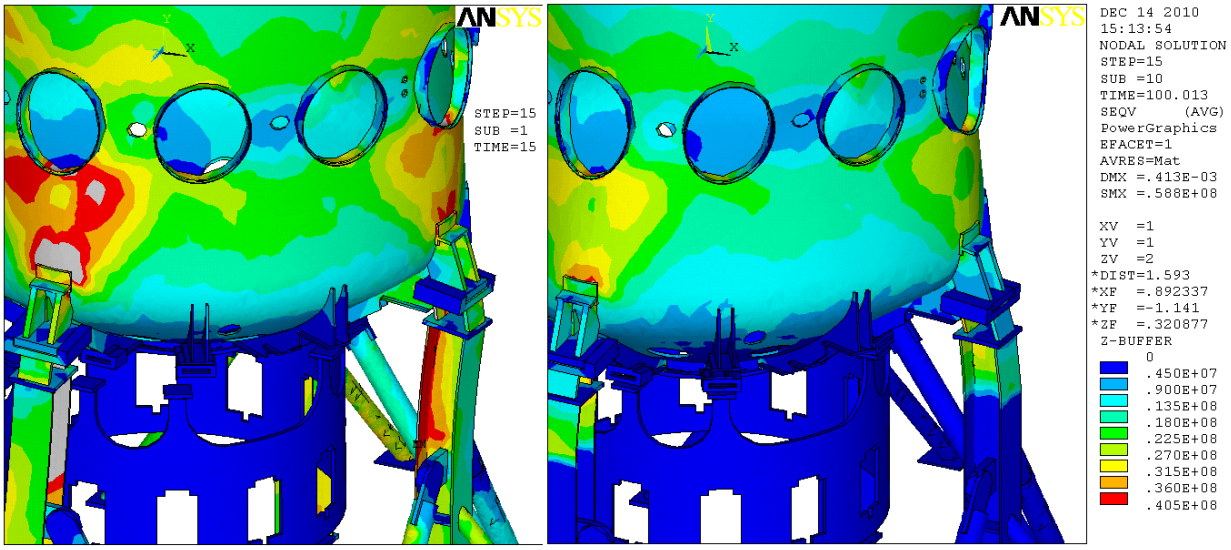

Static Dynamic

9.0 Passive Plate Disruption Analyses With Halo Currents

The Passive Plates are copper and are close to the plasma. They currently pick up large currents and are expected to see even larger currents and loads during the upgrade operation. In the test cases discussed in section 7, the passive plates were simply modeled because a solid model was not available. The passive plates were supplied by ORNL and the design drawings were entered into the NSTX Pro-E solid model of the machine in the summer of 2009. This work was done by Bruce Paul, with S. Avasarala interacting in the process to allow a meshable continuous solid. In order to facilitate creation of cyclic symmetry in ANSYS, 30 degrees of the desired section was created and reflected so that the nodes on the cyclic symmetry face would line-up. The model was still not fully merged at the backing plates, and a swept mesh was created that had reasonable bolt elements and would merge with the rest of the model.

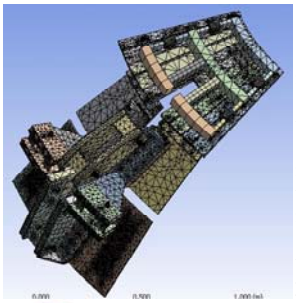

30 degree ProE model was meshed and then reflected to fit vessel 60 degree sector model. The vessel was added to model current sharing. Reflection was done to allow precise CP command coupling

Incorporation of the Detailed ProE model

To manage model size, 60 degree cyclic symmetry and up-down symmetry is used.

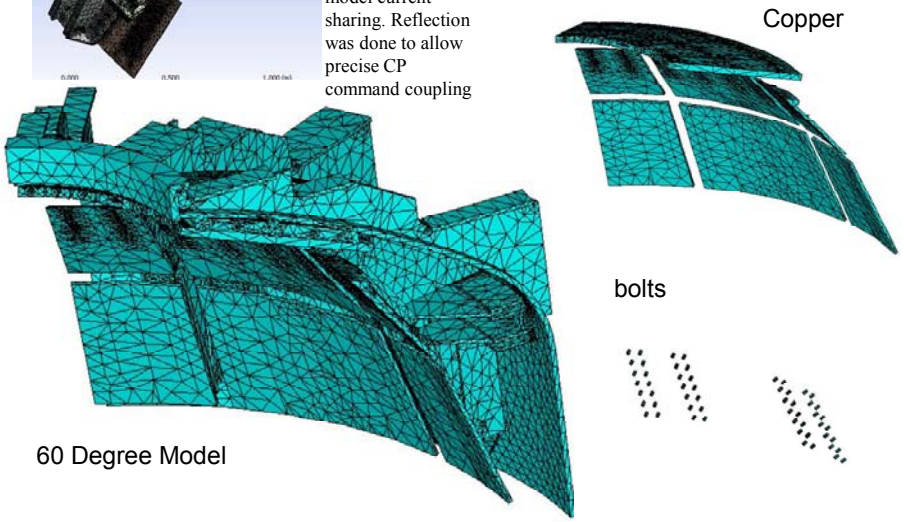

Figure 9.0-1 The ProE model and its Conversion to a meshed ANSYS cyclic Symmetry Model

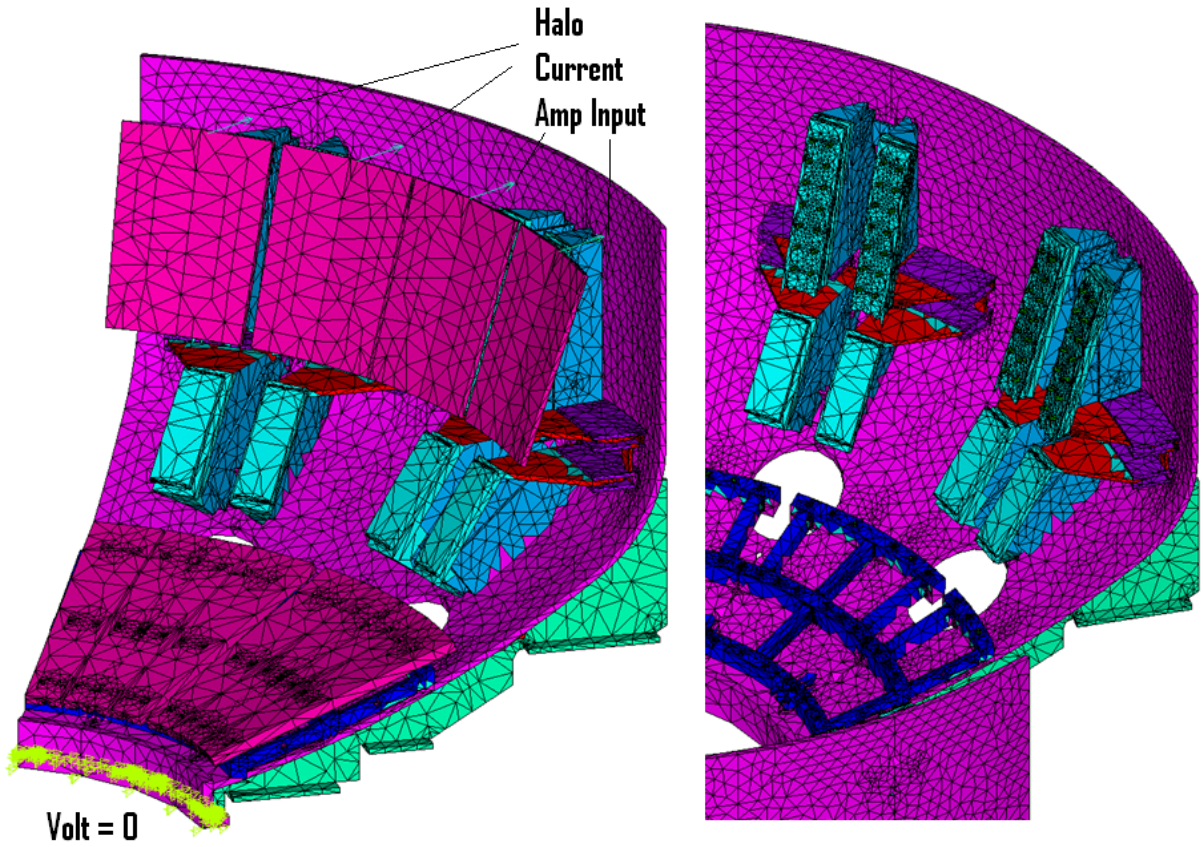

Figure 9.0-2 Halo Current Input Electromagnetic Model as of July 15th 2010. The secondary passive plates are not yet included

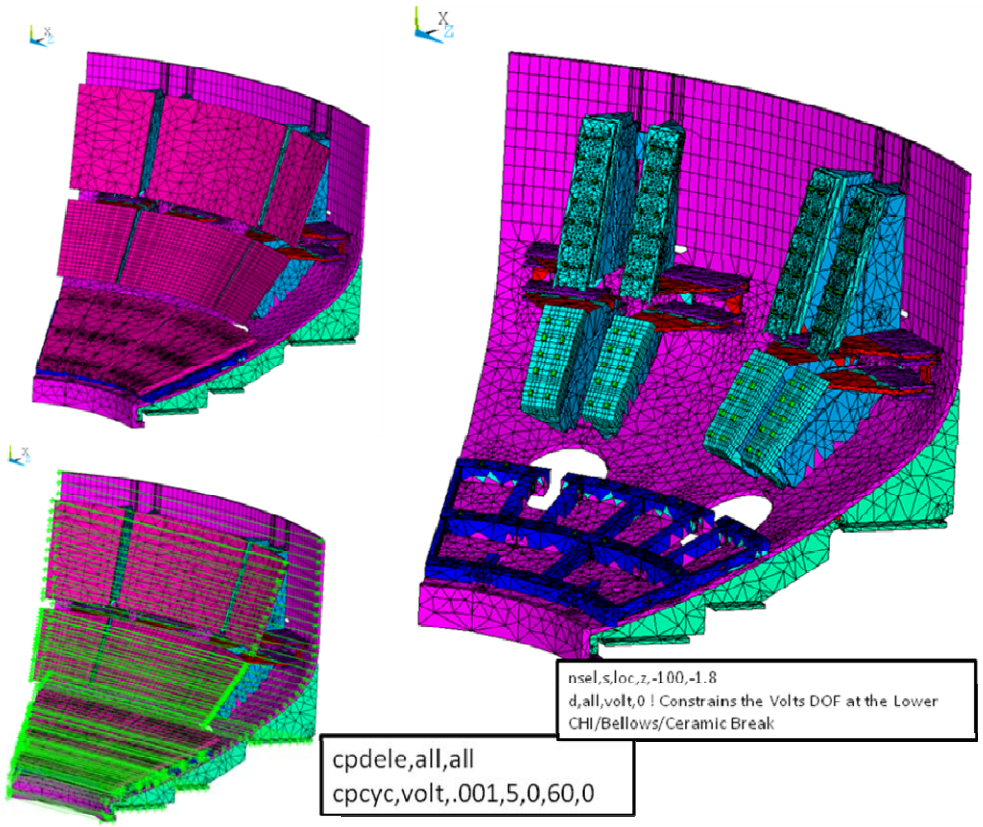

Figure 9.0-3 Halo Current Input Electromagnetic Model. The secondary passive plates have been added

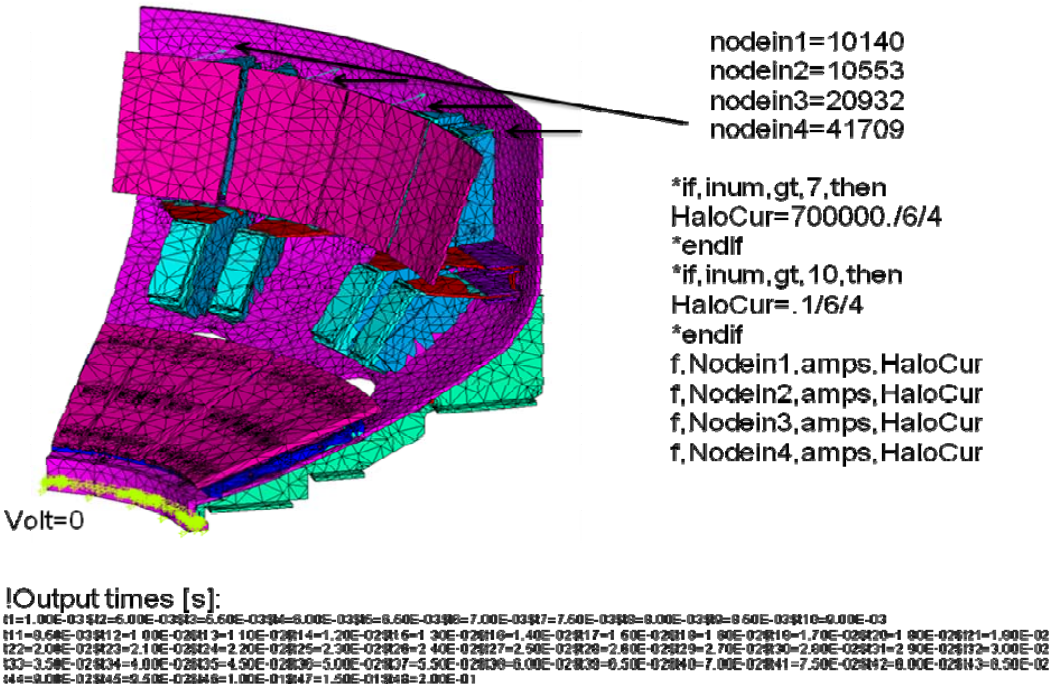

Figure 9.0-3 Halo Current Input Electromagnetic Model. Halo Current Input

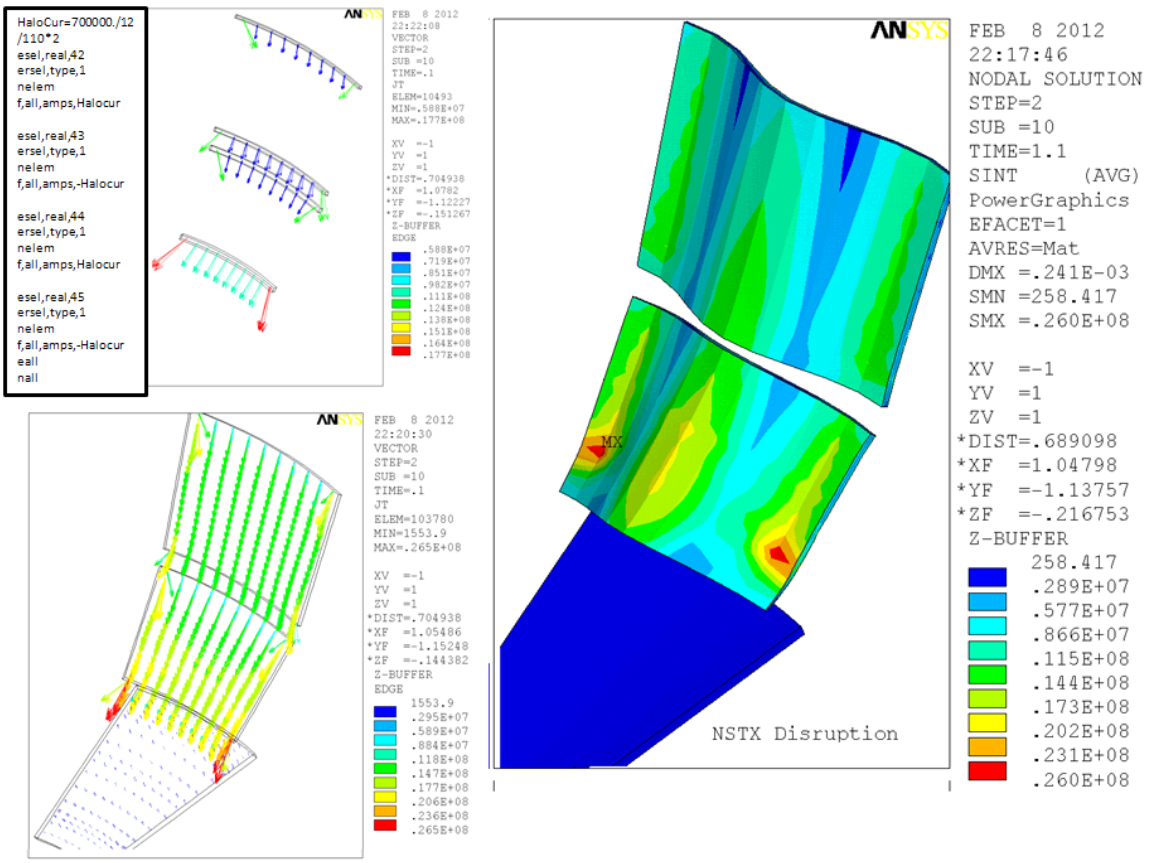

Figure 9.0-4 Halo Current Input in Attachment I Electromagnetic Model. Only the Halo Current is Applied -No Disruption Inductive Current

The halo loading in the passive plate model was not significant when included with the disruption loads. In addition, the choice of entry points caused the halo current to quickly go to the vessel which was grounded at the CHI gap. The analysis in Figure 9.0-4 forces the currents to flow through the passive plates. Halo currents were forced to enter into the top of the plate and exit through the bottom of the plates. See Appendix I for a more detailed discussion of this modeling. With the halo current forced to flow across the passive plates, the mid span bending stress is less than 20 MPa - The current direction and the toroidal field direction should have been chosen so that the halo current pressure pushed away from the plasma. The resulting stress mid span in the plate is much smaller than the 200 MPa found for the disruption inductively driven currents or about 10% additional to the bend stress reported in Appendices H and I

9.1 Drawing Excerpts and Photos

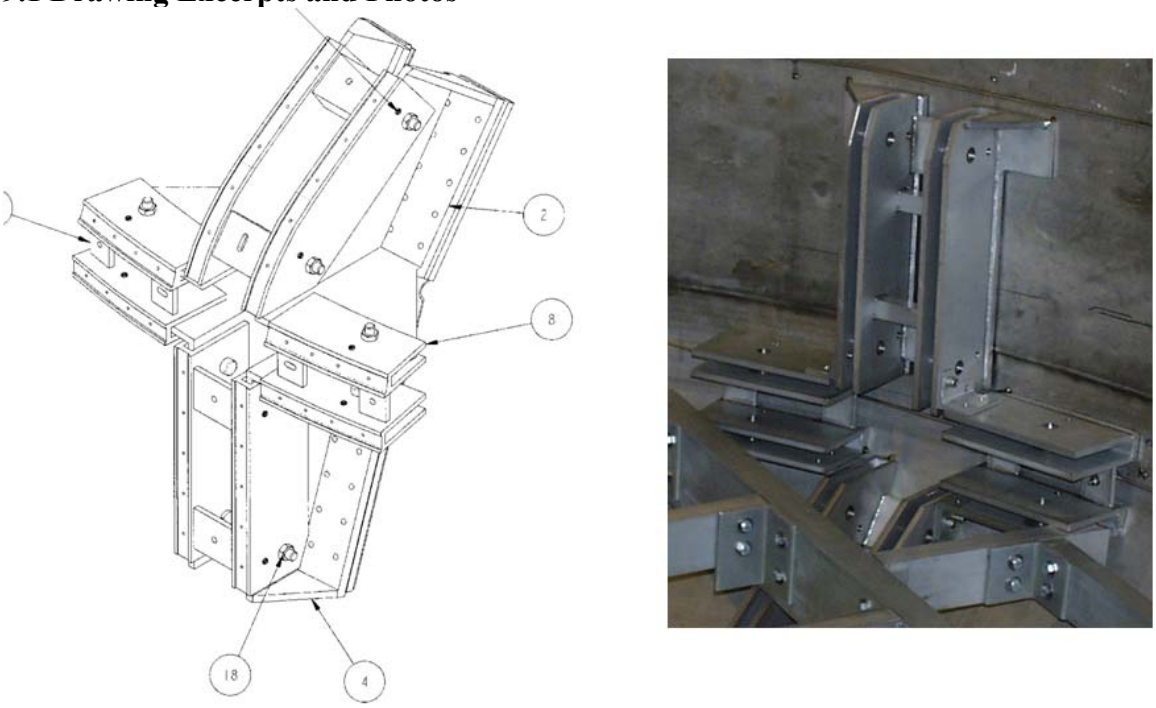

Figure 9.1-1 Bracket as it appears on the ORNL Drawing, and a photo of the bracket during installation. Not that the perimeter welds that connect the bracket to the vessel wall have not yet been made.

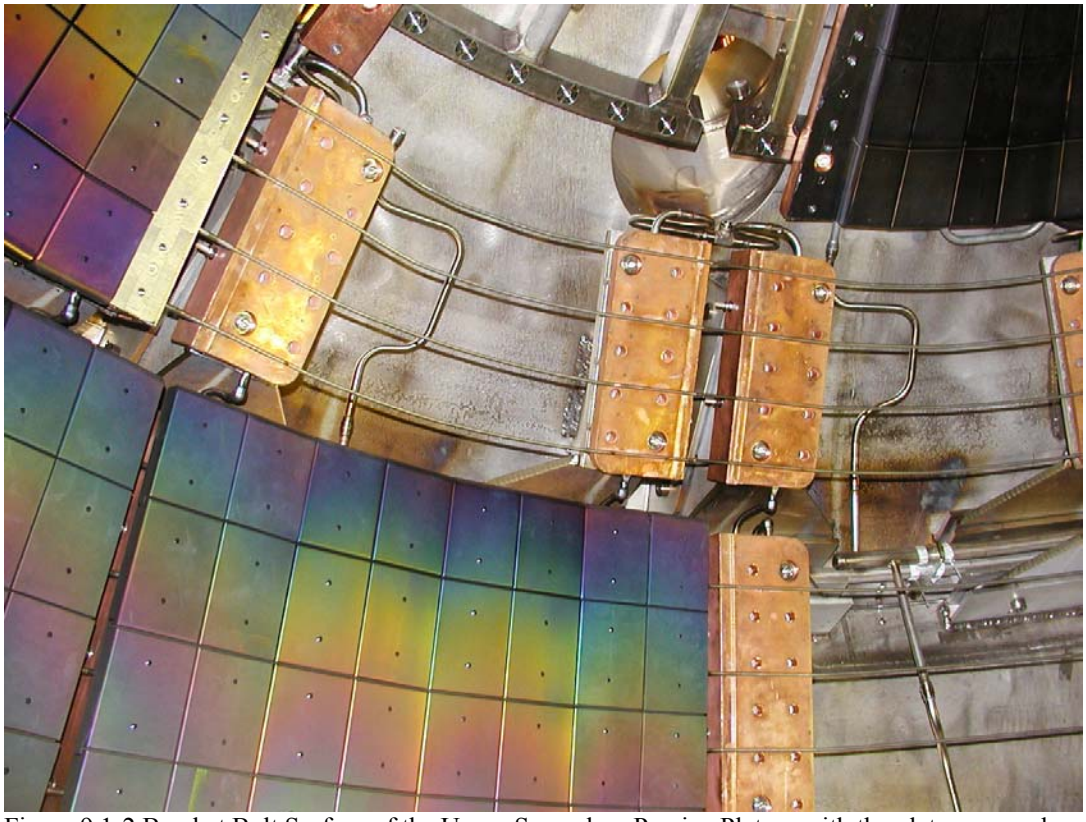

Figure 9.1-2 Bracket Bolt Surface of the Upper Secondary Passive Plate. - with the plate removed.

9.2 Passive Plates Loaded by a Mid-Plane Disruption

9.2.1 With and Without Halo Currents

The model was run with and without halo currents with the mid-plane disruption. In July 2010,the secondary passive plate had not been meshed. so the model was run without it to see the effects of the halo currents entering the passive plates and traveling through the vessel wall. Plots of with and without halo currents are shown below in figures 9.2-1 and 2

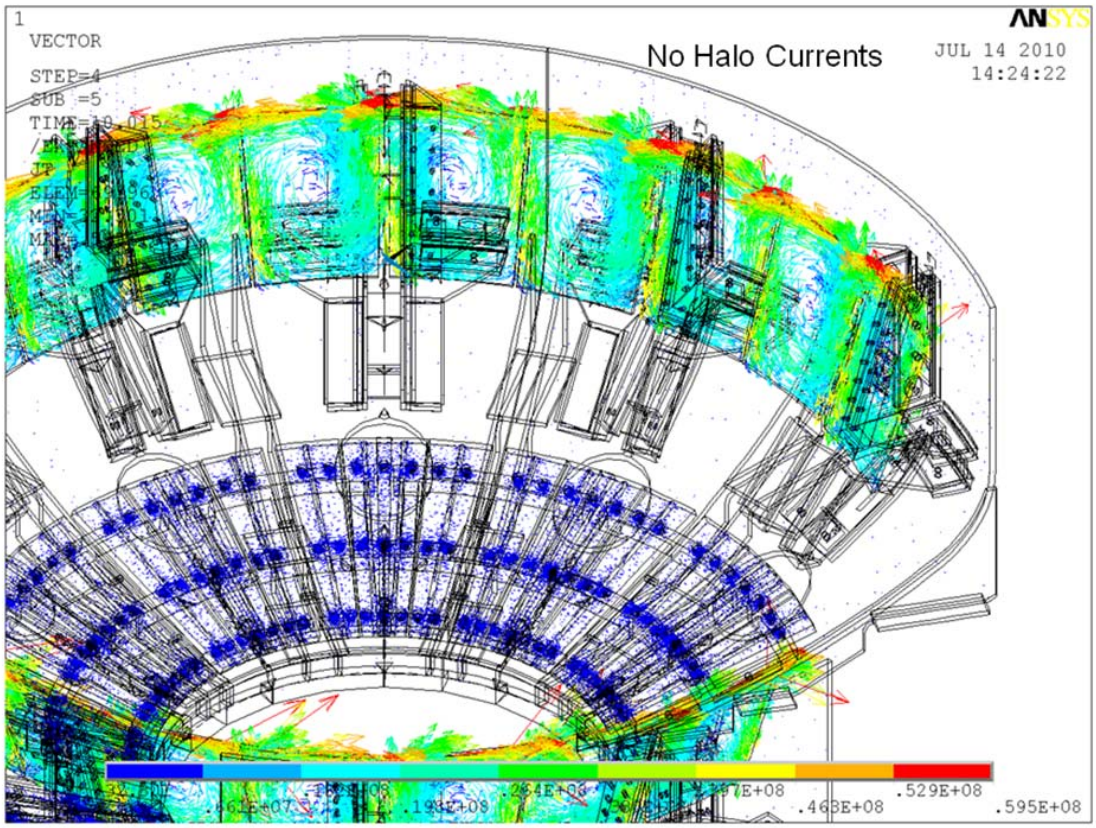

Figure 9.2-1 Results without halo currents

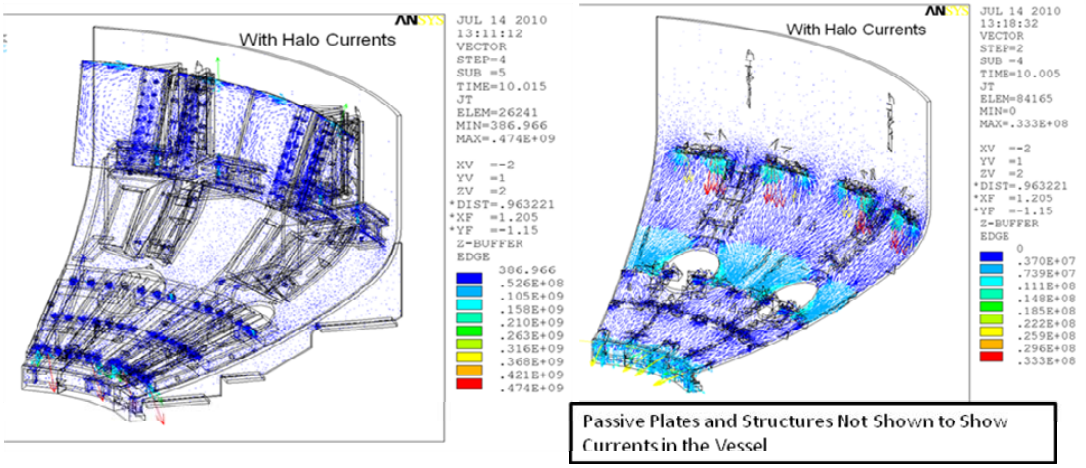

Figure 9.2-2 Results with halo currents

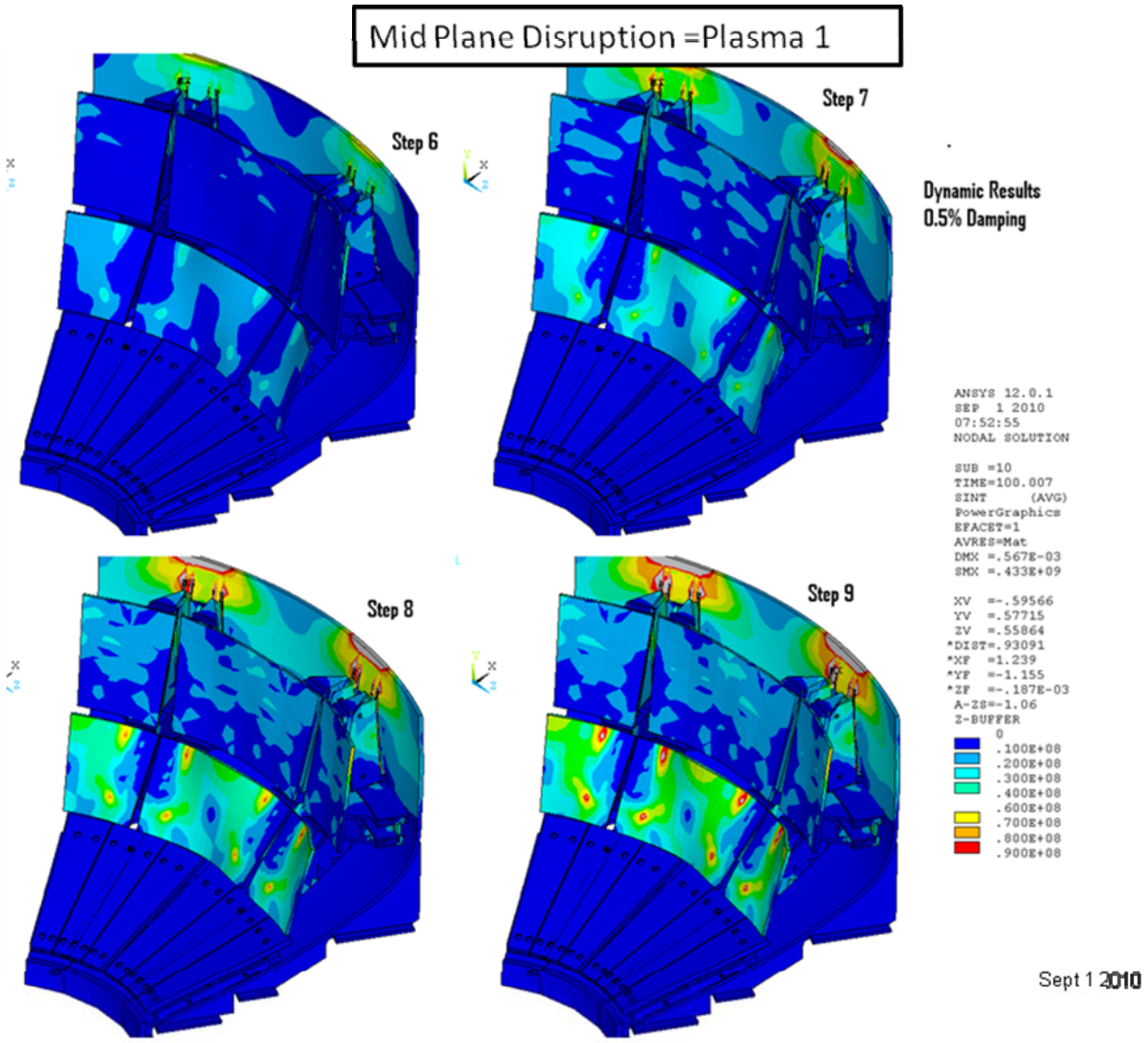

Figure 9.2-1 Static Stress in the middle of the Passive Plate

9.2.2 Currents Flowing in the Passive Plates, Mid-Plane Disruption, Plasma 1

The OPERA axisymmetric Analysis produces only toroidal currents.The results of the Opera/ANSYS disruption simulation show eddy currents in the plates. In the ANSYS results there is a clear net toroidal current in the primary passive plates represented by larger current densities at the top of the plate than at the bottom. Based on the top and bottom current densities, at the time in the disruption that produced the largest current densities , the conduction cross section of the primary passive plates and an assumed triangular current density distribution:

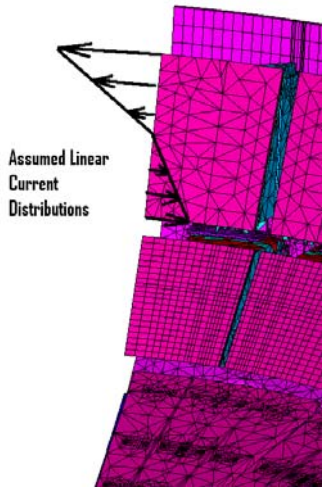

Figure 9.2.2-1

Fraction of IP flowing in the Primary Passive Plates is:

(.467e9-.311e9)*5.4848e-3/4/2E6 = .107

The upper bound of measured net currents [3] in the primary passive plates is also about 10% of the plasma current. Currents in the secondary passive plates are not as readily determined from the current vector plot but it is clear that they are lower, consistent with measured data.

```
tarea
 Element Group for which Area is to be Calculated
1
  TOTAL SURFACE AREA OF 4 NODE ELEMENTS IS BEING COMPUTED.
 TOTAL AREA =   5.4848189E-03
 CENTROID X,Y,Z=    1.437300      -0.7918749      -2.6471052E-02 MOMENTS OF INERTIA
 =   0.0000000E+00   1.9485991E-17   1.9029288E-20
 AXISYMMETRIC VOL=   4.9532536E-02
```

Figure 9.2.2-2 Passive Plate Cross Sectional Area

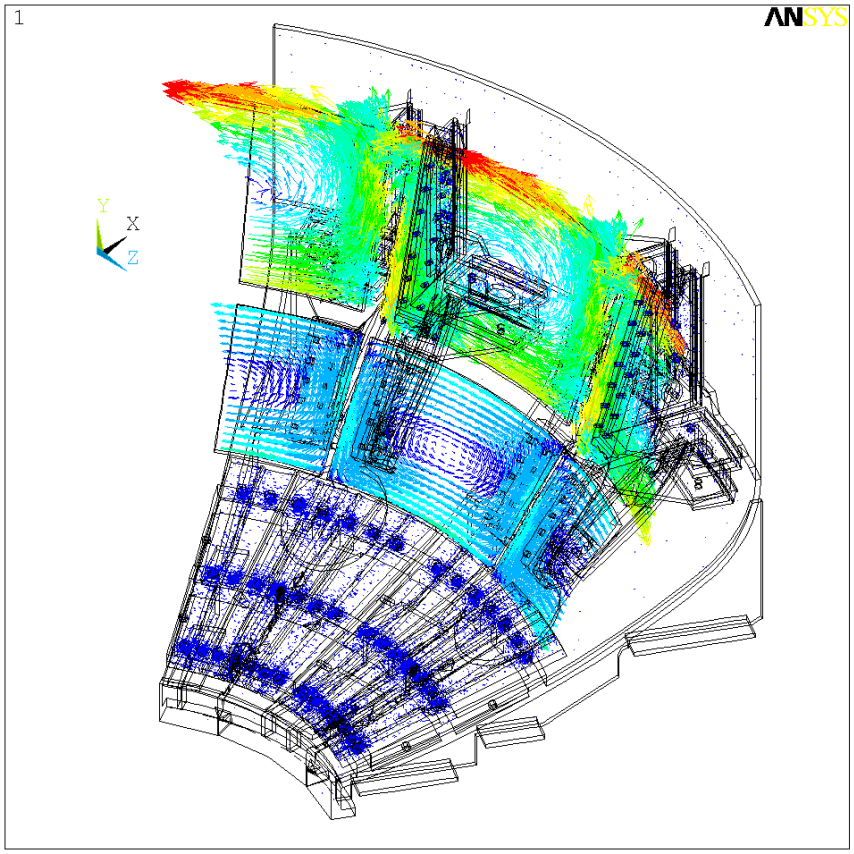

Figure 9.2.2-3

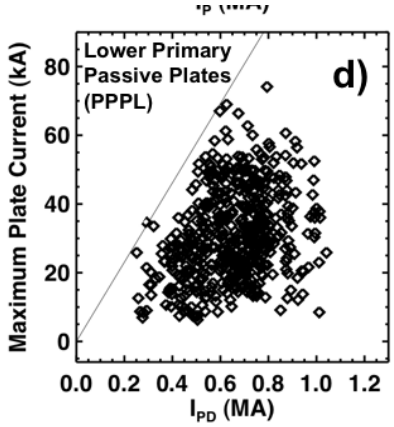

Figure 9.2.2-4 Figure from [3]

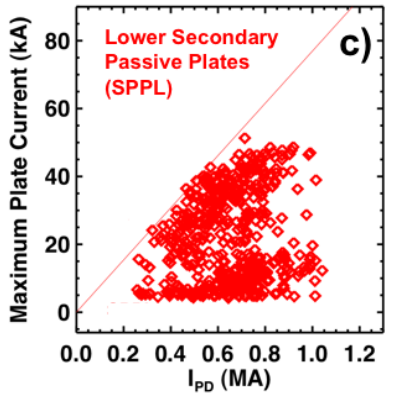

Figure 9.2.2-5 Figure 12 in Ref [3]

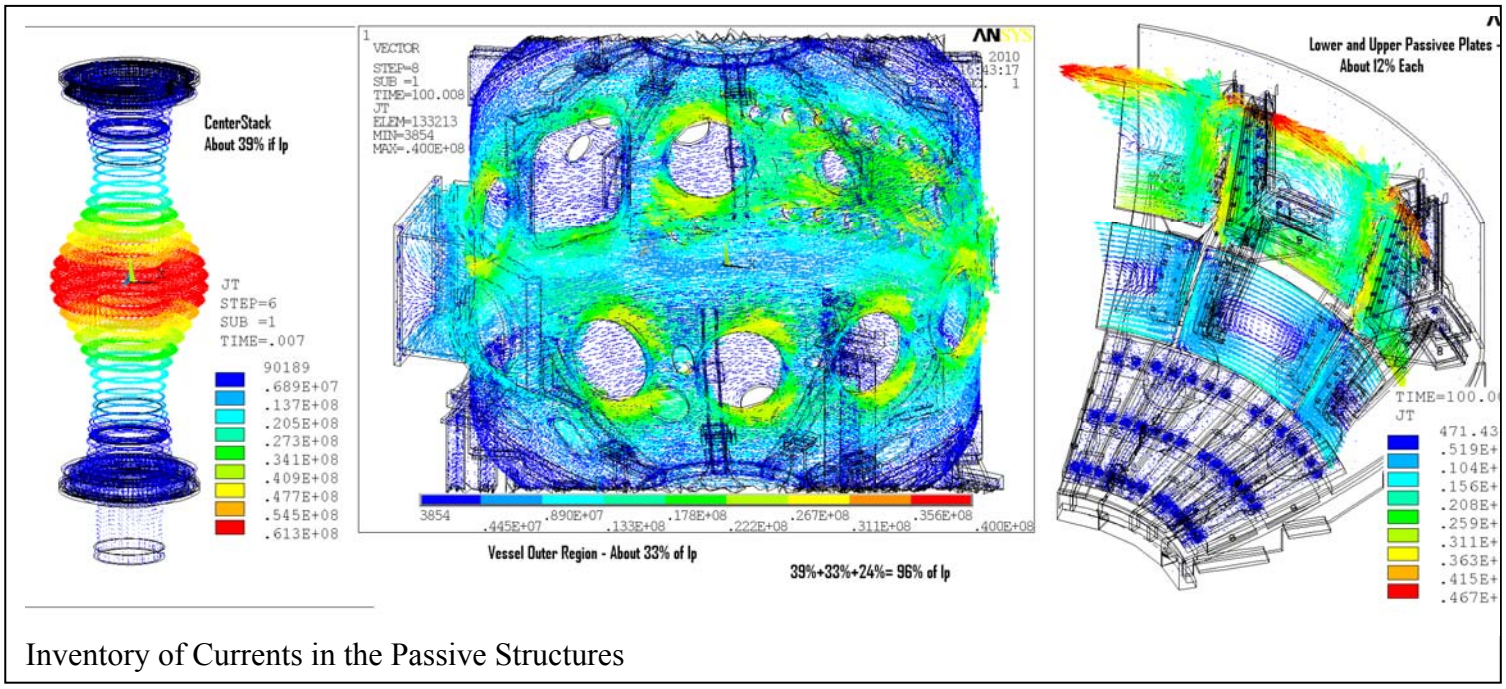

Figure 9.2.2-6 Inventory of Currents in the Passive Structures

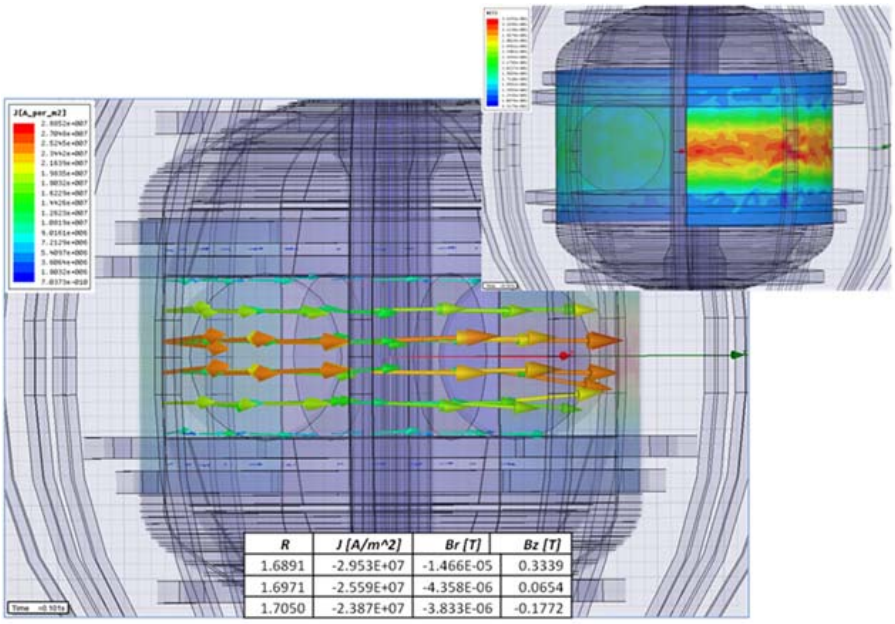

Figure 9.2.2-7 Maxwell and OPERA Mid-Plane Disruption Current Densities

9.3 Slow Plasma Translations

Slow VDE's sound less severe than quenchs. These are characterized by a translation from the mid-plane to another location. for the most significant of these with respect to the passive plates, the final position at a passive plate. The function of the passive plate is to resist this motion by developing counter currents which "push back" on the plasma. These forces are compressive i.e. push the passive plates back against the vessel. Consequently the tensile loads on the attachments should not be challenged.

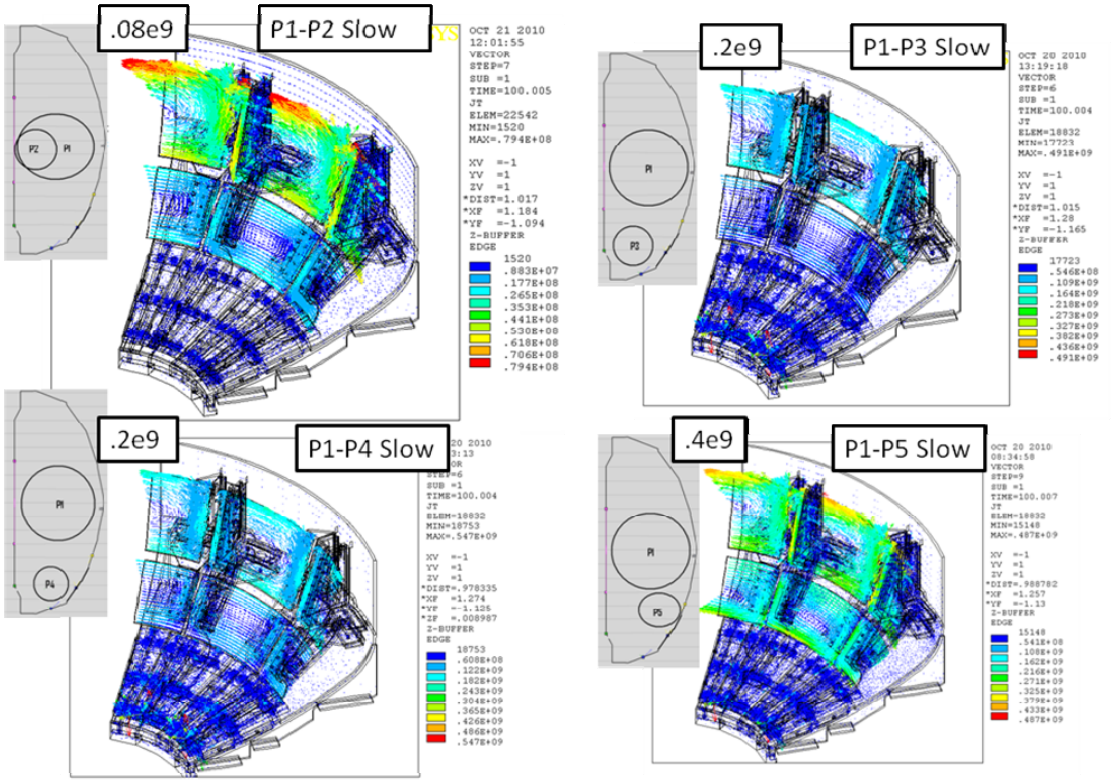

Figure 9.3-1 Comparison of Slow Translation Disruptions

9.3.1 P1-P2 Radial Slow Translation

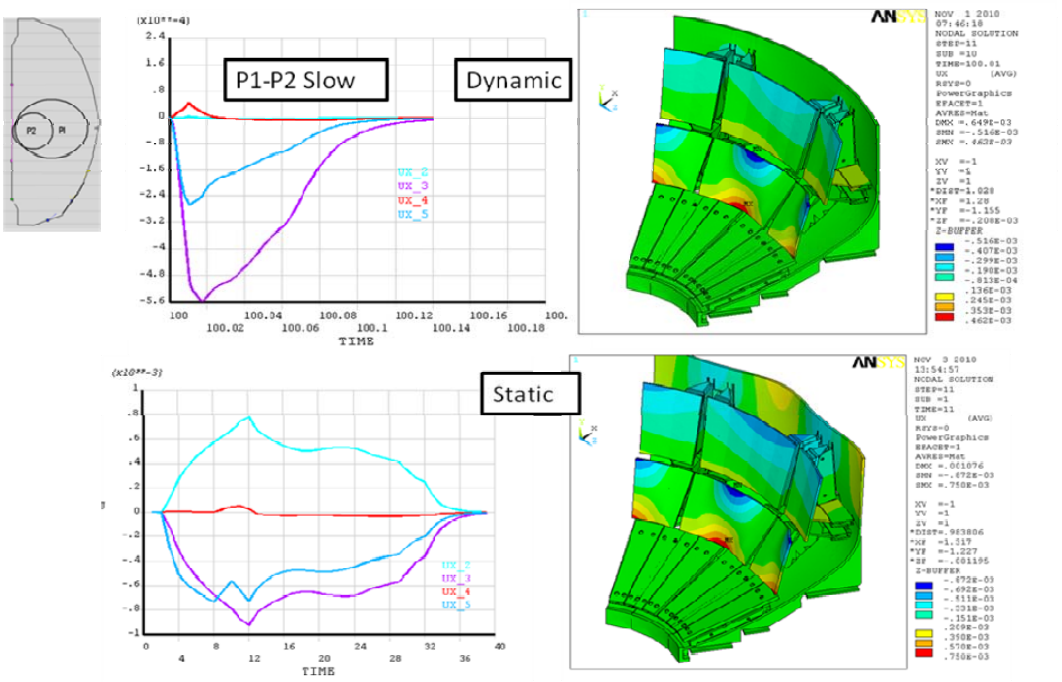

9.3-2 P1-P3 Slow

9.3.3 P1-P4 Slow

From figure 7.3.2, for loading of the secondary passive plate, .the following background fields would be appropriate: Bz=-.5, Br=.18. In the figure below, the fields are the total fields after the slow translation to P4. There are significant toroidal and poloidal fields in the secondary passive plates.

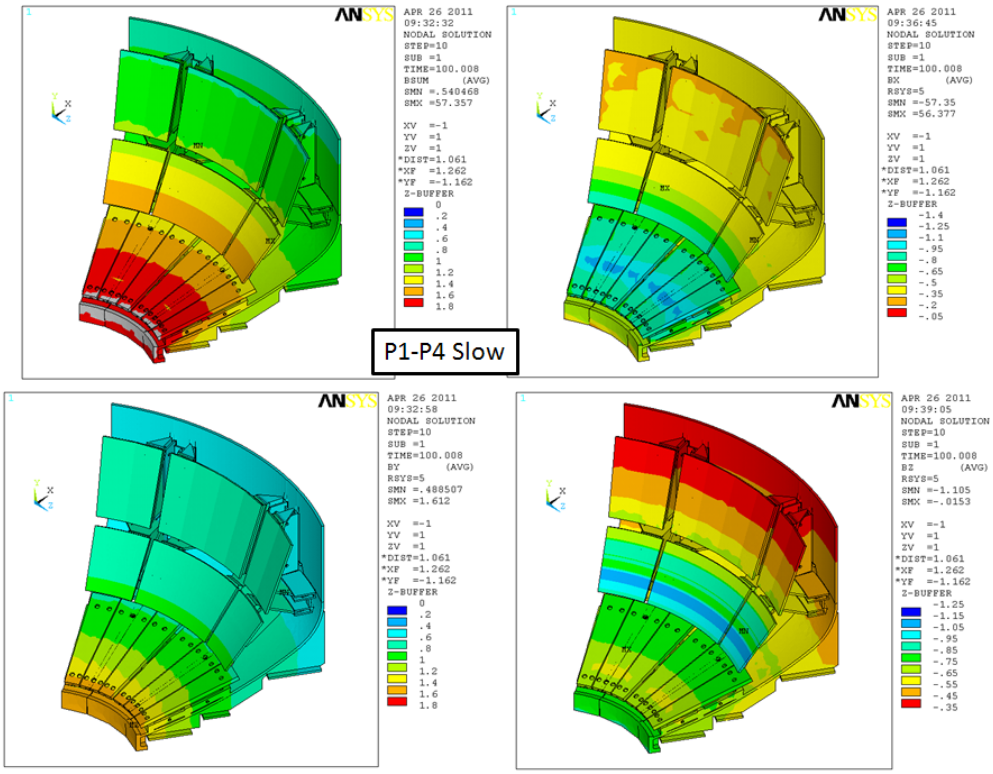

Figure 9.3.3-1 Field Plots at t=10 millisec, at completion of translation, P1-P4 Slow

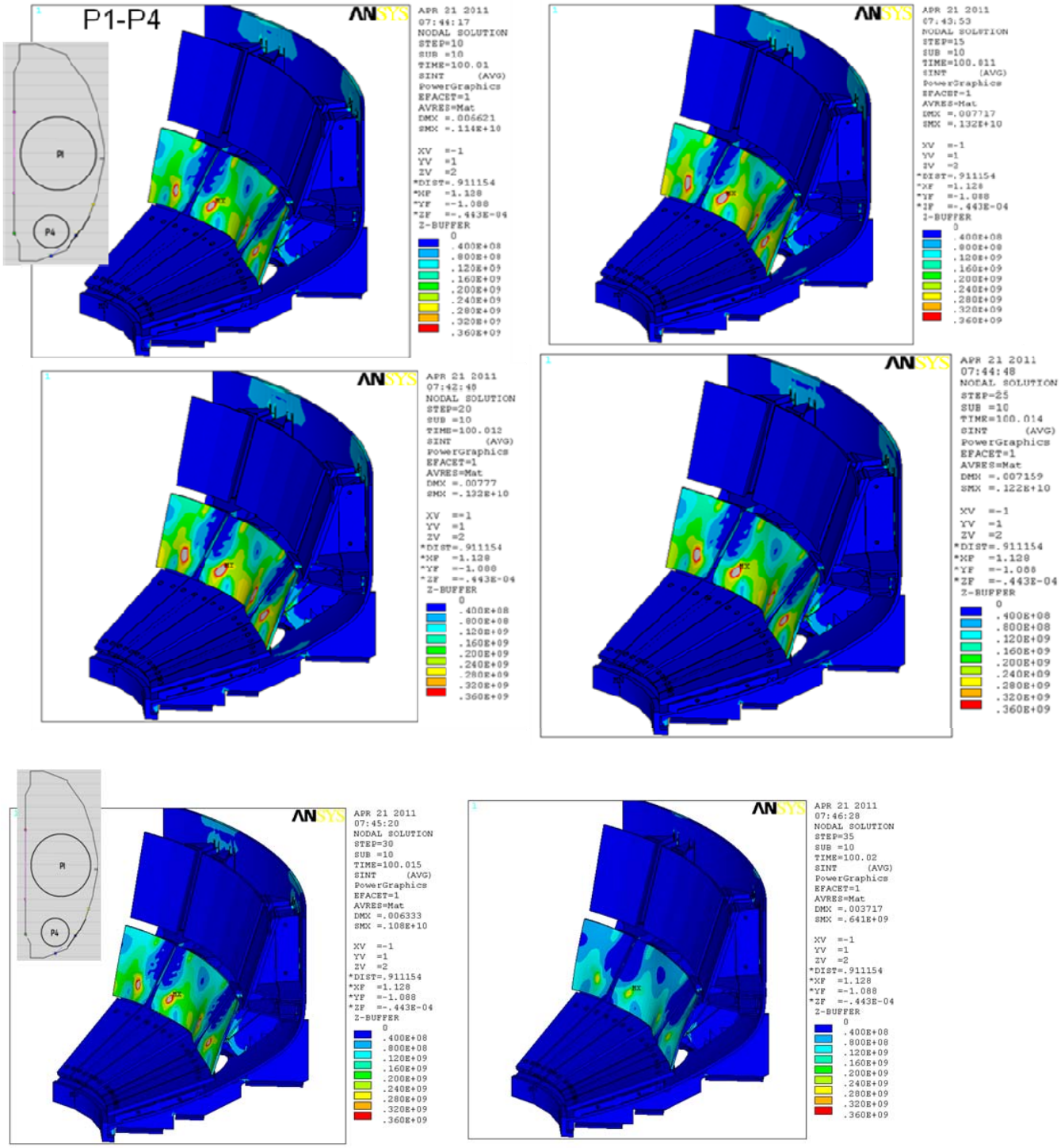

Figure 9.3.3-2 Tresca Stress from the Dynamic Solution, P1-P4 Slow

9.3.4 P1- P5 Slow

From figure 7.3.2, the following background fields would be appropriate: Bz=-.5, Br=.18 for loading of the secondary passive plate.

In July of 2011, a wedge of elements was run with the P1-P5 Slow Vector Potential data. The TF fields and background fields were turned off. The resulting field plots were generated:

P1 to P5 Slow BSUM Time History ½ inch PP

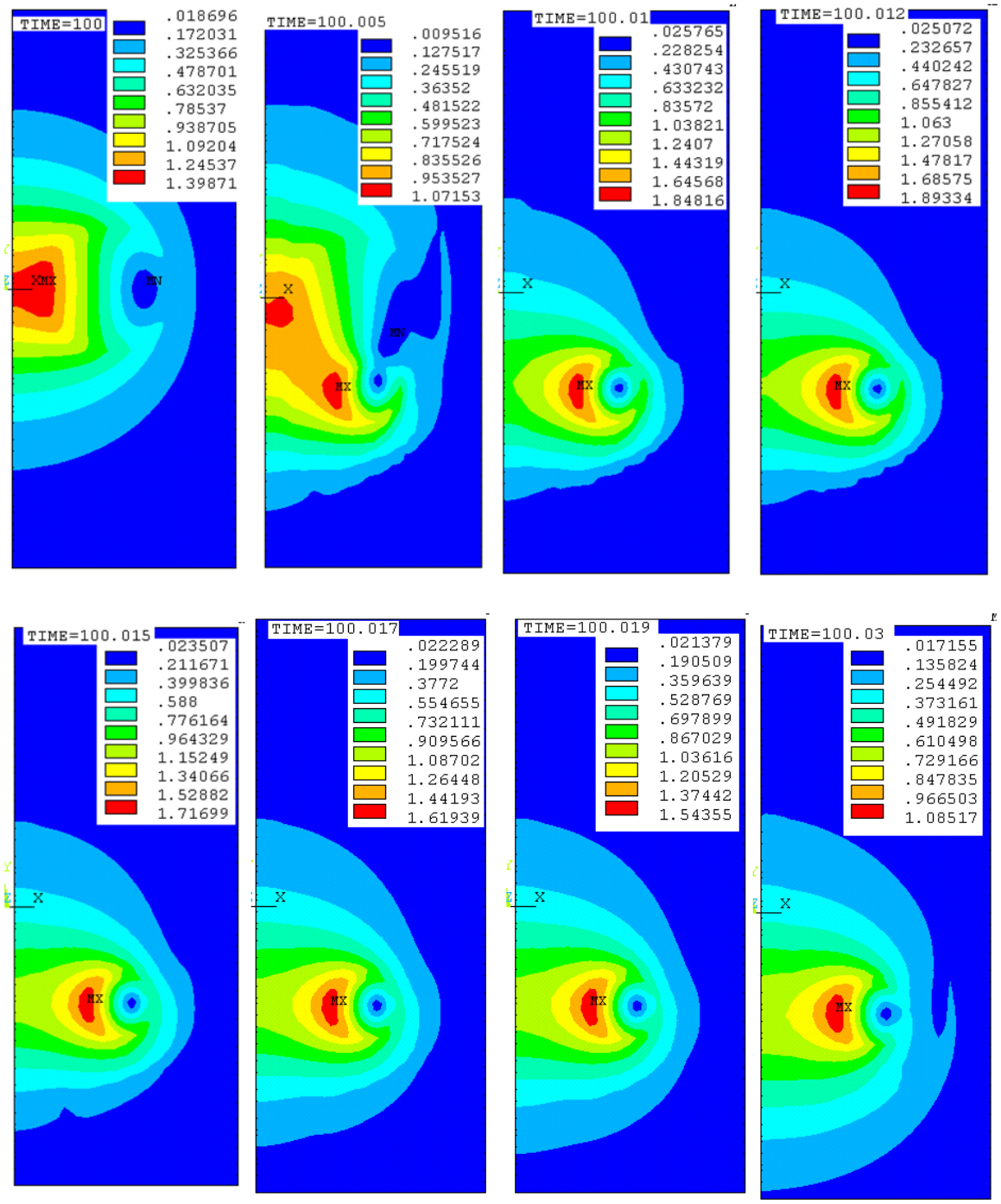

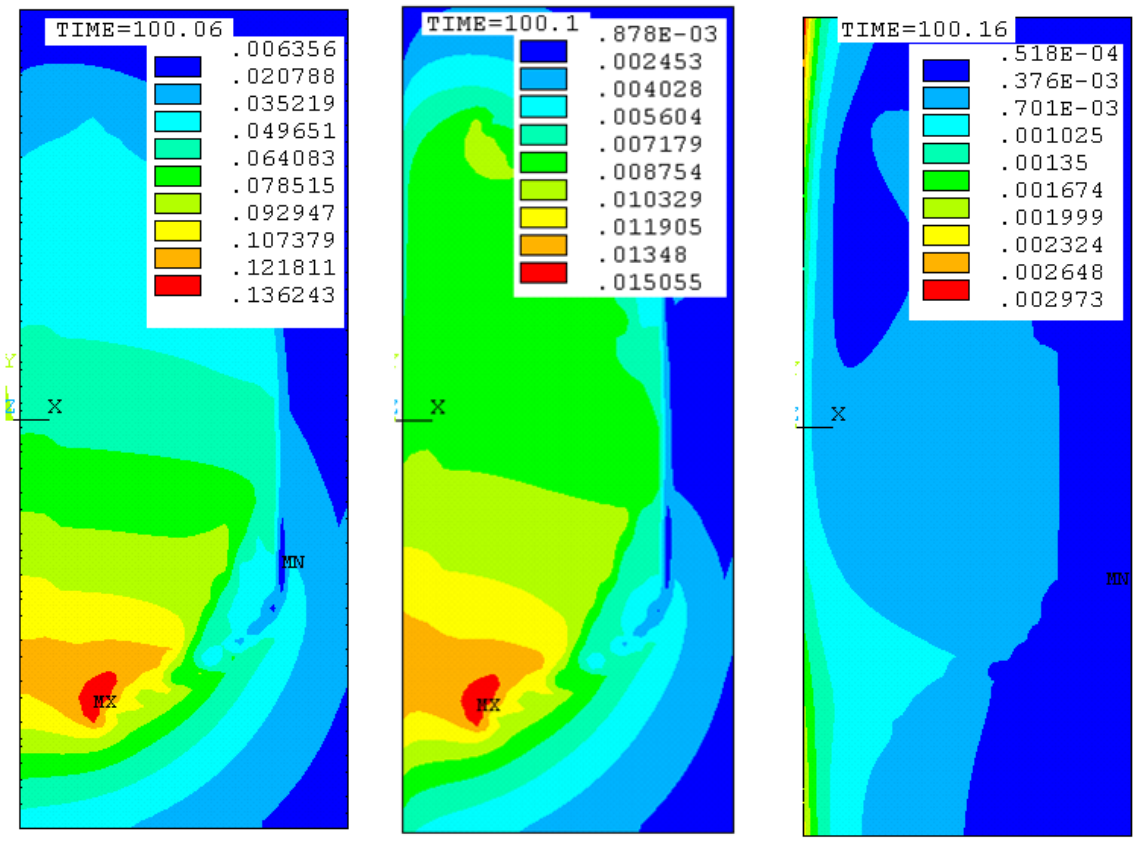

In these plots there are no inflection points or other indications of the presence of the passive plates.

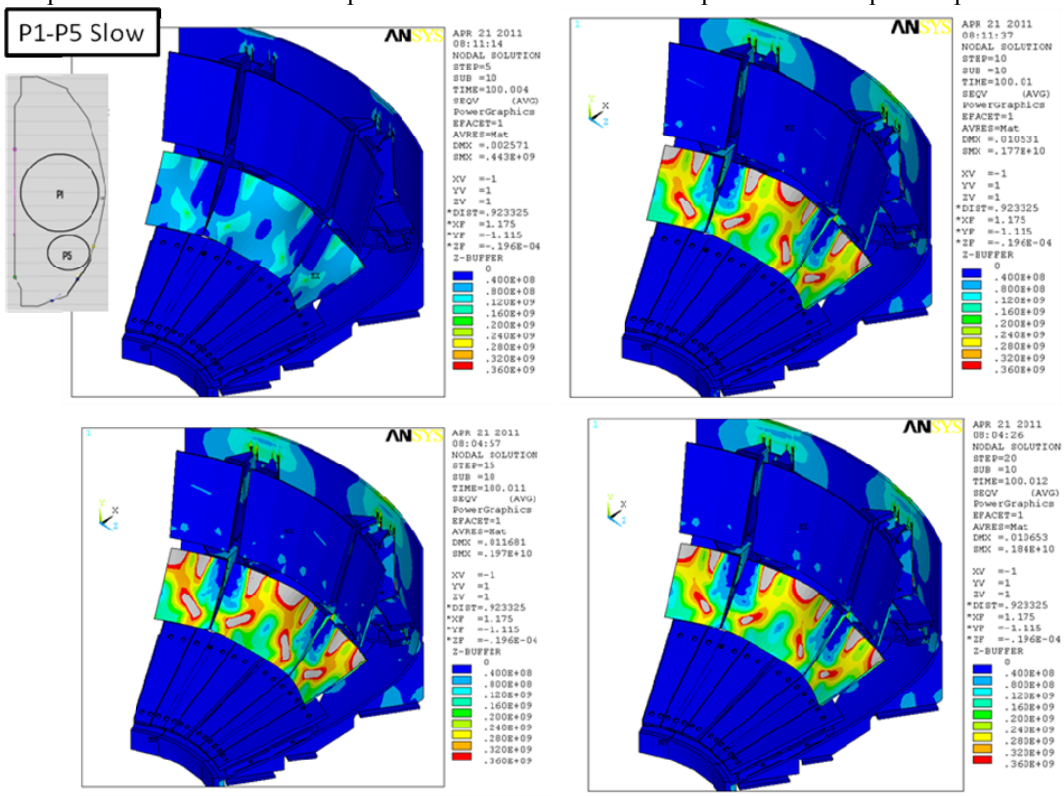

Figure 9.3.4-1 Tresca Stress from the Dynamic Analysis, P1-P5 Slow

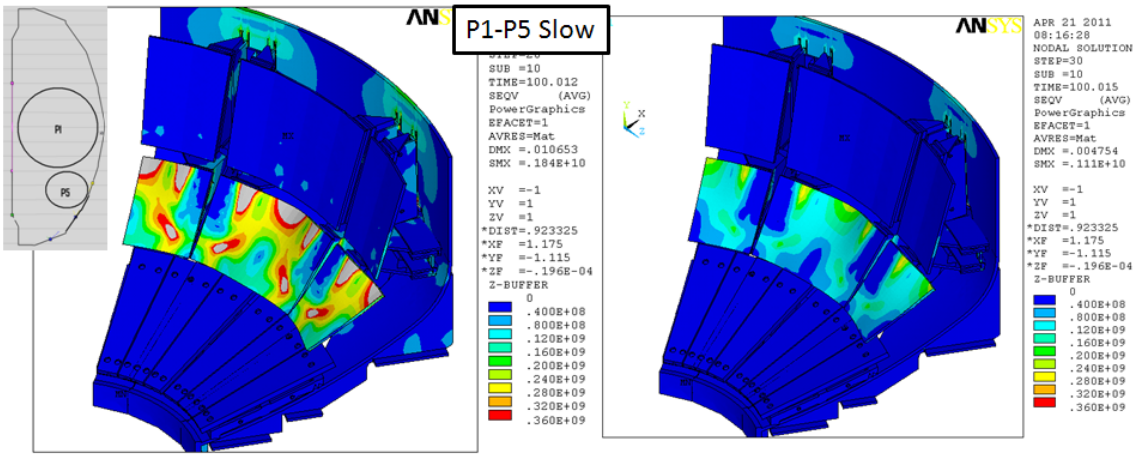

Figure 9.3.4-2 Tresca Stress from the Dynamic Analysis, P1-P5 Slow

The static analysis of the P1-P5 disruption with a slow quench was run. The resulrtsthe big difference I see is that the stresses in the secondary plate are much higher than the primary. So, I am extremely interested in seeing your results for the secondary plate. -Peter

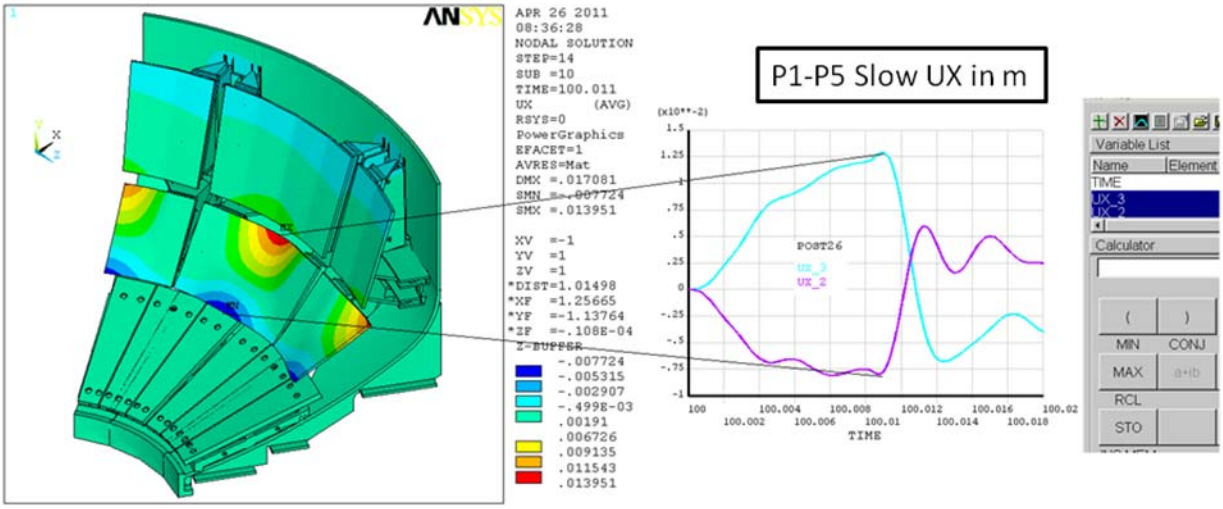

Figure 9.3.4-3 Radial Displacement from the Dynamic Analysis, P1-P5 Slow

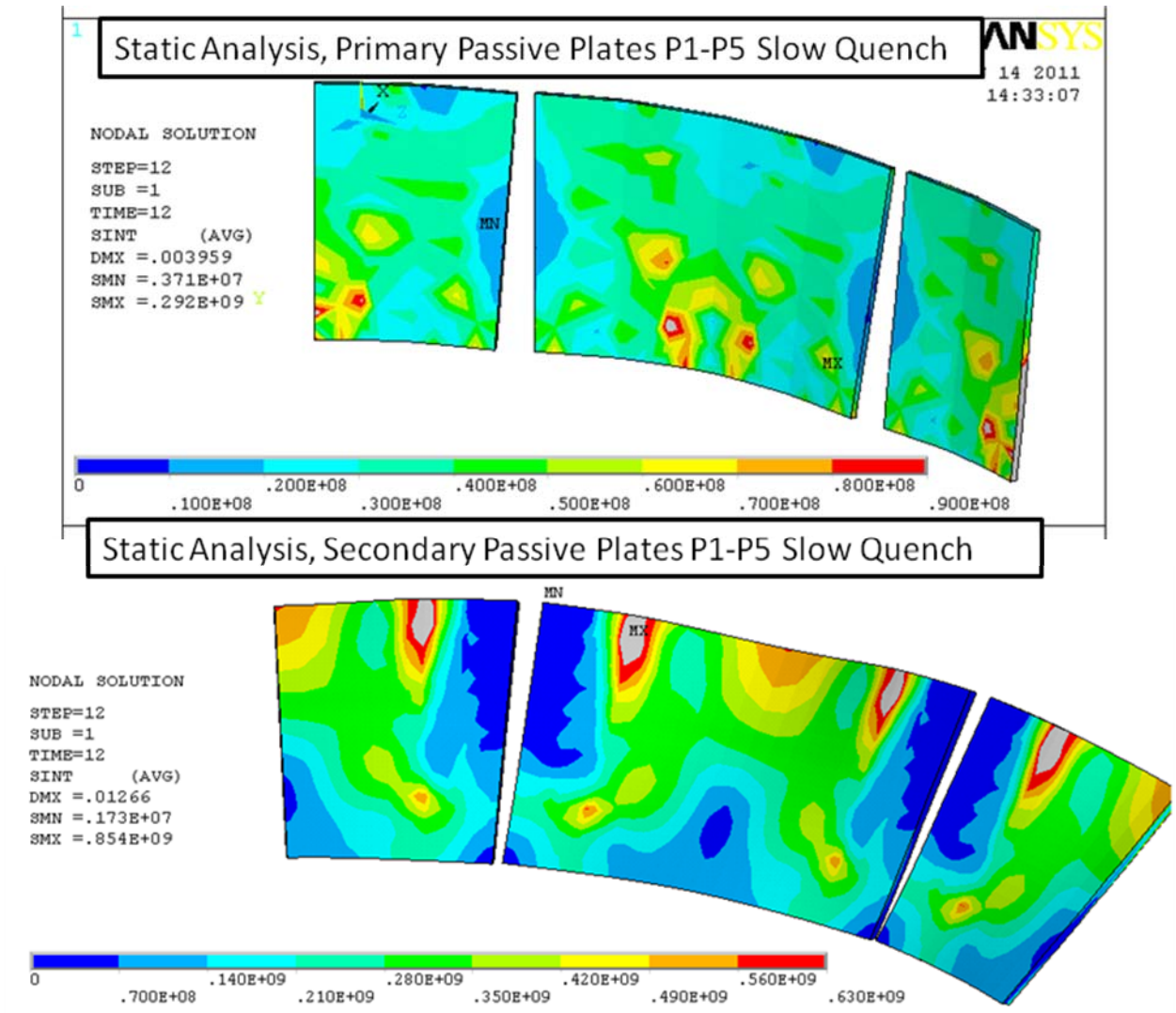

Figure 9.3.4-4 Stress from the Static Analysis, P1-P5 Slow

9.4 VDE to Plasma 4 Then Quench

This disruption simulation was expected to produce the largest loads on the lower passive plates and divertor, but it is not quite as severe as the slow translations.

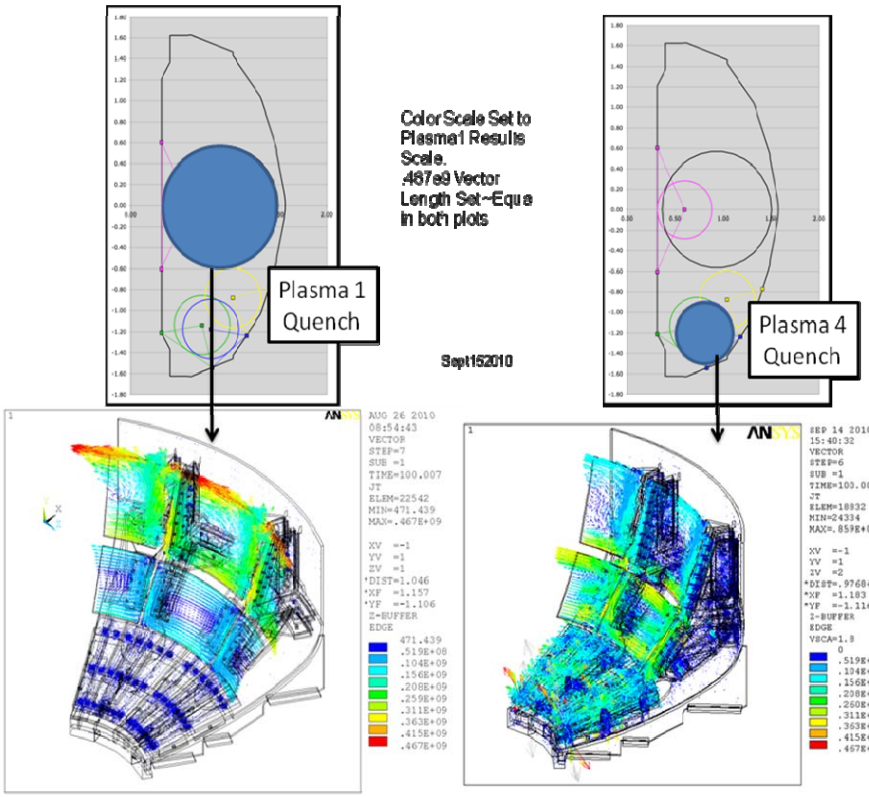

Figure 9.4.1 Comparison of Plasma 1 and Plasma 4 Quenches

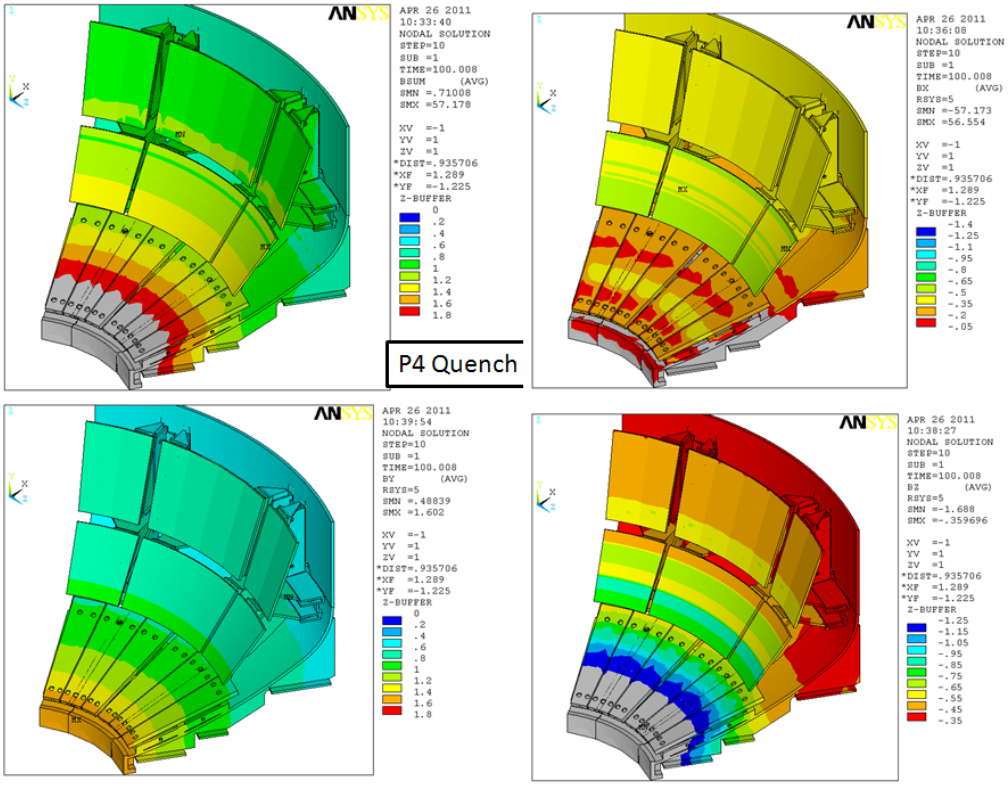

Figure 9.4.2 Field Components for the Plasma 4 Quench

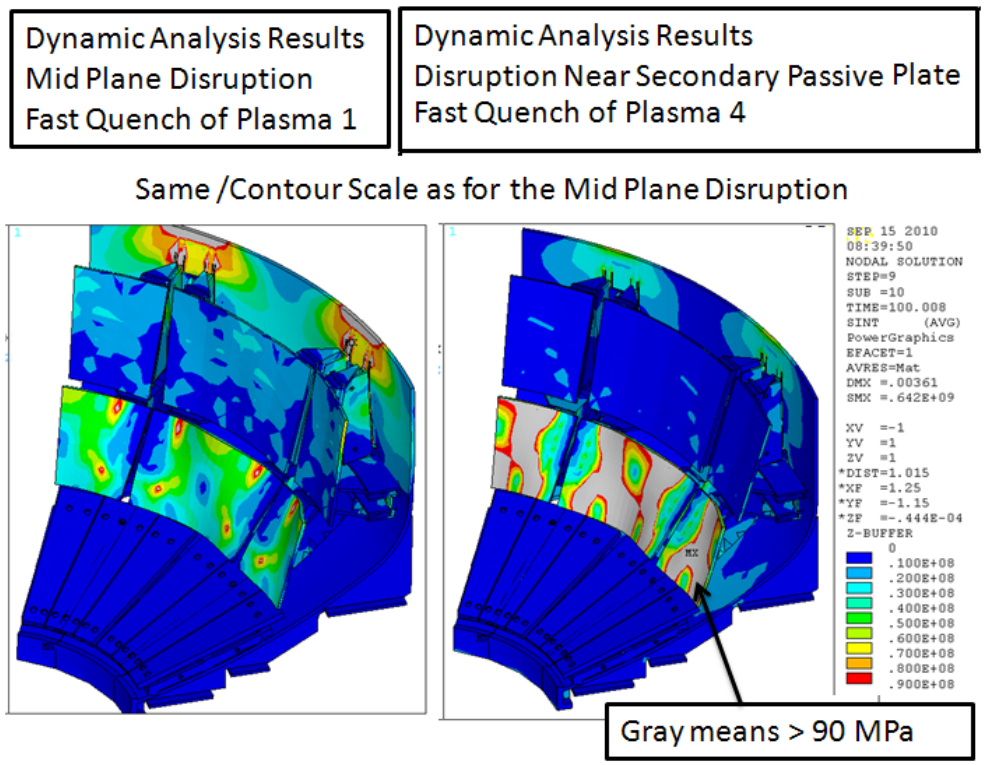

Figure 9.4.3 Comparison of Plasma 1 and Plasma 4 Dynamic Analysis Results

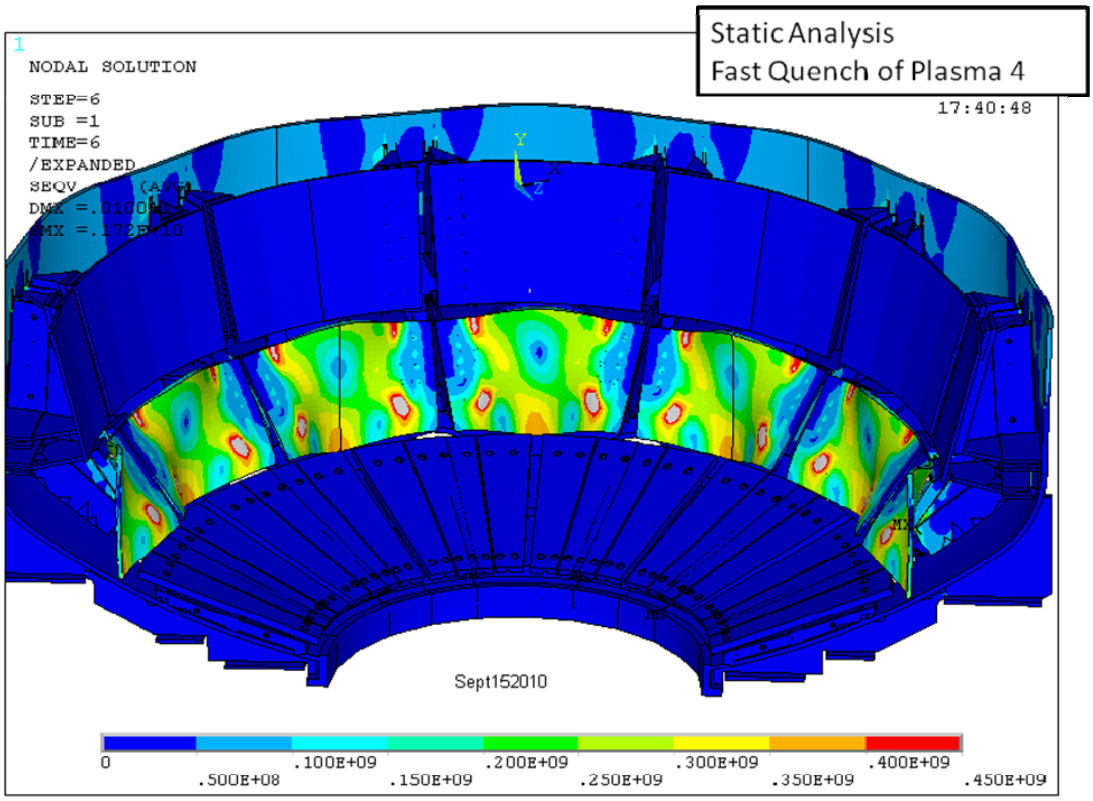

Figure 9.4-4 Static Analysis Results of the Plasma 4 Quench

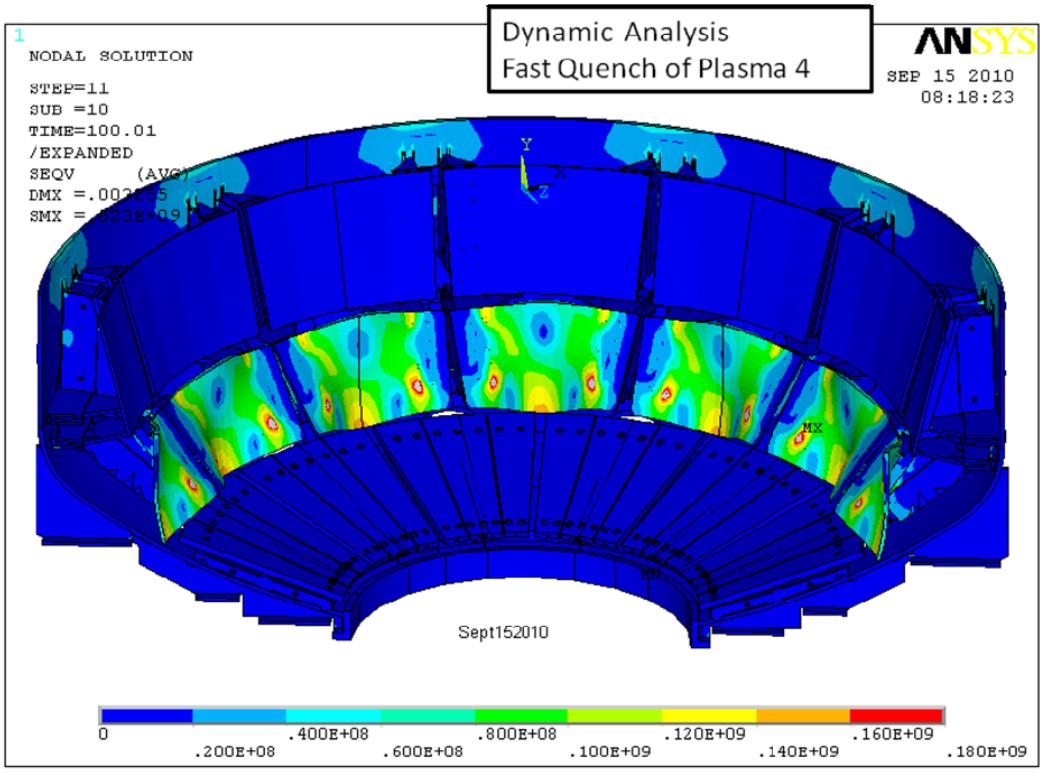

Figure 9.4-5 Dynamic Analysis Results of the Plasma 4 Quench

9.5 Bolting Analysis

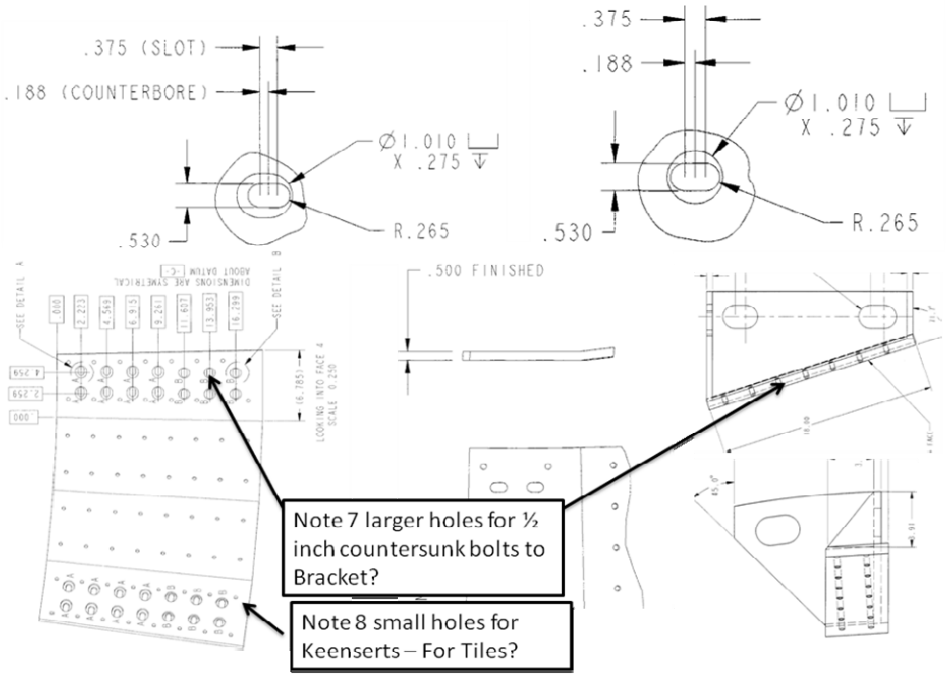

KEENSERT #KNHL420J	STN STL
PRIMARY PASSIVE PLATE	CDA 18150 COPPER
NOMENCLATURE OR DESCRIPTION	MATERIAL

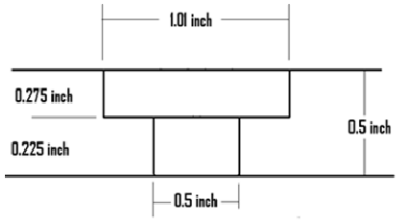

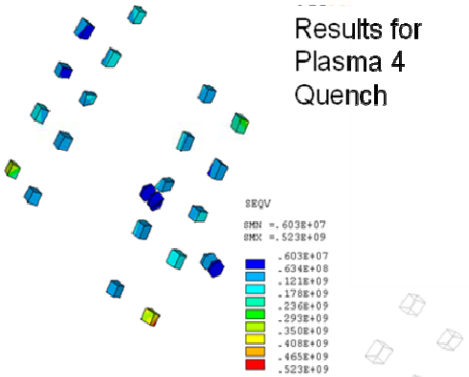

350e6*.01187*.0128*.2248=11954 lbs

Stress Area of a ½ inch bolt is .1416 in^2

Stress in worst corner bolt in the array=84.423psi

Shear Stress in Passive Plate Counterbore:
=11954/(1.01*pi*.225) = 16744 psi
Equivalent Tresca = 33488 psi = 231 MPa

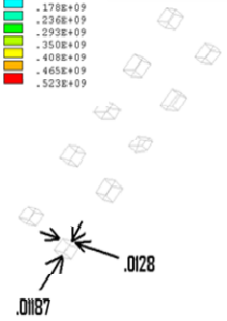

Tensile Property CuCrZr

Material	Yield (Mpa)	UTS(MPa)
Low strength (L)	78	248
Intermediate strength (I)	199.4	318.6
High strength (H)	297	405.3

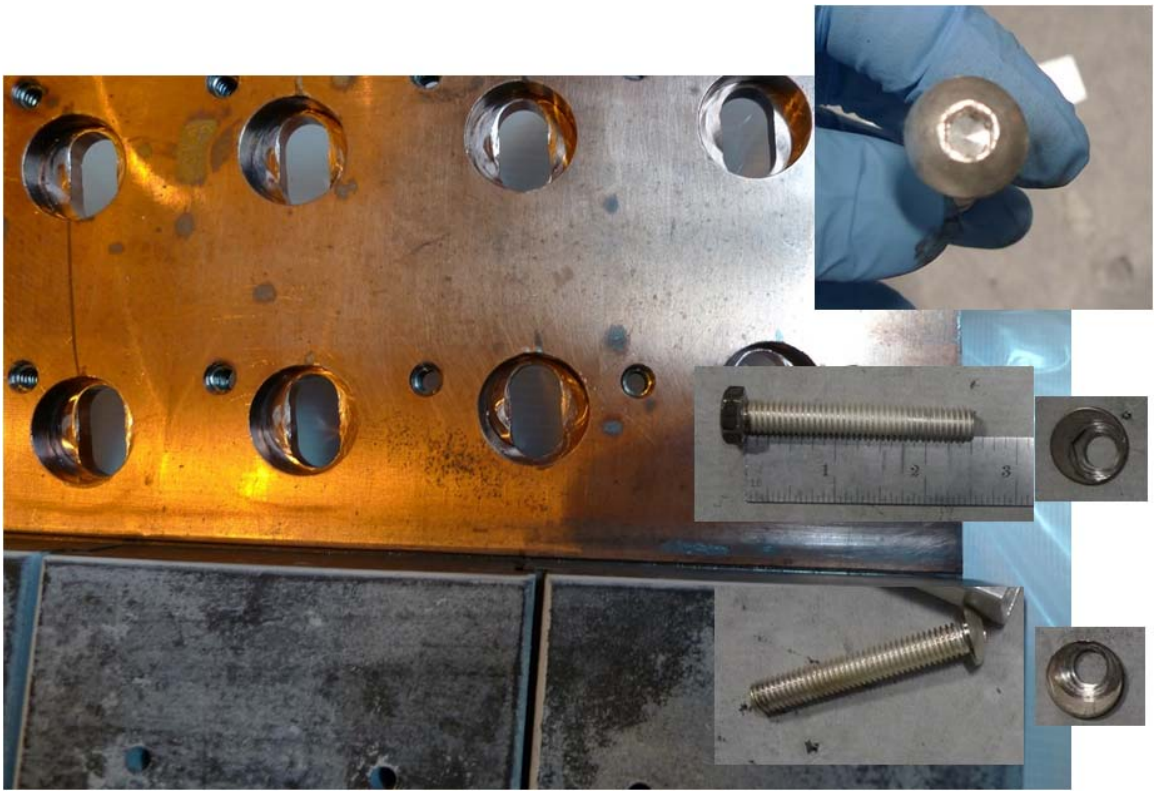

The passive Plates are made of CuCr1Zr UNS.C18150. Chromium Zirconium Copper C18150 is a copper alloy with high electrical conductivity, hardness, and ductility, moderate strength, and excellent resistance to softening at elevated temperatures. The addition of 0.1% zirconium (Zr) and 1.0% chromium (Cr) to copper results in a heat treatable alloy which may be solution treated and subsequently aged to produce these desirable properties.
NSTX Bake-out temperature is 350 degrees C. The softening temperature of properly heat treated C18150 rod exceeds 500°C as compared to unalloyed pure copper which softens at 200°C, and silver bearing coppers which soften at 350°C.

Copper Cr Zr Properties from ref [4]

Material	Yield strength (MPa)	UTS (MPa)	Average over
Low strength (L)	78	248	3
Intermediate strength (I)	199.4	318.6	3
High strength (H)	297	405.3	5

Ref 1, the original NSTX Passive Plate Calculation has slightly lower properties for CuCrZr

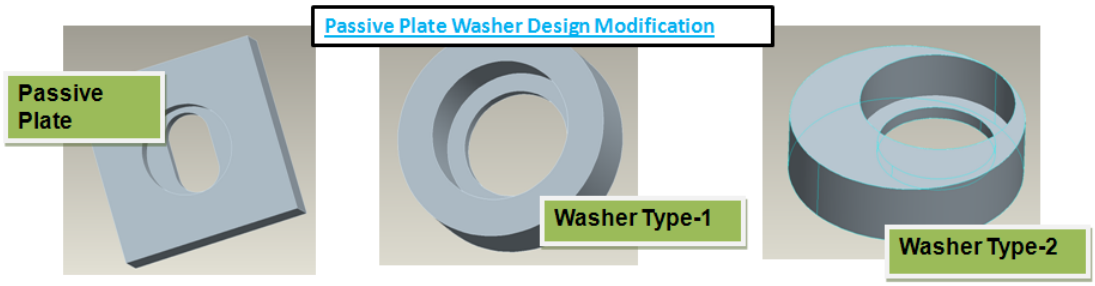

Washer Type-3

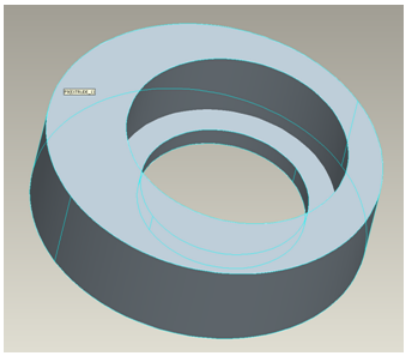

Stepped Geometry Needed at Lease for the Corner Washers. –The Passive Plate Would need to be Counter-bored with the step

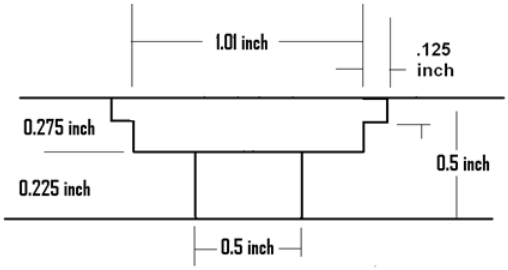

Estimate of 5/8 bolt shear load

Each bracket has 12 bolts, each in double shear, shear area =.306in^2
700000 amp halo current*.8m poloidally across the face of the PP *1Tesla toroidal field*1.5 peaking factor/12brackets/12bolts per bracket/2shear planes per bolt = shear load per shear area = 2916N = 655 lbs or 2142 psi shear or 4.2 ksi Tresca

Passive Plate 5/8 bolt Shear Stress Estimate for Halo Loads

- **Estimate of 5/8 bolt shear load**
-
- **Each bracket has 12 bolts, each in double shear, shear area =.306in^2**
-
- **700000 amp halo current*.8m poloidally across the face of the PP *1Tesla toroidal field*1.5 peaking factor /12brackets /12bolts per bracket / 2 shear planes per bolt = shear load per shear area = 2916N = 655 lbs or 2142 psi shear or 4.2 ksi Tresca**

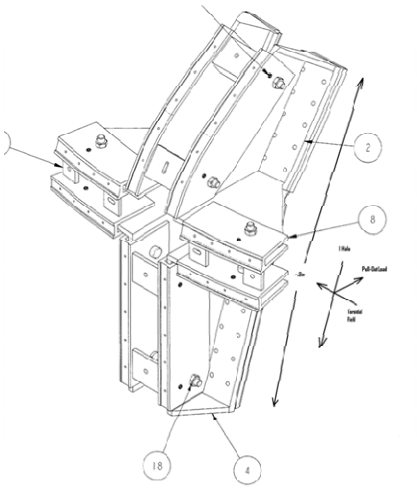

17

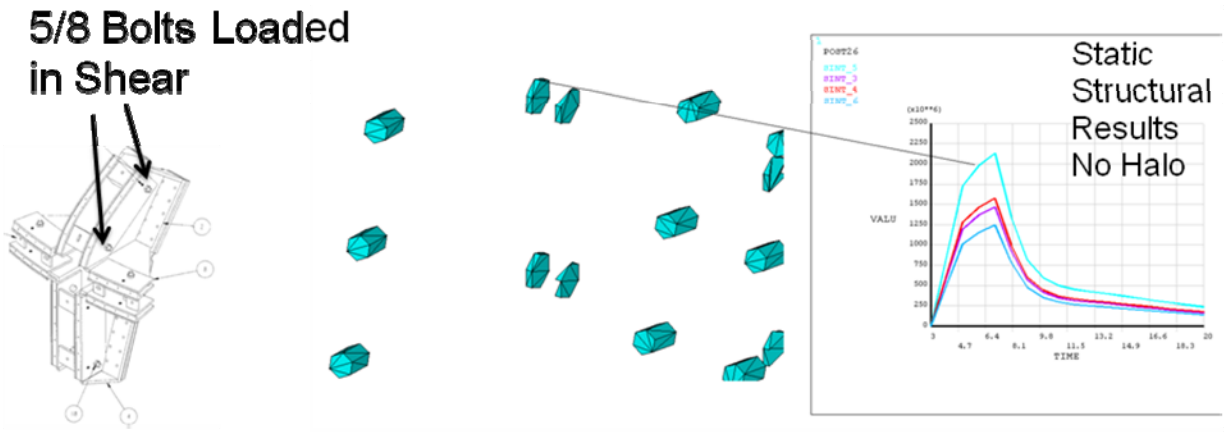

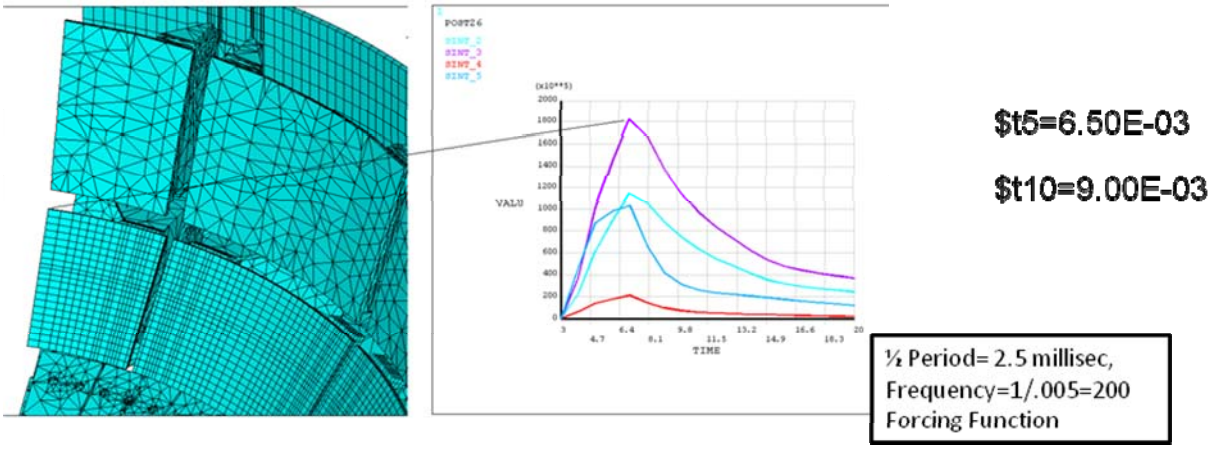

9.6 Bracket Welds

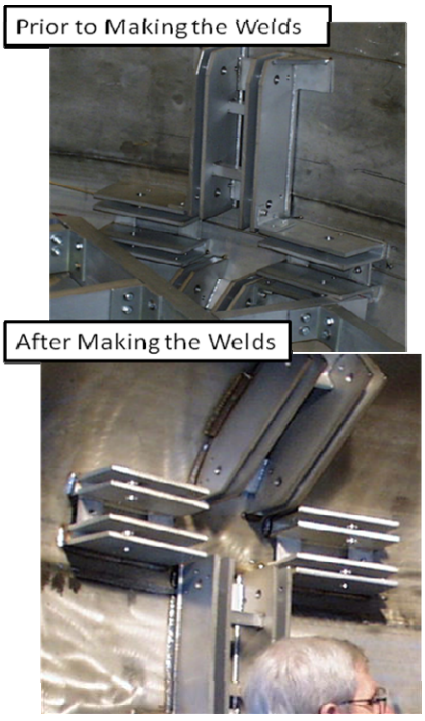

Bracket Welds

From Attachment F
Passive Plate Bracket Weld
QA Report

From J Boscoe To E Perry

Re: Welding of Vertical Straight (1053) and Vertical Curved Support Brackets (1055)

Because of fit-up - assembly gap issues on the above mentioned components & instructions (verbal) were given per Chrzanowski/Berner to use ¼" thick x ½" wide bridge-transition pieces to overcome these gaps. Due to worries about excessive installation time it was decided that doubling up on weld size ⅜" fillet to ¾" fillet would decrease required weld length by ½ or an increase of weld size from ⅜" fillet to ⅝" fillet would decrease the required weld length by ⅓. Welder - Tig torch accessibility for full length welds up both sides of pieces was also a factor in this decision. The design drawing - weld detail in question is EDB-1051. I believe it was intended for CR 70 to cover this (along with many other modifications - tweaking to original design). This change did not get included on CR 70.

In addition I noticed on inspection of the lower support-brackets that the unwelded portions of the vertical curved brackets #1055 ("bobsleds") are the ⅓ of length including the curved sections. My most recent concern was the remote possibility that this could adversely affect stress calculations

9.7 Frequency Analysis of the Passive Plate Model

The need of performing a modal analysis is reduced by the ability to run full dynamic analyses of the vessel and internal components. In this section, the results of modal analyses of the passive plates with a section of the vessel are presented for the purpose of aiding in the evaluation of the dynamic load factors that result from the dynamic analysis.

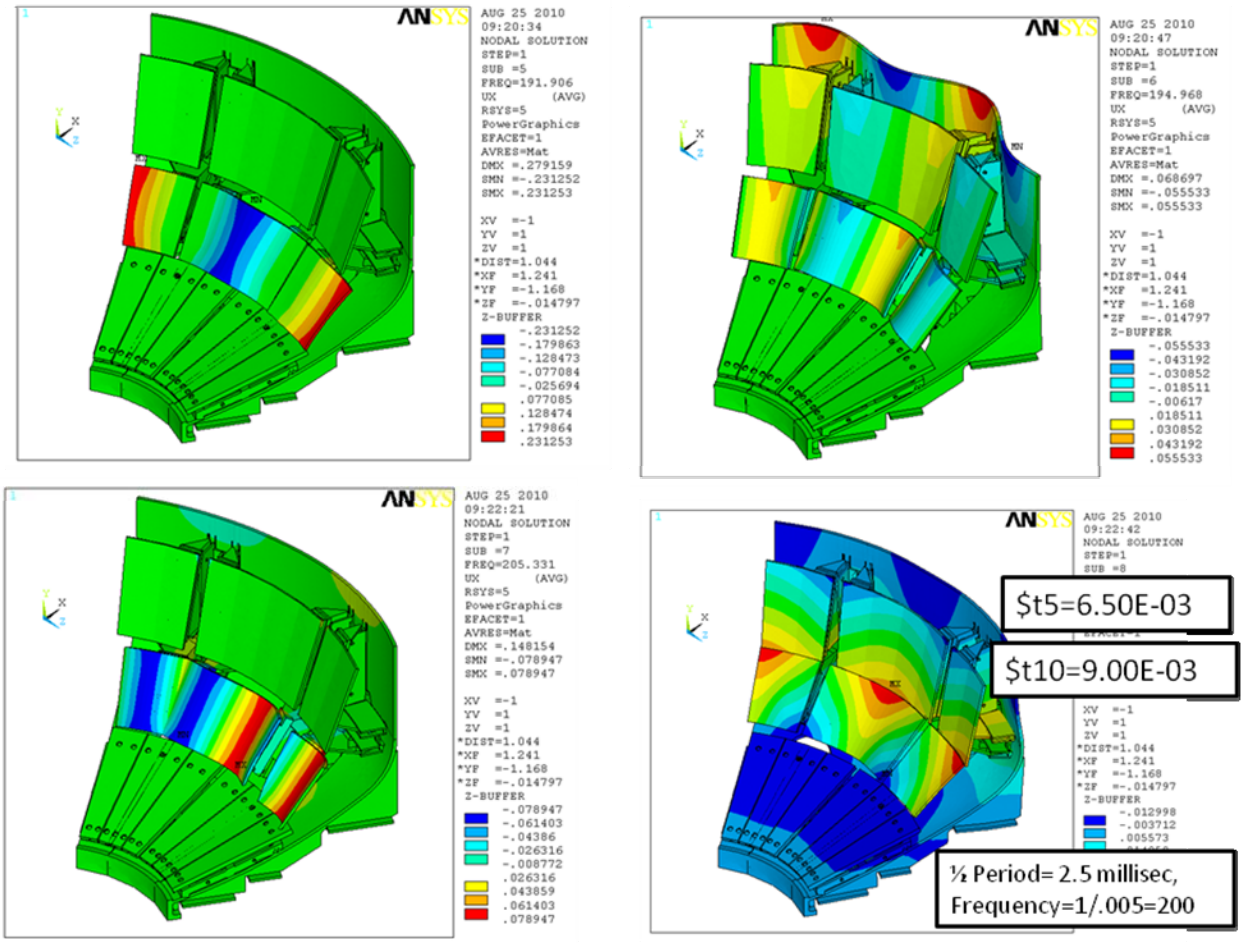

Figure 9.7.1 Frequencies of the Passive Plates: 191.9, 194.97, 205.33, 206.3

The disruption event for the fast quench is 9-6.5 milliseconds or 2.5 milliseconds. This is considered half a period thus the forcing function frequency is 1/.005 = 200 hz. The passive plate frequencies are in the range of the disruption excitation frequency. From this, it would be expected that the dynamic load factors would be greater than one.

Amplification factor, or DLF – Single degree of freedom oscillator with a "truncated" harmonic forcing function. Half a wavelength, or a load pulse of half a period would give a peak DLF of ~1.7 - if the frequency ratio is uncertain. For a high frequency pulsed load acting on a low frequency structure, the dynamic amplification factor is less than one.

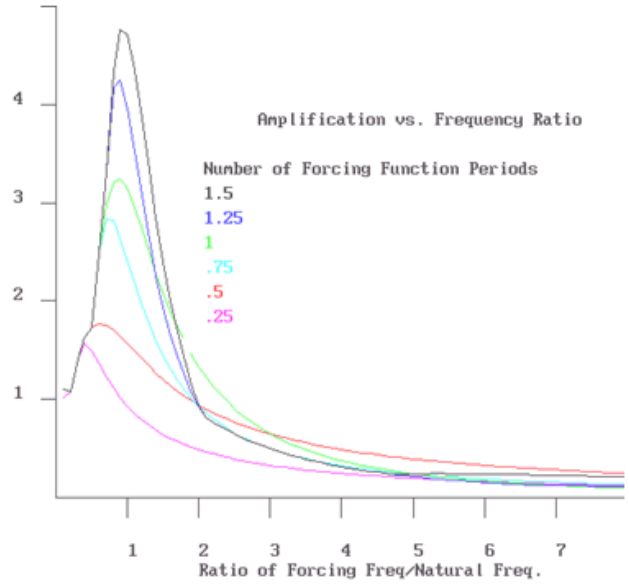

Figure 9.7.2 Response of a single Degree of Freedom oscillator to Partial Periods of Excitation

Ron Hatcher indicated in an email that all his fast quenches are 2 milliseconds

11.0 Centerstack Casing Analysis

11.1 Drawing Excerpts

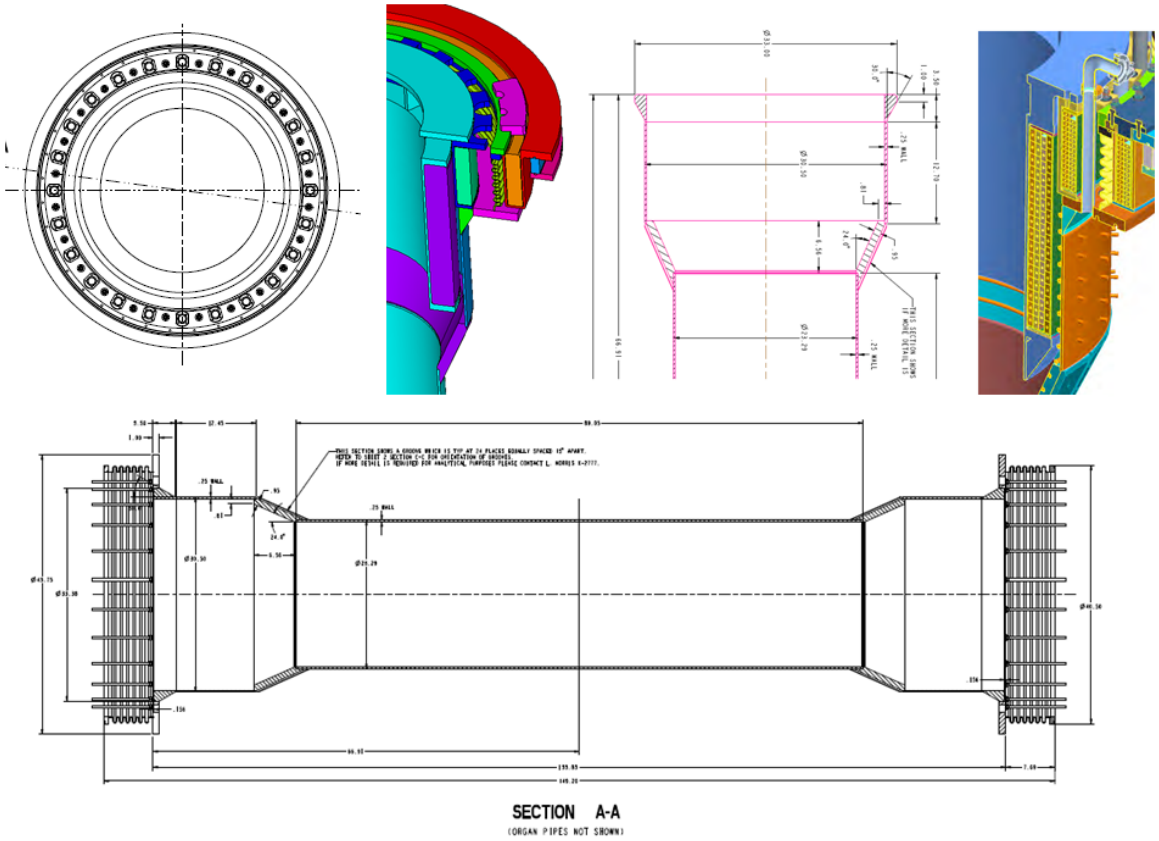

11.2 Inductively Driven Currents and Resulting Forces

Disruption analyses were performed on the centerstack casing using the procedures outlined in this calculation. Inductive eddy current loads have minimal effect on the casing because toroidal currents are induced. These are parallel to the toroidal field which then does not contribute to the Lorentz Loads. Only the poloidal fields and the toroidal currents produce significant loads..

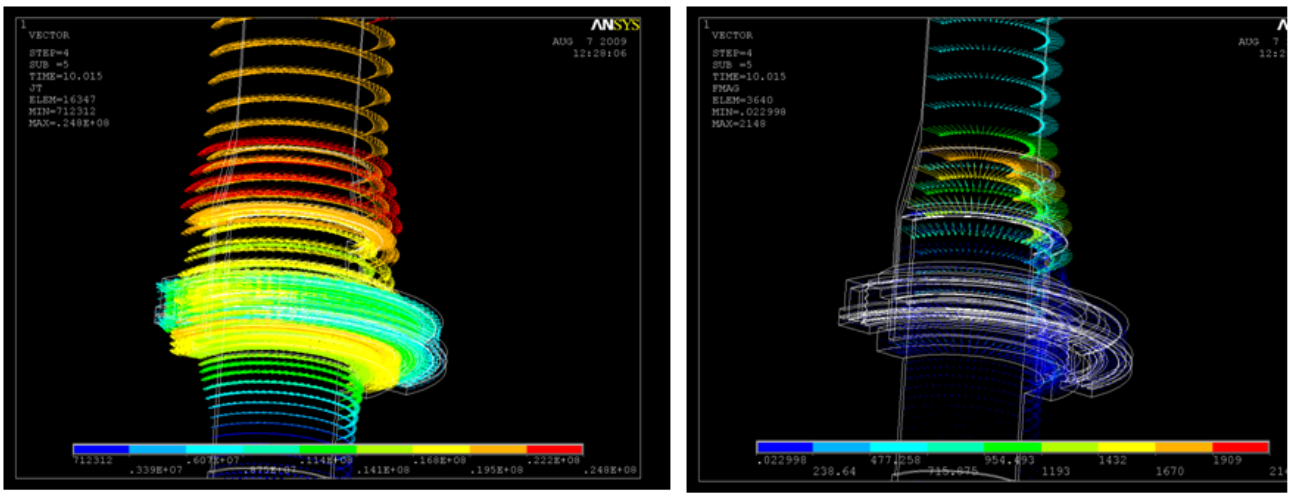

Inductively Driven Disruption Currents in the Casing Forces from Inductively Driven Disruption Currents

Figure 11.2-1 Inductively Currents and Forces from a Mid-Plane Disruption

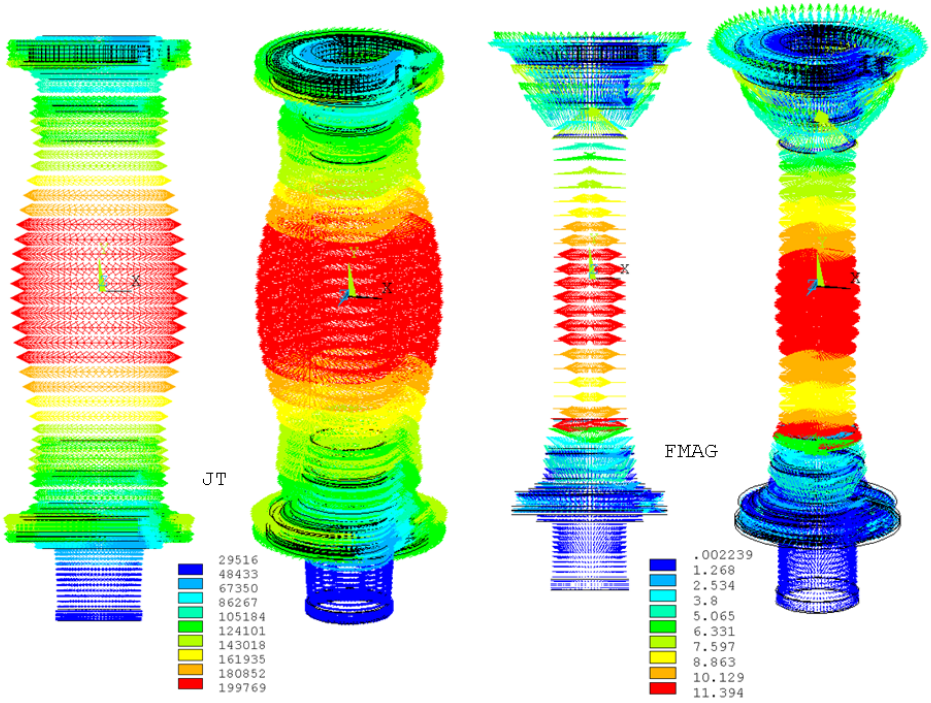

Figure 11.2-2 Inductively Currents and Forces from a Mid-Plane Disruption (April 2011)

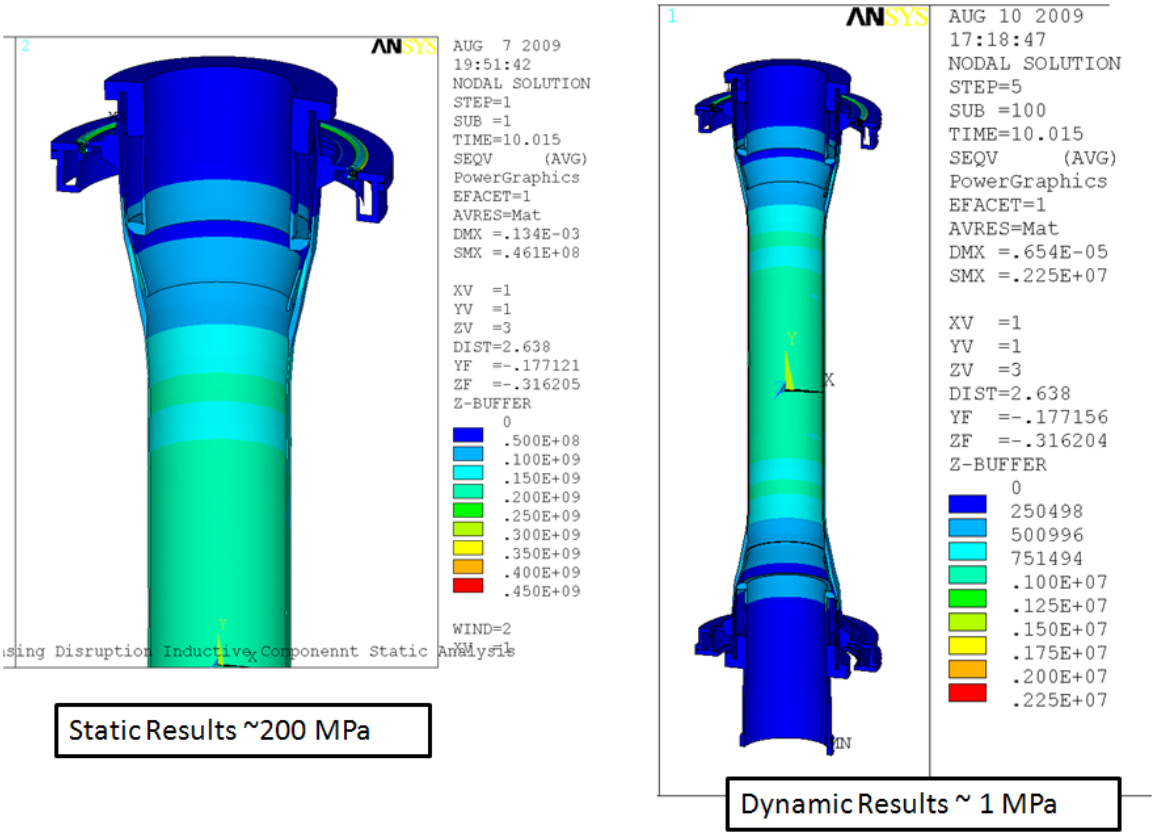

Figure 11.2-3 Stresses Due to Inductively Driven Currents and Forces from a Mid-Plane Disruption

11.3 Halo Currents and Resulting Forces

Halo currents have a large poloidal current component, are not axisymmetric, and potentially produce a large net lateral load. NSTX has some history regarding halo loads. .Neil Pomphrey and Jim Bialek studied the distribution of Halo Currents in NSTX [12]. Their understanding of the current re-distribution is that there is a resistive re-distribution of currents that minimizes the peaking factor or non axisymmetric loading over most of the height of the centerstack casing. . Art Brooks has studied the inductive component of the halo current derived from the poloidal inventory of current s in the plasma. Initially the peaking factor applies because inductive effects oppose resistive redistribution of the currents. In a short time, the currents redistribute resistively and reduce the peaking factor. This work is described in NSTX calculation " Halo Current Analysis of Center Stack" Calculation number NSTX-CALC--133-05-00-April 13, 2010 by Art Brooks [13]. Art Brooks' calculation is the calculation of record for Halo loading.

Halo loading was also investigated along with the inductively driven currents. The following spec is from the CDR Upgrade GRD:

Halo current [MA]	n.a	20%=	35%=	35%=	35%=
		400kA	700kA	700kA	700kA
Halo current entry point (r,z) [m]	n.a	0.3148	0.3148	0.8302	1.1813
		0.6041	-1.2081	-1.5441	-1.2348
Halo current exit point (r,z) [m]	n.a	0.3148	0.8302	1.1813	1.4105
		-0.6041	-1.5441	-1.2348	-0.7713

Addition of the halo currents was done in two ways. The first was to develop a cosine distribution of loads on the centerstack casing. These were then added to the Lorentz loads obtained from the inductively driven

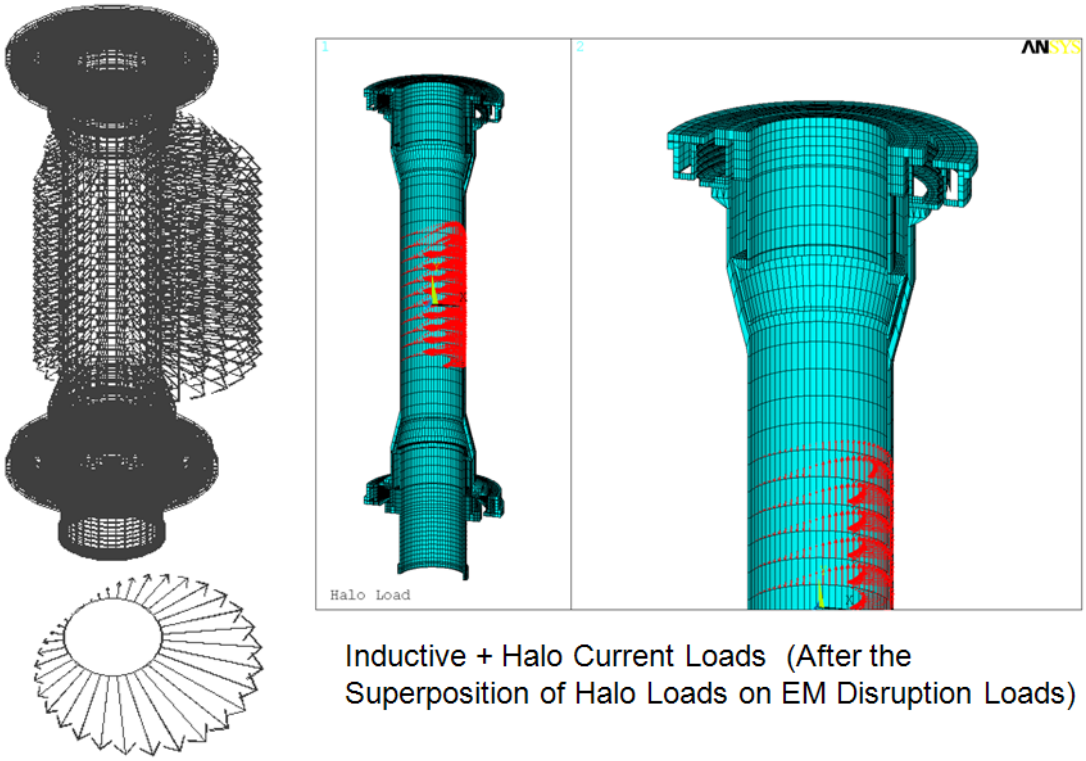

Figure 11.3-1 Disruption Forces, Including Halo Loads

currents/loads in the shell. Halo loads were calculated outside of ANSYS and read in after reading the inductive loads with the LDREAD command, and with FCUM,ALL

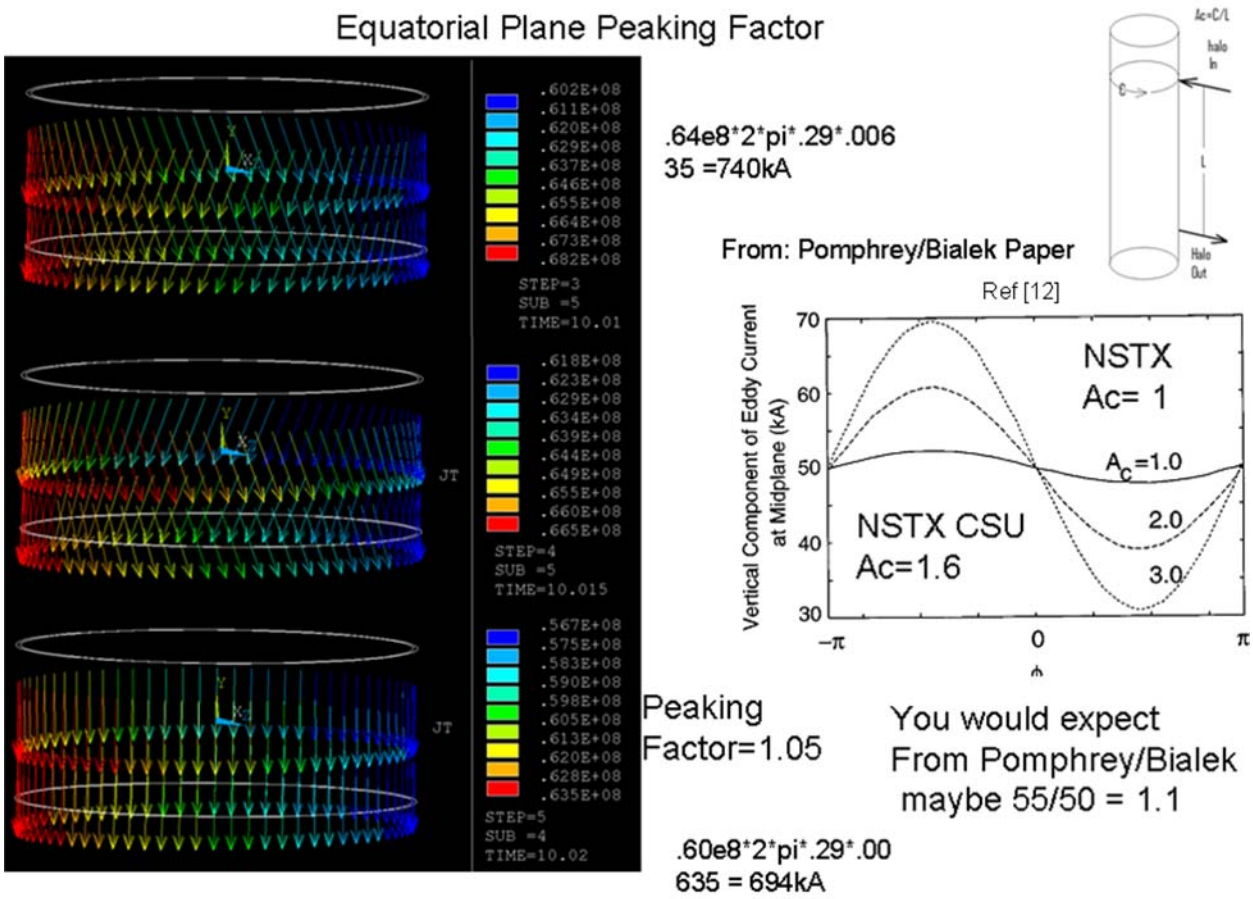

The second way to include halo loading is to introduce the halo currents during the ANSYS electromagnetic simulation in the same way the halo loads were included in the passive plate analyses. This was done, but the work was superseded by a more rigorous treatment by Art Brooks. [13]

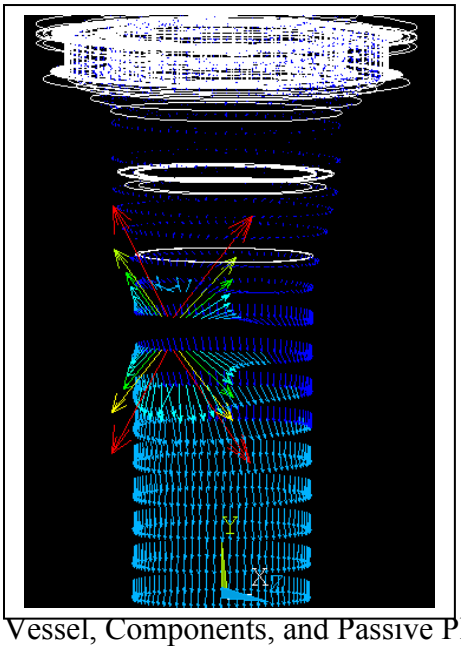

```
BR=130000*12*3*2e-7
*get,nmax,node,,num,max
*do,i,1,nmax
z=nz(i)
x=nx(i)
d,i,ay,vect4(x,z)
d,i,az,-0.5*BR*log(x*x)
*enddo
d,all,ax,0.
f,32437,amps,700000.0
f,18830,amps,-700000.0
lswrite,4
time,10.02
autots,1
deltim,.001,.0005,.002
kbc,0
*dim,vect5,table,81,81,1,x,z,,5
*tread,vect5,'5','txt'
nall
BR=130000*12*3*2e-7
*get,nmax,node,,num,max
```

12.0 Bellows Analysis

The analysis of the bellows is presented in detail in calculation number NSTXU-CALC-133-10-0 by Peter Rogoff. Presented here is the initial analysis of the electromagnetic analysis of the bellows. P. Rogoff's calculation includes the EM analysis and structural analyses for all loading of the bellows. Also Rogoff sizes the convolutions and bellows thicknesses to satisfy the EJMA standards and the NSTX criteria. The finite element model used in the EM calculations derives from Rogoff's NASTRAN plate element model. This was converted to 8 node brick solids that allow use of the procedure developed in this calculation.

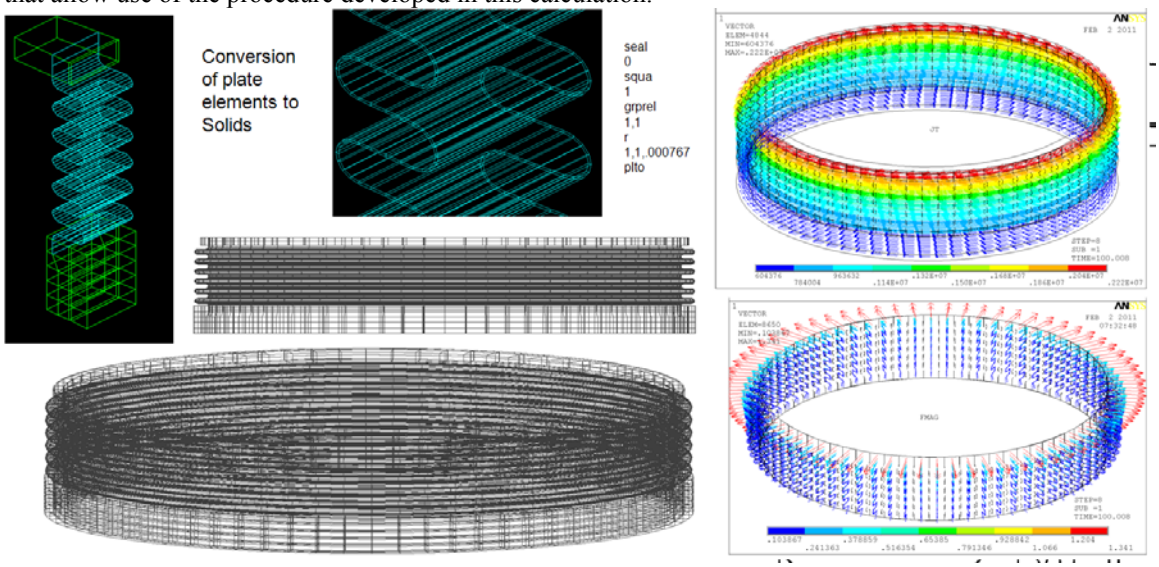

Figure 12.0-1 Bellows mesh (Left) Current Density (Right, Upper) Forces (Right Lower).

13.0 NB Backing Plate Analysis

This is another application of the procedure that is covered in more detail in the calculation of record by Larry Bryant This procedure has been applied to the neutral beam armor plate backing structure, various diagnostic components, and the centerstack casing, using a common set of OPERA disruption VP files.

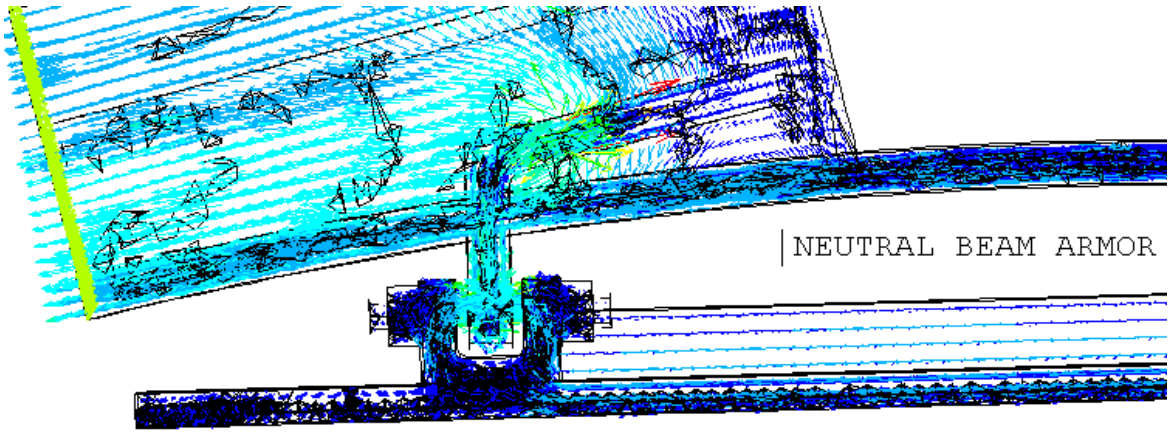

Figure 13.0-1 Current Densities in the Neutral Beam Armor Plate Backing Plate,

14.0 Moly Shield for the TAE antenna

The TAE antenna is a stand alone antenna utilizing five turns of 10 gauge copper wire on stud-mounted Macor standoffs shielded by molybdenum strips. Figure 14-1 shows the position of the antenna and the inset shows some of the details of the TAE corner spoolpieces, and the shield cross sections/ The Moly strips and attachments proposed for shielding of the TAE antenna were sized to experience eddy current forces equivalent to the Moly shields installed over the existing RWM sensor coils (I believe this was analyzed by Art brooks Michael Bell's). The first e-mail included in attachment is calculations for the maximum forces on the moly shields being proposed for the new antenna. We would to either have Michael's calculations checked, or further analysis done as you see appropriate.

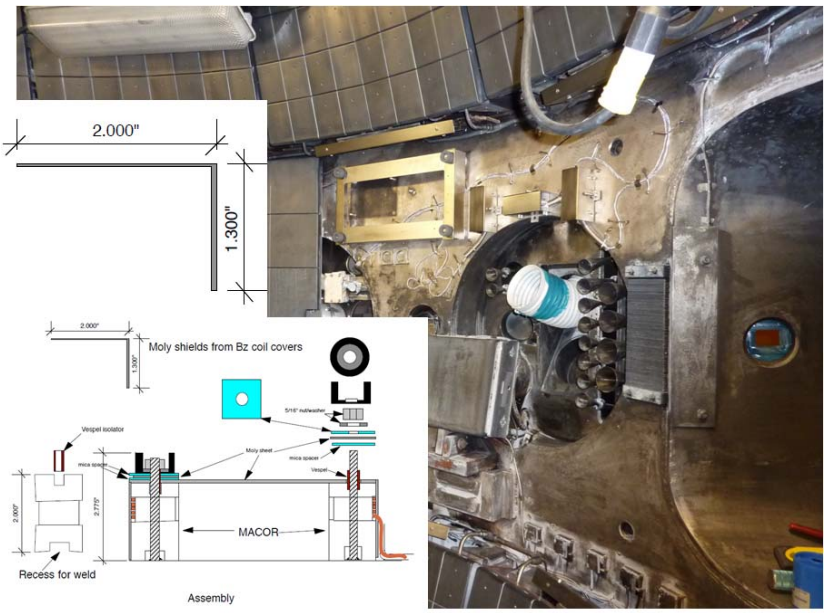

Figure 14.0-1 TAE Antenna with trial mounted shield

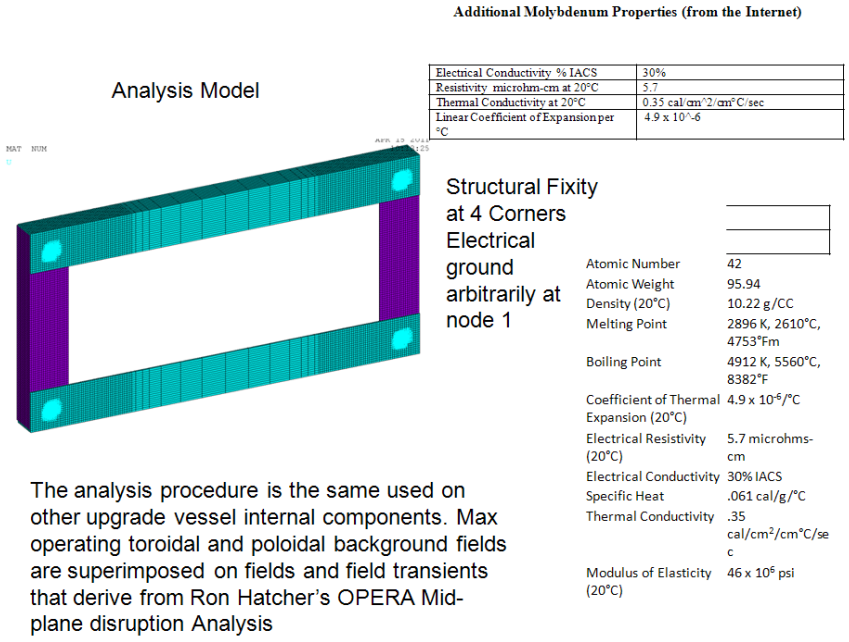

Figure 14.0-2 TAE Antenna Analysis Model

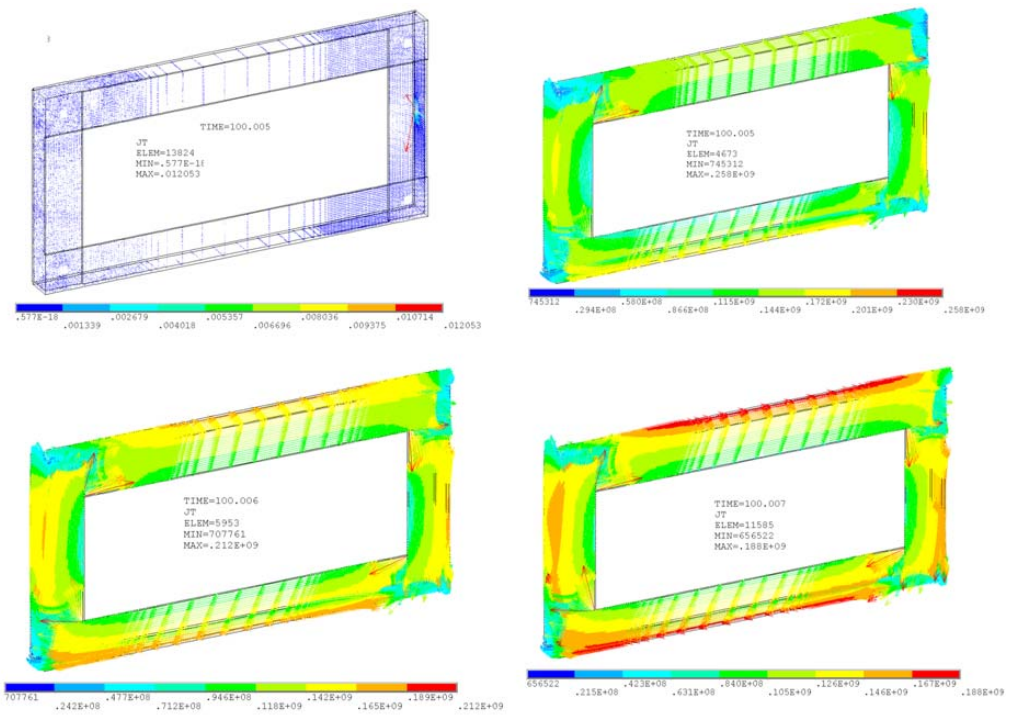

Figure 14.0-1 TAE Antenna with trial mounted shield

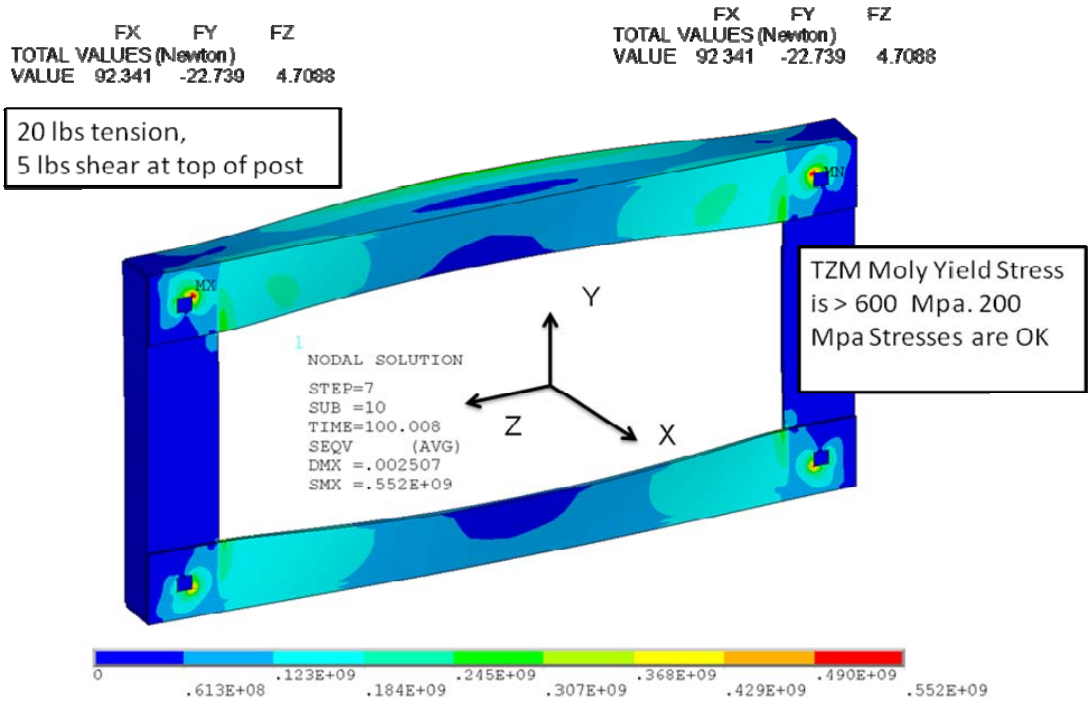

- Figure 14.0-3 TAE Antenna Stress and Reaction Results

15.0 Liquid Lithium Divertor

The Liquid Lithium Divertor (LLD) survived operation in NSTX marginally. The 1/4 inch screws that hold the corners were damaged significantly but did not break. This was considered a benchmark of what types of structures and attachment details could take disruption loads that were typical of NSTX Scenarios. If the analysis procedure being employed for the passive plates showed that the 1/4 inch bolts would survive, then this would be one level of confirmation for transferring vector potential data from the axisymmetric OPERA model.

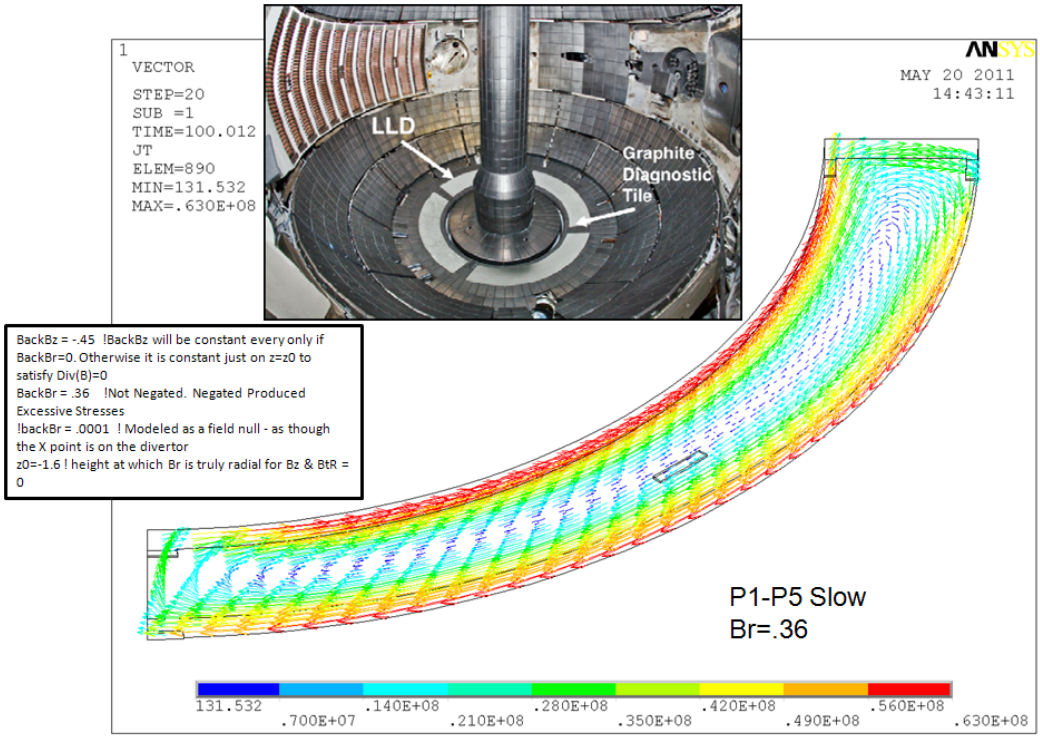

Figure 15.0-1 Current Density Plot Along with a Photo of the LLD, and Background Field Information

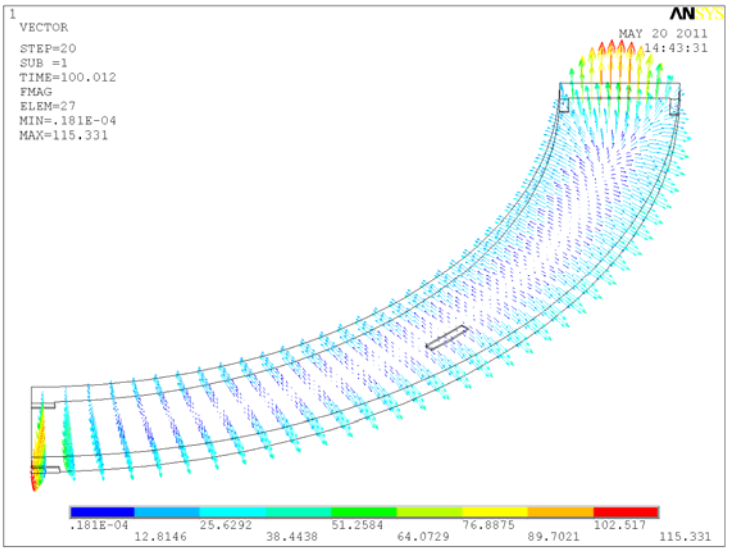

Figure 15.0-2 Lorentz Force Plot

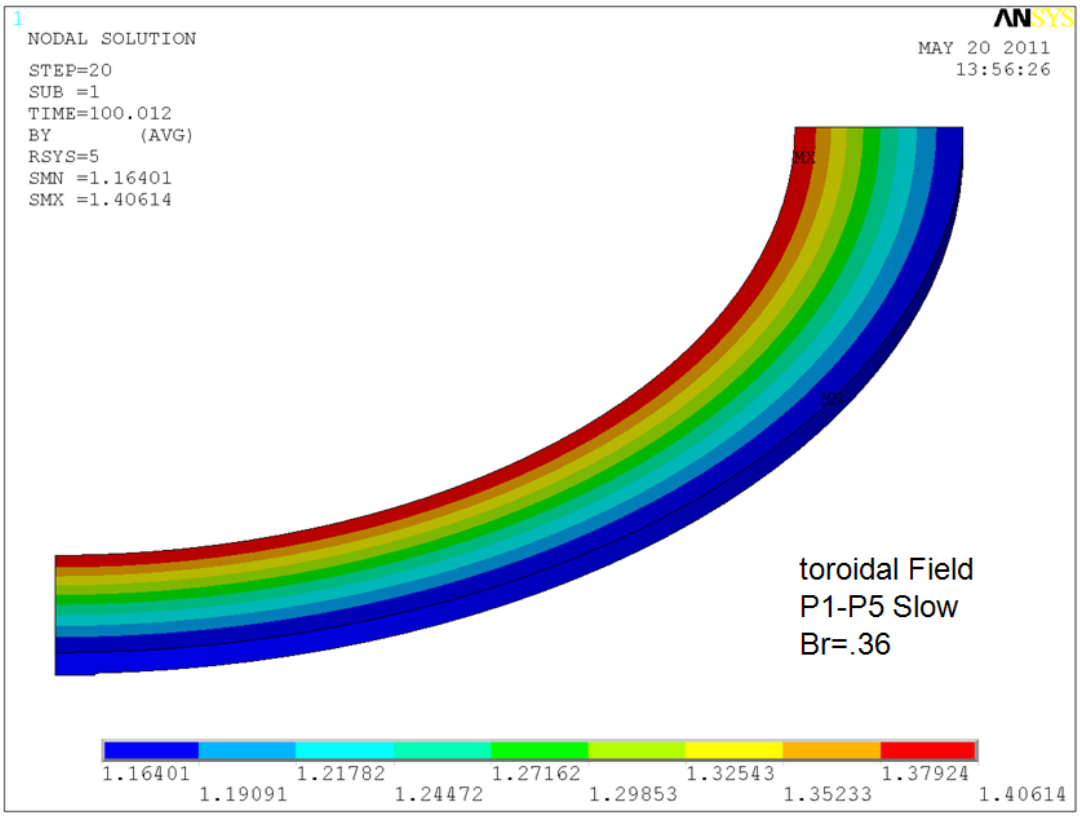

Figure 15.0-3 Toroidal Field Plot

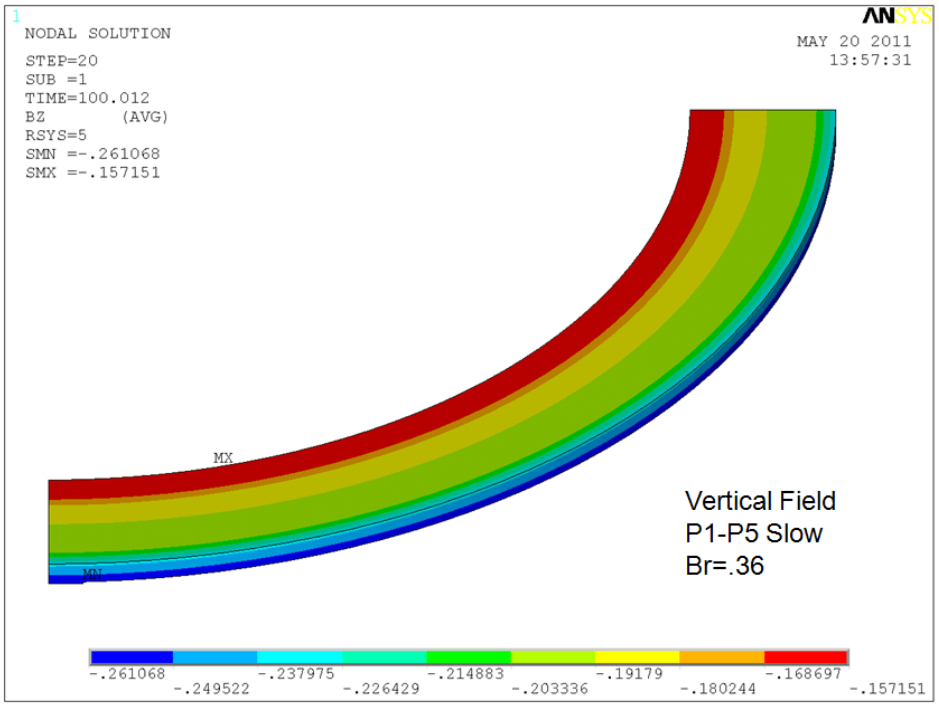

Figure 15.0-4 Vertical Field Plot

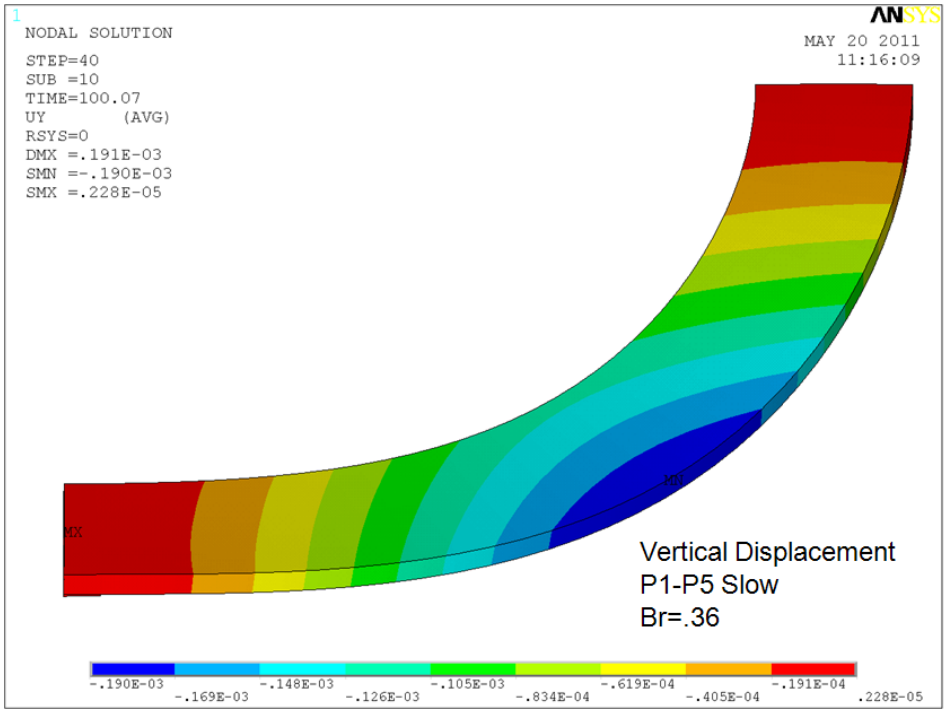

Figure 15.0-5 Vertical Displacement Plot

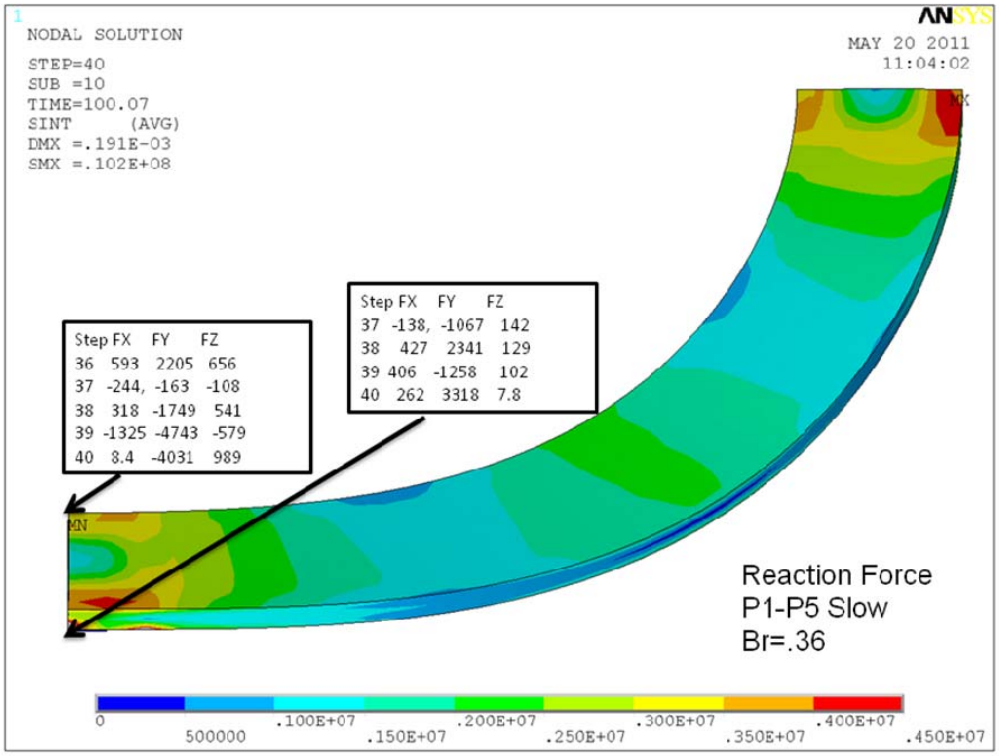

Figure 15.0-6 Stress Plot and Reaction Forces, Br=.36T

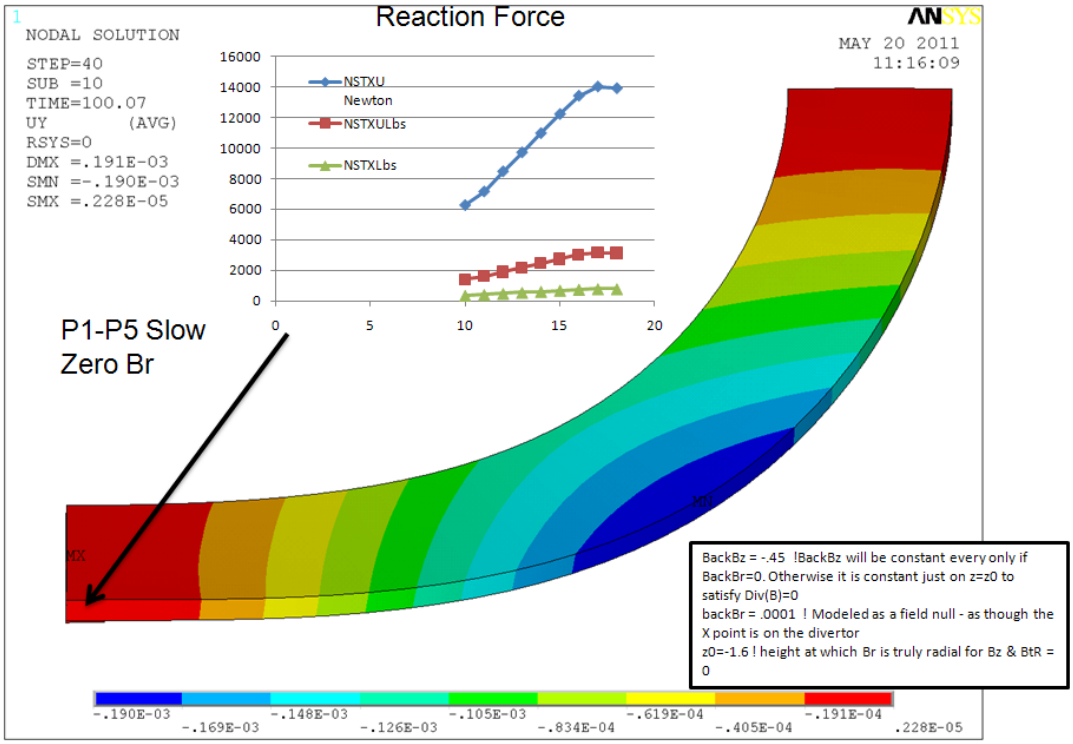

Figure 15.0-6 Vertical Displacement Plot and Reaction Forces, Br=0.0 T

In the EXCEL Plot, the estimate of the corner reactions peaks at 781 Lbs. Assuming the 1/4 inch bolt or pin takes the load in shear, The average shear stress is 781 lbs divided by pi/4*.25^2, which yields 15.9ksi or a Tresca of 32ksi - which is consistent with a commercial bolt that was near failure.

Appendix A

MACRO FOR GENERATING EDDY CURRENTS

!!!(Used for P1-P5 Slow VDE)

```
/filename,halo2
/prep7
/nerr,1000000,1000000

BackBz =-.5
BackBr = .18
et,1,45
ex,1,200e9     !Vessel
ex,5,117e9     !passive Plates
ex,8,200e9     !Vessel Shell
ex,10,200e9    !Diverto2 Support
ex,11,200e9    !ribs
ex,12,200e9    !PPL Support
ex,13,200e9    !Vessel Bracket
ex,14,200e9    !Vessel Bracket
ex,15,200e9    !Vessel Bracket
ex,17,200e9    !bolts


shpp,off
/input,lowd,mod
!/input,ves2,mod
nummer,node,.000001
nsel,y,-3,-1.8
d,all,all,0.0
nall
eall
csys,5
!nrotate,all
!nsel,y,-15.001,-14.999
!nasel,y,14.999,15.001
!d,all,uy,0.0
nrotate,all
cpdele,all,all
cpcyc,ux,.001,5,0,60,0
cpcyc,uy,.001,5,0,60,0
cpcyc,uz,.001,5,0,60,0
nall
eall
save
```

```
fini

/solu
f,31523,fy,1.0
solve
save
fini
!/exit   ! remove for the electromagnetic part

/filename,elect2
/prep7
/nerr,,99999997,,0,,
resume,halo2,db ! 360 degree model of the vessel, legs, umbrella & passive plates
et,1,97,1  !Center Stack Casing
et,5,97,1 ! vessel, legs and umbrella structure
et,12,97,1 ! passive plates

!ex,1,200e9     !Vessel
!ex,5,117e9     !passive Plates
!ex,8,200e9     !Vessel Shell
!ex,10,200e9    !Diverto2 Support
!ex,11,200e9    !ribs
!ex,12,200e9    !PPL Support
!ex,13,200e9    !Vessel Bracket
!ex,14,200e9    !Vessel Bracket
!ex,15,200e9    !Vessel Bracket
!ex,17,200e9    !bolts

*do,imat,1,20
mp,dens,imat,8950
mp,murx,imat,1.0
mp,rsvx,imat,74.0e-8
*enddo
mp,dens,1,8950 ! vessel, legs and umbrella structure
mp,rsvx,1,74.e-8
mp,dens,20,8950 ! Center Stack Casing Inconel 625
mp,rsvx,20,1.3e-6
mp,dens,5,8950 ! Passive plates
mp,rsvx,5,.85*2.443e-8 ! @400K
mp,dens,6,8950 ! Passive plates
mp,rsvx,6,74e-8
csys,5 ! Opera output is in Cylindrical System
nrotat,all
!nsel,s,loc,z,-3.9342,-3.9215 ! Selects nodes at the base
nsel,s,loc,z,-100,-1.8
```

!nasel,y,29.99,30.001
!nasel,y,-30.001,-29.99
d,all,volt,0 ! Constrains the Volts DOF at the Lower CHI/Bellows/Ceramic Break
nall
eall
cpdele,all,all
cpcyc,volt,.001,5,0,60,0
!nsel,y,29.99,30.001
!nasel,y,-30.001,-29.99
!d,all,volt,0 ! Constrains the Volts DOF Vessel Cyc Symm
nsel,all
allsel,all
save
!
fini
/solu
HaloCur=.1/6/4

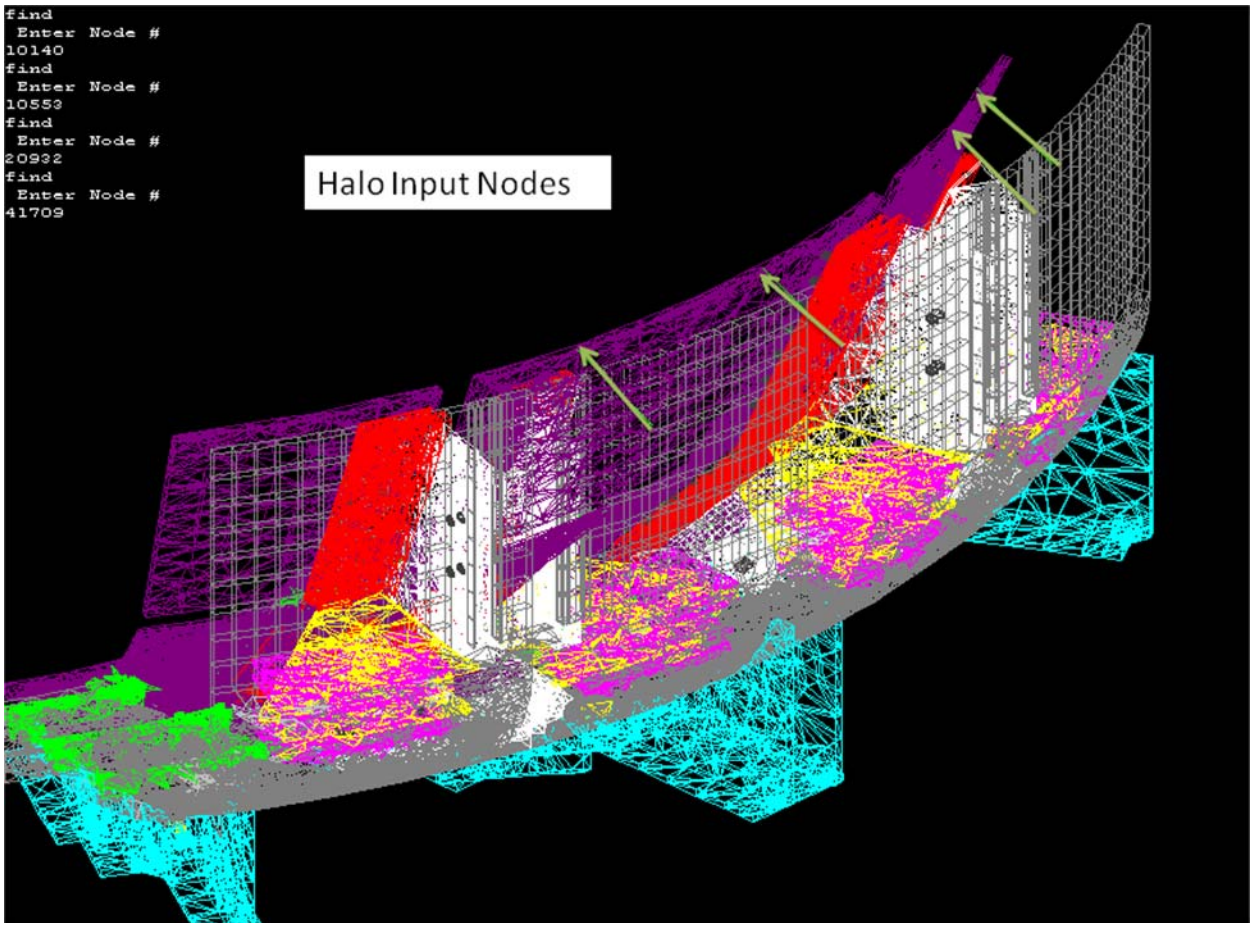

nodein1=10140
nodein2=10553
nodein3=20932

nodein4=41709
Nodeout=10841
!Output times [s]:
 t1= 0.0
 t2= 1.0E-03
 t3= 2.0E-03
 t4= 3.0E-03
 t5= 4.0E-03
 t6= 5.0E-03
 t7= 6.0E-03
 t8= 7.0E-03
 t9= 8.0E-03
t10= 0.01
t11= 0.01025
t12= 0.0105
t13= 0.01075
t14= 0.011
t15= 0.01125
t16= 0.0115
t17= 0.01175
t18= 0.012
t19= 0.01225
t20= 0.0125
t21= 0.01275
t22= 0.013
t23= 0.01325
t24= 0.0135
t25= 0.01375
t26= 0.014
t27= 0.01425
t28= 0.0145
t29= 0.01475
t30= 0.015
t31= 0.016
t32= 0.017
t33= 0.018
t34= 0.019
t35= 0.02
t36= 0.03
t37= 0.04
t38= 0.05
t39= 0.06
t40= 0.07
t41= 0.08
t42= 0.09
t43= 0.1

```
t44= 0.11
t45= 0.12
t46= 0.13
t47= 0.15
t48= 0.16
t49= 0.17
t50= 0.18
t51= 0.19
t52= 0.2
t53= 0.225
t54= 0.25



BackBz = -.4  !BackBz will be constant every only if BackBr=0. Otherwise it is constant
just on z=z0 to satisfy Div(B)=0
BackBr = -.3
z0=-.6 ! height at which Br is truely radial for Bz & BtR = 0
antype,4
!antype,static
trnopt,full
outres,all,last
autots,1
deltim,1,.5,3
kbc,0

time,.001
lswrite,1

*do,inum,1,44,1
time,t%inum%+100
*dim,vect%inum%,table,81,81,1,x,z,,5 ! Specfies a 81X 81 parameter table

*tread,vect%inum%,'VecPot_case_%inum%','txt' ! Reads the file 1.txt into the table

nall
BR=130000*12*3*2e-7 ! Toroidal current
*get,nmax,node,,num,max
*do,i,1,nmax
z=nz(i)
x=nx(i)

!           Applying Poloidal Fields
!d,i,ay,vect%inum%(x,z) ! Intrepolates and applies the Vector Potential on the node
                    !/x removed because Ron's Files have been corrected for 1/r
```

```
d,i,ay,BackBz*x/2-BackBr*(z-z0)+vect%inum%(x,z) ! Intrepolates and applies the
Vector Potential on the node
                !/x removed because Ron's Files have been corrected for 1/r
!d,i,ay,BackBz*x/2-BackBr*(z-z0)! Applies only the background fields
!          Applying the Toroidal Field
d,i,az,-0.5*BR*log(x*x) ! applies vector potential for toroidal magnetic field
*enddo
d,all,ax,0.
*if,inum,gt,7,then
HaloCur=700000./6/4
*endif
*if,inum,gt,10,then
HaloCur=.1/6/4
*endif
f,Nodein1,amps,HaloCur
f,Nodein2,amps,HaloCur
f,Nodein3,amps,HaloCur
f,Nodein4,amps,HaloCur
!f,nodeout,amps,-HaloCur
lswrite,inum+1
*enddo


!
lssolve,1,40,1 ! solves 9 load steps
save
fini
/post1
plnstr,bsum
/exit
```

Appendix B
MACRO FOR STATIC STRUCTURAL ANALYSIS

```
/batch
/filename,struct2
!/pmacro
/nerr,,99999997,,0,,
/prep7
!resume,elect,db  ! resume your model

shpp,off

et,1,45                ! Use appropriate element type numbers
et,5,45
dof,delete
dof,ux,uy,uz
```

```
mp,dens,6,8900

ex,1,200e9     !Vessel
ex,5,117e9     !passive Plates
ex,8,200e9     !Vessel Shell
ex,10,200e9    !Diverto2 Support
ex,11,200e9    !ribs
ex,12,200e9    !PPL Support
ex,13,200e9    !Vessel Bracket
ex,14,200e9    !Vessel Bracket
ex,15,200e9    !Vessel Bracket
ex,17,200e9    !bolts
*do,imat,1,20
mp,dens,imat,8950
mp,prxy,imat,0.3
mp,dens,imat,8900
*enddo

/input,lowd,mod
eusel,mat,90
nelem

csys,5                  ! Use the same coordinate system as the one in magnetic analysis
nrotat,all
      ! Constraints the base of the structure
ddele,all
nsel,z,-3,-1.8
d,all,all,0.0
nsel,z,-1.47,-1.45
nrsel,x,1.5,2
d,all,all,0.0
nall
eall
!nsel,y,-15.001,-14.999
!nasel,y,14.999,15.001
!d,all,uy,0.0
cpdele,all,all
cpcyc,ux,.001,5,0,60,0
cpcyc,uy,.001,5,0,60,0
cpcyc,uz,.001,5,0,60,0
nall
eall
nall
eall
save
```

```
!
fini
/solu
!antype,4      ! Use 4 for dynamic analysis
antype,0     ! Use 0 for static analysis
!outres,all,3     ! writes results every three load steps.  Use smaller # for more resolution

!Output times [s]:
t1=1.00E-03 $t2=5.00E-03$t3=5.50E-03$t4=6.00E-03$t5=6.50E-03$t6=7.00E-
03$t7=7.50E-03$t8=8.00E-03$t9=8.50E-03$t10=9.00E-03
t11=9.50E-03$t12=1.00E-02$t13=1.10E-02$t14=1.20E-02$t15=1.30E-02$t16=1.40E-
02$t17=1.50E-02$t18=1.60E-02$t19=1.70E-02$t20=1.80E-02$t21=1.90E-02
t22=2.00E-02$t23=2.10E-02$t24=2.20E-02$t25=2.30E-02$t26=2.40E-02$t27=2.50E-
02$t28=2.60E-02$t29=2.70E-02$t30=2.80E-02$t31=2.90E-02$t32=3.00E-02
t33=3.50E-02$t34=4.00E-02$t35=4.50E-02$t36=5.00E-02$t37=5.50E-02$t38=6.00E-
02$t39=6.50E-02$t40=7.00E-02$t41=7.50E-02$t42=8.00E-02$t43=8.50E-02
t44=9.00E-02$t45=9.50E-02$t46=1.00E-01$t47=1.50E-01$t48=2.00E-01

!nsubst,100        ! For more finer results use larger #.
!betad,0.005         !Damping
kbc,0
fdele,all,all
lswrite,1

*do,inum,2,40,1
time,t%inum%
fdele,all,all
ldread,forc,inum,,,,elect2,rst,   ! Use the appropriate file name.
lswrite,inum+1
*enddo


!lssolve,4,6,1
lssolve,1,40,1
```

Appendix C
MACRO FOR DYNAMIC STRUCTURAL ANALYSIS

```
!!!(Used for P1-P5 Slow VDE)

/batch
/filename,Dynamic
!/pmacro
/nerr,,99999997,,0,,
/prep7
!resume,elect,db  ! resume your model (If needed to Obtain the Mesh)
```

```
shpp,off

et,1,45                 ! Use appropriate element type numbers
et,5,45
dof,delete
dof,ux,uy,uz

mp,dens,6,8900

ex,1,200e9     !Vessel
ex,5,117e9     !passive Plates
ex,8,200e9     !Vessel Shell
ex,10,200e9    !Divertor Support
ex,11,200e9    !ribs
ex,12,200e9    !PPL Support
ex,13,200e9    !Vessel Bracket
ex,14,200e9    !Vessel Bracket
ex,15,200e9    !Vessel Bracket
ex,17,200e9    !bolts
*do,imat,1,20
mp,dens,imat,8950
mp,prxy,imat,0.3
mp,dens,imat,8900
*enddo

/input,lowd,mod
eusel,mat,90
nelem

csys,5                  ! Use the same coordinate system as the one in magnetic analysis
nrotat,all
      ! Constraints the base of the structure
ddele,all
nsel,z,-3,-1.8
d,all,all,0.0
nsel,z,-1.47,-1.45
nrsel,x,1.5,2
d,all,all,0.0
! restrain vessel around ports
nsel,z,-.468,-.467
d,all,all,0.0
nall
eall
!nsel,y,-15.001,-14.999
!nasel,y,14.999,15.001
```

```
!d,all,uy,0.0
cpdele,all,all
cpcyc,ux,.001,5,0,60,0
cpcyc,uy,.001,5,0,60,0
cpcyc,uz,.001,5,0,60,0
nall
eall
nall
eall
save
!
fini
/solu
antype,4      ! Use 4 for dynamic analysis
!antype,0     ! Use 0 for static analysis
outres,all,1     ! writes results every sub step.  Use smaller # for more resolution
!Output times:
 t1= 0.0
 t2= 1.0E-03
 t3= 2.0E-03
 t4= 3.0E-03
 t5= 4.0E-03
 t6= 5.0E-03
 t7= 6.0E-03
 t8= 7.0E-03
 t9= 8.0E-03
t10= 0.01
t11= 0.01025
t12= 0.0105
t13= 0.01075
t14= 0.011
t15= 0.01125
t16= 0.0115
t17= 0.01175
t18= 0.012
t19= 0.01225
t20= 0.0125
t21= 0.01275
t22= 0.013
t23= 0.01325
t24= 0.0135
t25= 0.01375
t26= 0.014
t27= 0.01425
t28= 0.0145
t29= 0.01475
```

```
t30= 0.015
t31= 0.016
t32= 0.017
t33= 0.018
t34= 0.019
t35= 0.02
t36= 0.03
t37= 0.04
t38= 0.05
t39= 0.06
t40= 0.07
t41= 0.08
t42= 0.09
t43= 0.1
t44= 0.11
t45= 0.12
t46= 0.13
t47= 0.15
t48= 0.16
t49= 0.17
t50= 0.18
t51= 0.19
t52= 0.2
t53 =0.225
t54= 0.25

nsubst,10       ! For more finer results use larger #.
betad,0.005        !Damping
alphd,0.005        !Damping
kbc,0
fdele,all,all
time,.001
lswrite,1
time,100.0
lswrite,2
*do,inum,3,40,1
time,t%inum% + 100
fdele,all,all
ldread,forc,inum,,,,elect2,rst,   ! Use the appropriate file name.
time,t%inum% + 100
lswrite,inum
*enddo


!lssolve,4,6,1
                                        lssolve,1,40,1
```

Appendix D

From Art Brooks:

The Magnetic Potential needed to produce a (near) Uniform Magnetic Field in Cylindrical Coordinates

The magnetic flux density can be expressed in terms of the curl of a vector potential

$$\mathbf{B} = \nabla \times \mathbf{A} \tag{1.1}$$

In cylindrical coordinates equation (1.1) becomes

$$\nabla \times \mathbf{A} = \frac{1}{r}\begin{vmatrix} u_r & u_\theta & u_z \\ \frac{\partial}{\partial r} & \frac{\partial}{\partial \theta} & \frac{\partial}{\partial z} \\ A_r & rA_\theta & A_z \end{vmatrix} \tag{1.2}$$

Which expands to

$$B_r = \frac{1}{r}\left\{\frac{\partial A_z}{\partial \theta} - \frac{\partial (rA_\theta)}{\partial z}\right\}u_r \tag{1.3}$$

$$B_\theta = \frac{1}{r}\left\{\frac{\partial A_r}{\partial z} - \frac{\partial A_z}{\partial r}\right\}ru_\theta \tag{1.4}$$

$$B_z = \frac{1}{r}\left\{\frac{\partial (rA_\theta)}{\partial r} - \frac{\partial A_r}{\partial \theta}\right\}u_z \tag{1.5}$$

The above can be solved for the vector potential for a constant field in any one of the directions. An expression of the total field in terms of vector potential is obtained by superposition. However as will be shown below, while the expressions are linear in A and B, they are coupled in the coordinate directions, so that the presence of a radial field induces a non uniform vertical field. The specified field can be obtained only over a limited range from the field point chosen.

For the 2D field in a plane normal to the z-axis where $B_z = 0$ equation (1.5) can be satisfied by setting $A_r = A_\theta = 0$ so B_r and B_θ becomes functions of A_z only. Then (1.3) and (1.4) become

$$B_r = \frac{1}{r}\frac{\partial (A_z)}{\partial \theta} \tag{1.6}$$

$$B_\theta = -\frac{dA_z}{dr} \tag{1.7}$$

With a 1/r toroidal field $B_\theta = \frac{B_o R_o}{r}$ and $B_r = 0$ we have

$$dA_z = -\frac{B_o R_o}{r} dr \tag{1.8}$$

plus an arbitrary constant which can be set equal to zero.
Integrating both sides of the equation we have

$$A_z = -B_o R_o \ln(r) \tag{1.9}$$

For $B_\theta = 0$ equation (1.4) can be satisfied by setting $A_r = A_z = 0$ so B_r and B_z becomes functions of A_θ only. Then (1.3) and (1.5) become

$$B_r = -\frac{1}{r}\frac{\partial(rA_\theta)}{\partial z} \tag{1.10}$$

$$B_z = \frac{1}{r}\frac{\partial(rA_\theta)}{\partial r} \tag{1.11}$$

For constant B_r assume A_θ is a function of z only and integrate (1.10)

$$\begin{aligned} rA_\theta &= -B_r rz \\ A_\theta &= -B_r z \end{aligned} \tag{1.12}$$

For constant B_z assume A_θ is a function of r only and integrate (1.11)

$$\begin{aligned} rA_\theta &= \frac{B_z r^2}{2} \\ A_\theta &= \frac{B_z r}{2} \end{aligned} \tag{1.13}$$

For constant B_r and B_z we have from summing (1.12) and (1.13)

$$A_\theta = -B_r z + \frac{B_z r}{2} \tag{1.14}$$

Back substituting (1.14) into (1.10) to verify B_r we have

$$\begin{aligned} B_r &= -\frac{1}{r}\frac{\partial}{\partial z}\{-B_r zr + \frac{B_z r^2}{2}\} \\ &= -\frac{1}{r}(-B_z r) \\ &= B_r \text{ everywhere} \end{aligned} \tag{1.15}$$

However for B_z we get

$$
\begin{aligned}
B_z &= \frac{1}{r}\frac{\partial}{\partial r}\{-B_r zr + \frac{B_z r^2}{2}\} \\
&= \frac{1}{r}(-B_r z + B_z r) \\
&= B_z - B_r \frac{z}{r} \\
&= B_z \text{ only on the plane z= 0}
\end{aligned}
\tag{1.16}
$$

```
fini
/clear
!
! Test of producing B field from vector potential in cylindrical coordinates
!
BtR=1.  ! Telsa-meters   $Br=1
z0=0.5  ! height at which Br is truely radial for Bz & BtR = 0
Bz=1 ! Bz will be constant every only if Br=0. Otherwise it is constant just on z=z0 to
satisfy Div(B)=0
!
! Choose if y is up ('no' leaves z up)
!
yup='yes'
*if,yup,eq,'yes',then
csys,5
wpcsys,-1,5
*else
csys,1
*endif
!
/prep7
et,1,97,0
mp,murx,1,1.
cylind,.5,1.5,-1,1,0,90
esize,.1
vmesh,all!
!
! apply 1/R toroidal field, constant Bz field and near constant Br field
!  using magnetic vector potential thru body
!
nrotat,all ! into cyclindrical cord sys (1 for z up, 5 for y up)
d,all,ax,0.
!
*get,nmax,node,,num,max
*do,i,1,nmax
rr=nx(i)
zz=nz(i)
d,i,az,-.5*BtR*log(rr*rr)
d,i,ay,Bz*rr/2-Br*(zz-z0)
*enddo
!
fini
/solu  $solve  $fini
/post1
/WIND,ALL,OFF   $/WIND,1,LTOP  $/WIND,2,RTOP  $/WIND,3,LBOT  $/WIND,4,RBOT
/view,1,1  $/view,2,,1  $/view,3,,,1  $/view,4,1,1,1  $/vscale,1,.25,1
plvect,b,,,,vect,,on
```

Appendix E
Background Poloidal Fields…(By J. Boales&R. Hatcher)

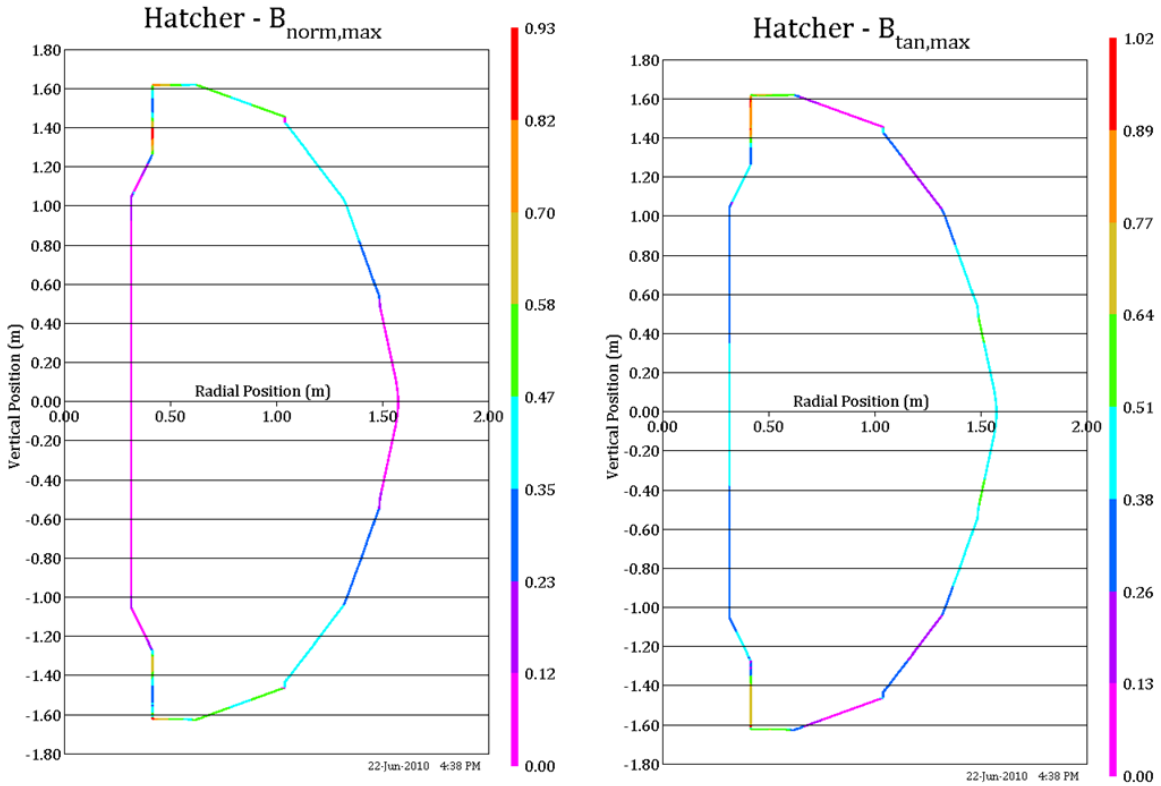

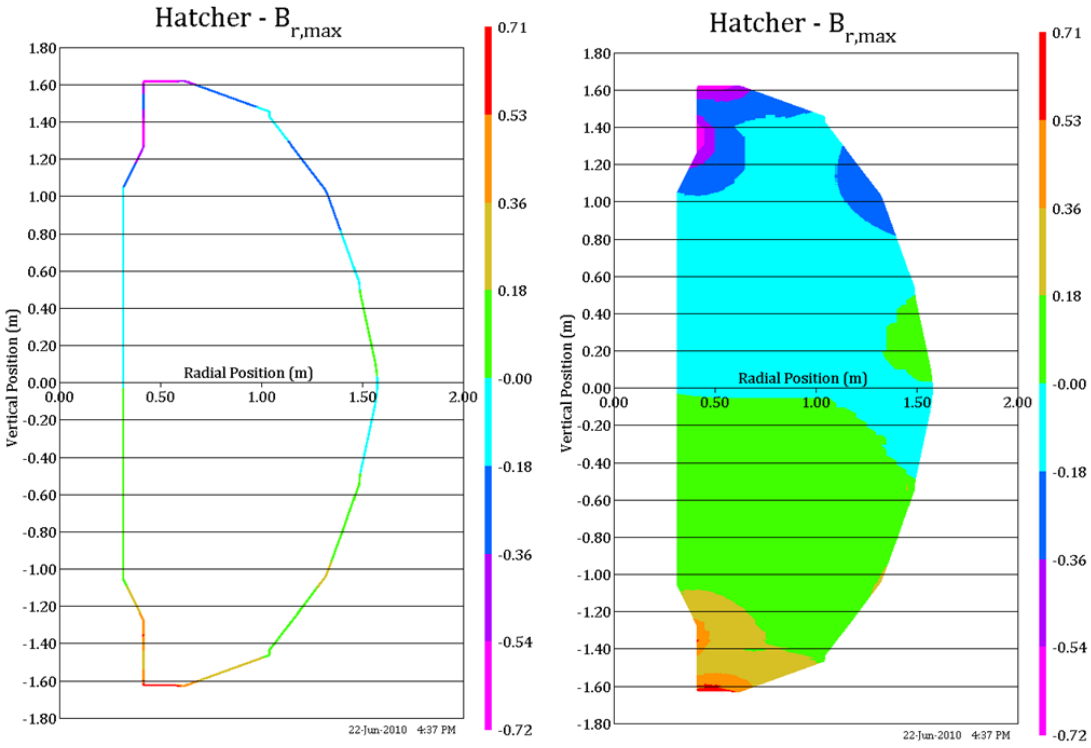

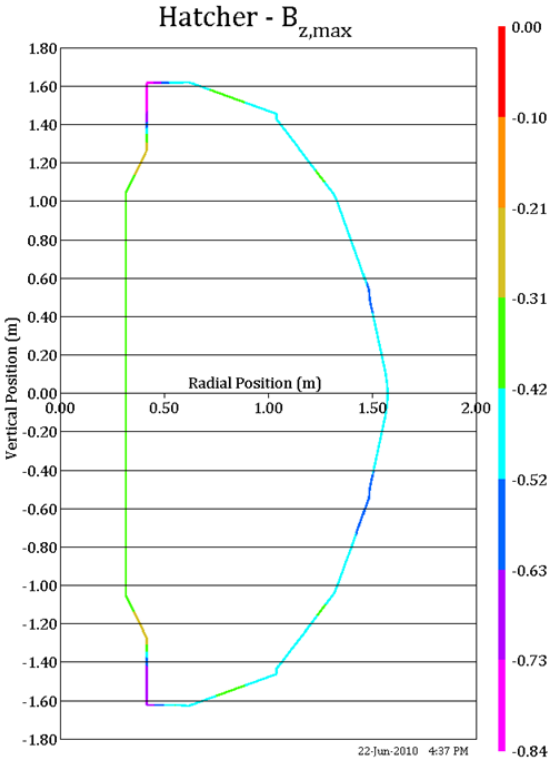
Hatcher - $B_{z,max}$
Vertical Position (m)
Radial Position (m)
0.00
0.50
1.00
1.50
2.00
1.80
1.60
1.40
1.20
1.00
0.80
0.60
0.40
0.20
0.00
-0.20
-0.40
-0.60
-0.80
-1.00
-1.20
-1.40
-1.60
-1.80
0.00
-0.10
-0.21
-0.31
-0.42
-0.52
-0.63
-0.73
-0.84
22-Jun-2010 4:37 PM

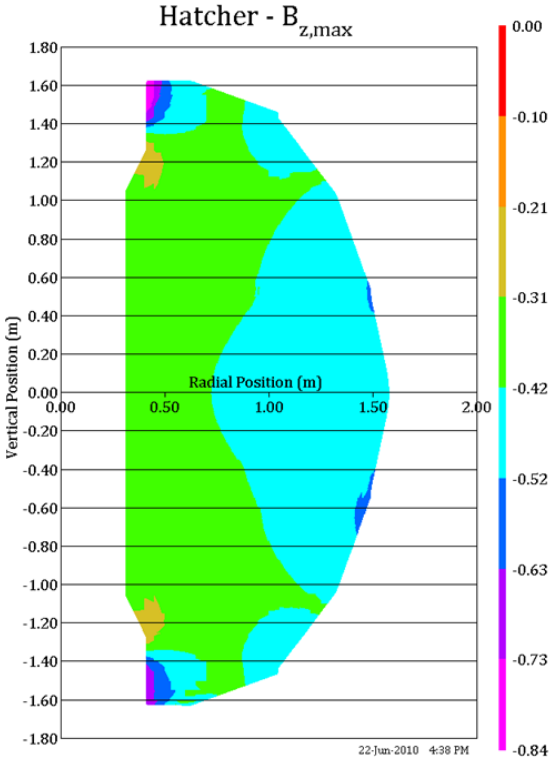
Hatcher - $B_{z,max}$
Vertical Position (m)
Radial Position (m)
0.00
0.50
1.00
1.50
2.00
1.80
1.60
1.40
1.20
1.00
0.80
0.60
0.40
0.20
0.00
-0.20
-0.40
-0.60
-0.80
-1.00
-1.20
-1.40
-1.60
-1.80
0.00
-0.10
-0.21
-0.31
-0.42
-0.52
-0.63
-0.73
-0.84
22-Jun-2010 4:38 PM

Attachment F
Passive Plate Bracket Weld QA Report

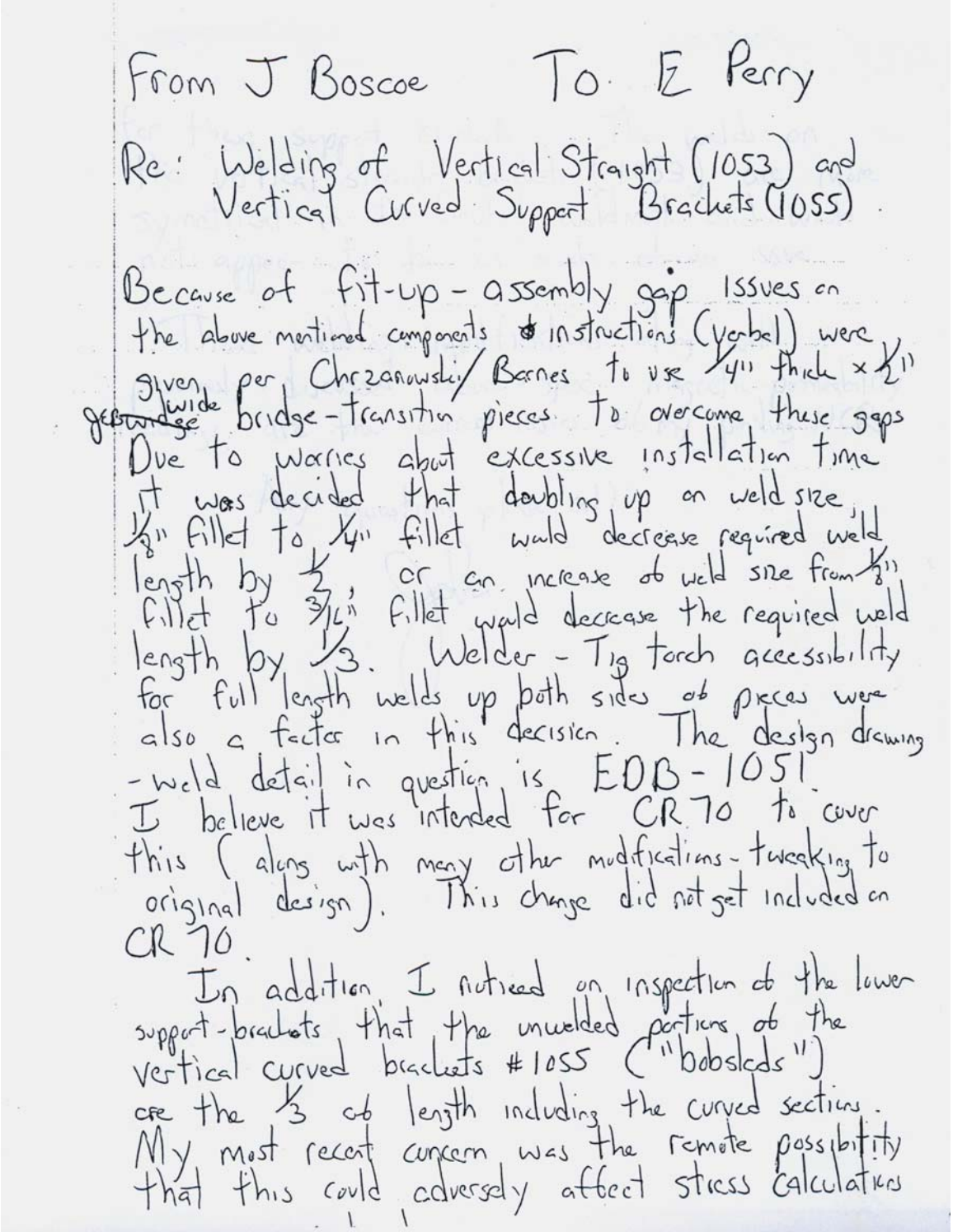

From J Boscoe To E Perry

Re: Welding of Vertical Straight (1053) and Vertical Curved Support Brackets (1055).

Because of fit-up - assembly gap issues on the above mentioned components ~~&~~ instructions (verbal) were given per Chrzanowski/Barnes to use 1/4" thick x 1/2" ~~gerwidge~~ wide bridge-transition pieces to overcome these gaps Due to worries about excessive installation time it was decided that doubling up on weld size, 1/8" fillet to 1/4" fillet would decrease required weld length by 1/2, or an increase of weld size from 1/8" fillet to 3/16" fillet would decrease the required weld length by 1/3. Welder - Tig torch accessibility for full length welds up both sides of pieces were also a factor in this decision. The design drawing - weld detail in question is EDB-1051. I believe it was intended for CR 70 to cover this (along with many other modifications - tweaking to original design). This change did not get included on CR 70.

In addition I noticed on inspection of the lower support-brackets that the unwelded portions of the vertical curved brackets #1055 ("bobsleds") are the 1/3 of length including the curved sections. My most recent concern was the remote possibility that this could adversely affect stress calculations

Attachement G
email from Michael Belll
On Mar 29, 2011, at 9:43 PM, Michael G. Bell wrote:

Masa,
You asked me to send you some estimates for the maximum forces that could affect the moly shields on the proposed *AE antenna.
The shields are L-shaped pieces of molybdenum sheet 0.040" thick that are 2" wide on one side and 1.3" wide on the other (data from drawing B-9D11037 and from Lane Roquemore). This cross-section is the same as that of the new moly shields fixed over the 24 RWM B_p coils just behind the graphite tiles at the top or bottom of the lower and upper passive plates, respectively. The two horizontal shields will span a distance
of 16" and the verticals will span 8" between their mounting studs.

When we were designing the moly shields for the B_pol sensors, Jim Bialek did a calculation of the eddy current induced in them by rapid changes in the poloidal field, such as during a disruption. He considered the case of a poloidal field of 0.8T disappearing in 3ms, which is a worst case. In this case, the eddy currents in the normal face of the shield reached a maximum of 2.8kA, limited by the resistance (i.e. determined by the rate of change of the flux, not the total flux change). The largest face of the shield (2" x 17.5") has an area of of about 0.023m^2, so the dipole moment induced in the shield is less than 2.8kA x 0.23m^2 = 64A.m^2. I then plugged these numbers into my code which
calculates the force and torque on a magnetic
dipole in NSTX. The worst case forces I calculated were 20N, less than 5 lbf, and the torque 25 N.m, i.e. 18 ft.lbf. Given that each of these is divided between two 1/4" bolts welded to the vessel and Macor standoffs 1.5" in diameter, these worst-case loads are not excessive. We had concluded the same thing when we analyzed their
use on the RWM sensors.

The calculation above assumed that the eddy currents flowed in the shields independently because they are insulated from each other at the corners. If all the insulators failed, then eddy currents could circulate in the loop formed by all four shields which has an area of 17.5" x 9.5" ‰ 0.1m^2. This could intercept a radial field up to 0.1T maximum for a total flux of 10mWb. I estimate that this loop has an inductance of about 1µH and a resistance of about 1m‡ for an L/R time of 1ms. If the field disappeared in 3ms (conservative), the induced current would be ~3kA (resistance limited). The radial force on each horizontal element due to a vertical field of 0.8T would then be about 1000N, about 220lbf (one would be pushed towards and one pulled away from the wall). The radial force on the vertical elements crossing the TF would be less than half this. These forces are much greater, but they should be within the capability of the shields and mounts to withstand. They also require that all four insulators fail to zero resistance and they result from truly awesome disruptions. I have suggested to Lane that we make the insulators between the shields out ot two layers of Micamat with the inner layer undercut so that any lithium condensing on the shields would have to bridge 4 gaps of about a millimeter to complete the circuit.

I believe that the risk of mechanical faiure of the proposed antenna due to eddy-current forces is low.

Michael
--

Michael Bell
Princeton Plasma Physics Laboratory
Email: MBell@pppl.gov
Mail: MS34, P.O. Box 451, Princeton, NJ 08543-0451 U.S.A.
Phone: +1-609-243-3282
FAX: +1-609-243-2874

Attachment H
3D Disruption Analysis of Passive Plates for NSTX Upgrade
Prepared by Yuhu Zhai

1. Executive summary

This FE based 3D analysis is an amendment to NSTXU-CALC-12-01-01 to check previous 2D disruption analysis of passive plates, vacuum vessel and components during plasma disruption and VDEs for NSTX upgrade. The ½" passive plates are electrically connected and structurally supported by the vacuum vessel through the supporting bracket. Each plate is bolted onto the bracket with 28 steel bolts at the back of the plate and the bracket is welded onto the vessel. The passive plates are made of Chromium Zirconium Copper C18150, a copper alloy with high electrical conductivity. The bracket and the vessel are made of stainless steel.

Since the output disruption forces on the center stack, the vessel and its components from the NSTXU-CALC-12-01-01 are used as input for a number of other calculations for NSTX upgrade, it is important to validate methodology used in this analysis and cross check magnetic field distribution and eddy current forces during plasma disruption.

In the 2D disruption analysis, magnetic vector potentials from OPERA 2D simulation are transferred to classical ANSYS APDL for stress analysis. The 2D OPERA model is an axisymmetric model assuming copper and bracket averaged material electrical conductivity based on available measurement data. This averaged electrical conductivity, however, is an order of magnitude smaller than that of the copper plate. Therefore, skin effect, which is important for passive plates during transient plasma disruption and fast VDEs, cannot be captured in previous analysis. The skin depth of copper plates is ~2 mm for 1 ms disruption, which means that the eddy current flowing in the plate during disruption penetrates only ~1/6 of the plate thickness. The skin depth increases to ~6 mm for the 10 ms plasma VDEs – eddy current flows only in half of the plate thickness. Therefore, due to this limitation, 2D analysis will overestimate the disruption force and bending moment on the passive plates.

A 3D OPERA EM model is created for accurate disruption analysis and a new OPERA to ANSYS load transferring procedure has been established. The new EM model includes not only the plates, but also the supporting bracket, the vacuum vessel and center stack casing. Various plasma shapes from square, trapezoid to octagon (close to circular) are studied to understand its impact on the disruption loads for passive plates for fast (1 ms) mid-plane disruption, P1 to P5 10 ms translation and then fast (1 ms) and slow (40 ms) disruption. The elemental disruption forces on the primary and secondary plates are mapped onto ANSYS Workbench structural model for static and dynamic stress analysis. A sensitivity study with varying electrical conductivity for the bracket is performed to study its impact on the disruption loads on the plate. An adjusted conductivity of the bracket that matches the overall DC loop voltage measurement with electrical conducting path from the plate to bracket and the vessel is used. The 3D model is benchmarked against a Maxwell 3D model used for vessel disruption analysis as well as the magnetic field from results of Woolley Green's function formulation for various coil current scenarios. The new 3D model in an axisymmetric form is also benchmarked against

Hatcher's 2D analysis using the same electric conductivity as that from direct measurements.
The main conclusion based on the new 3D disruption analysis is that current primary and secondary plates should be adequate although there is local high stress region close to the bolts. The washers and bolts are therefore recommended to be replaced for better support of the plates. Following is a summary of main observations from the new disruption analysis with a list of main assumptions used for the 3D analysis.

1) The worst disruption loads on primary plates are from P1 to P5 VDEs – 10 ms translation and 1ms fast quench. The peak pushing force from the primary plate against the bracket is 60~100 kN at the end of plasma translation and the peak force pulling the plate out of the bracket is 80~120 kN at the end of 1ms plasma disruption.

2) The Tresca stress of membrane plus bending in primary plates during disruption is less than ~200 MPa and the stress in secondary plate is smaller. Although stress in regions near the corner bolts is higher than 200 MPa, it is still lower than the stress limit for CuCrZr. The maximum deflection of the plate during disruption is less than 5 mm.

3) Results show higher stresses in the corner bolts due to bending and twisting of the plate with non-uniformly distributed eddy current loop during disruption. The linearized stress in worst corner bolt is ~280 MPa membrane stress and ~445 MPa membrane plus bending stress. The current 3/8" corner bolts are recommended to be replaced with larger size bolts – at least ½" bolts with Fine Grade 2 or replaced with higher strength bolts such as Inconel bolts.

4) The peak net toroidal current in the plate is 250~300 kA. This is from the worst case for P1 to P5 VDE and fast disruption.

5) To be consistent with Hatcher's 2D model, a close to circular plasma shape is used in my final analysis. Plasma shape has some limited impact on the net disruption loads but skin depth, which is missing in the 2D model, is the most dominant factor.

6) Dynamic Amplification Factor – Results from dynamic analysis with 0.5% damping factor for the disruption cases we studied show a relatively small dynamic response, the dynamic amplification factor is ~1.1.

7) Impact of halo current during disruption on the passive plate is still under investigation but not included in my current analysis.

8) Instead of using the worst background field from all scenarios, current scenario #79 is used for coil background field and the real background field spatial distribution is represented in the new 3D model. It is possible to explore current scenarios with the worst background field but it will take some time and the transient field from plasma disruption is far more important than the influence from the background.

2. OPERA 3D Model

The NSTX PF, OH, TF coils, and a 60 degree OPERA 3D model of the passive plates with support bracket, vacuum vessel and center stack casing are shown in Figure 1. The small fringe fields of TF flex joints are neglected for the purpose of this analysis. All TF, PF and OH coils are treated as Biot-Savart conductors in OPERA to extract magnetic background field distribution of coils anywhere in 3D space without involving finite element analysis. The model with PF and OH coils only is used for benchmark the OPERA 3D model against Woolley Design Sheet and Willard 3D Maxwell model to ensure that the Opera model produces an accurate fringe fields.

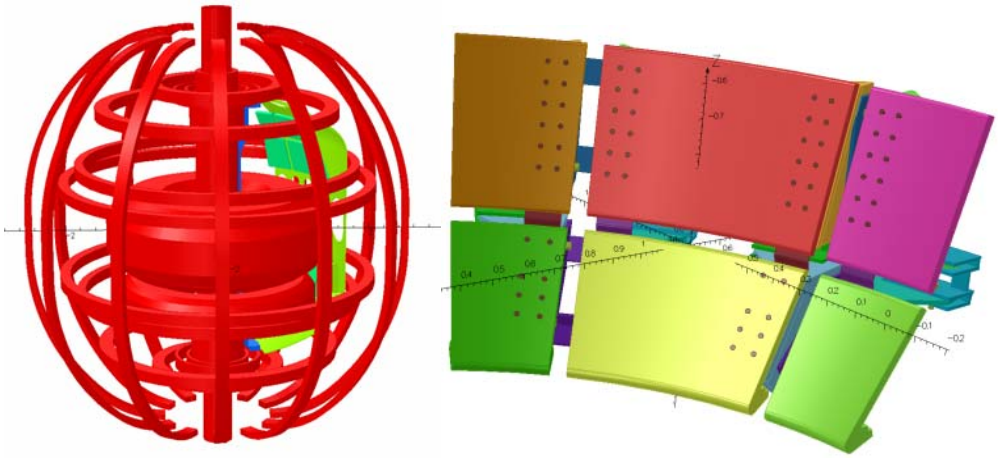

Figure 1 - NSTX PF, OH, TF coils with 60 degree model of passive plates and support bracket, VV and CS casing (left); passive plates, support brackets and connecting bolts only (right)

The right panel of Figure 1 presents the 60 degree model of passive plates, its support bracket as well as the connecting bolts – 14 bolts on each side of the primary plate and 10 bolts on each side of the secondary plate (2 bolts are missing in secondary plate due to 3D meshing difficulty). The electrical conductivity and corresponding skin depth during 1 ms fast disruption of each material are listed in Table 1. For a 1 ms fast disruption, the eddy current penetrates only 2.25 mm into CuCrZr passive plates. For 10 ms slow VDEs, the skin depth is ~6-7 mm, still only half of the ½" plate thickness.

Table 1 – Electrical conductivity and skin depth during 1ms disruption

	Conductivity (S/m)	Skin depth
Passive Plate	5.07×10^{7} (85% Cu)	2.25 mm
Bracket	1.389×10^{6} (SS)	13.7 mm
VV	1.389×10^{6} (SS)	13.7 mm
CS Casing	0.7576×10^{6} (INCONEL)	18.3 mm

Several different plasma shapes are used in the 3D model for disruption analysis. Our results show plasma shape has a limited impact (<5-10%) on the disruption load. To be

consistent with Hatcher 2D model, a close to circular plasma shape is used in the following analysis.

3. Model Validation

The NSTX background magnetic fields for upgrade from the 3D model are benchmarked against 3D Maxwell results as well as that from Woolley Design Sheet (Zhai, 2011) in the vacuum pump magnetic shielding analysis. The field from a close to circular shape plasma during disruption has also been checked against Ron Hatcher 2D OPERA analysis using the same averaged electrical conductivities for the passive plate as shown in Table 2. However, the skin depth of LPP used in Hatcher model at 1 ms disruption is 18 mm (more than the plate thickness) and the skin depth increases to 57 mm for 10 ms VDEs.

Table 2 – Electrical conductivity (S/m) used in Hatcher 2D OPERA model

upper primary PP	8.387×10^5
upper secondary PP	6.113×10^5
lower primary PP	8.207×10^5
lower secondary PP	6.668×10^5
VV	1.389×10^6 (SS)
CS Casing	7.576×10^5

Figure 2 presents the plasma disruption scenarios defined in the GRD for NSTX upgrade. Figures 3 and 4 present the comparison of radial and vertical magnetic field between Hatcher 2D cyclic symmetric model and Zhai 3D cyclic symmetric model from circular plasma at 10 ms during P1-P5 slow VDEs. For model validation, the same conductivities listed in Table 2 from measurement data are used in my cyclic symmetric OPERA model. The field contour lines shown in left panels agree well with color contours shown in the right panels from OPERA 3D model. Looking at the cross section of the plate, the radial field penetrates through lower secondary plate from ~0.9T in the middle of the front surface to ~0.6-0.7T at the plate back surface. This is because the averaged electrical conductivity shown in Table 2 is used for the plate, and therefore skin depth is much larger than that of copper conductivity during disruption. The magnetic field during disruption penetrates into the plate.

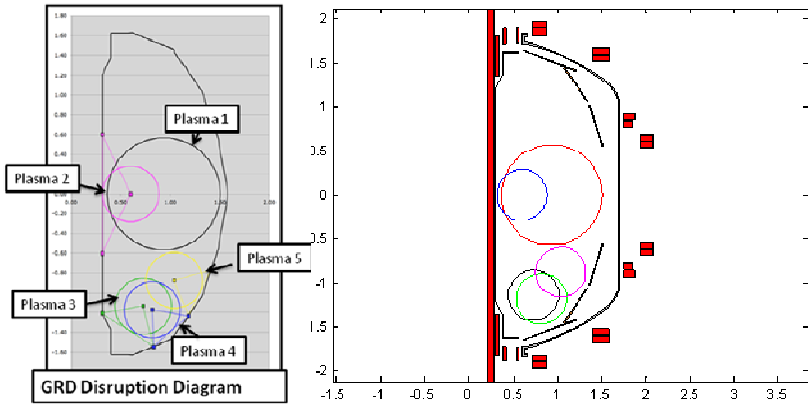

Figure 2 – Plasma disruption scenarios described in GRD; we focus on mid-plane disruption (P1- 1ms) and P1-P5 Slow and Fast VDEs.

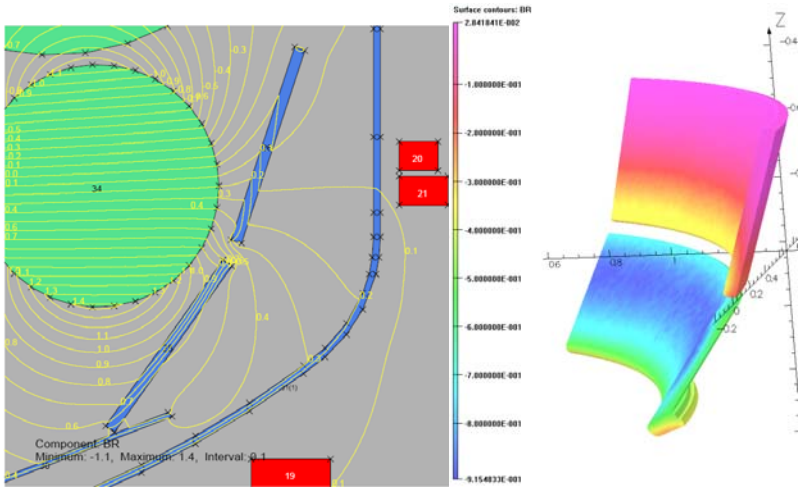

Figure 3 – Radial field (in Tesla) from cyclic symmetric models (Left-Hatcher and Right-Zhai) during P1-P5 Slow VDE at 10 ms; close agreement if same material property in Table 2 is used

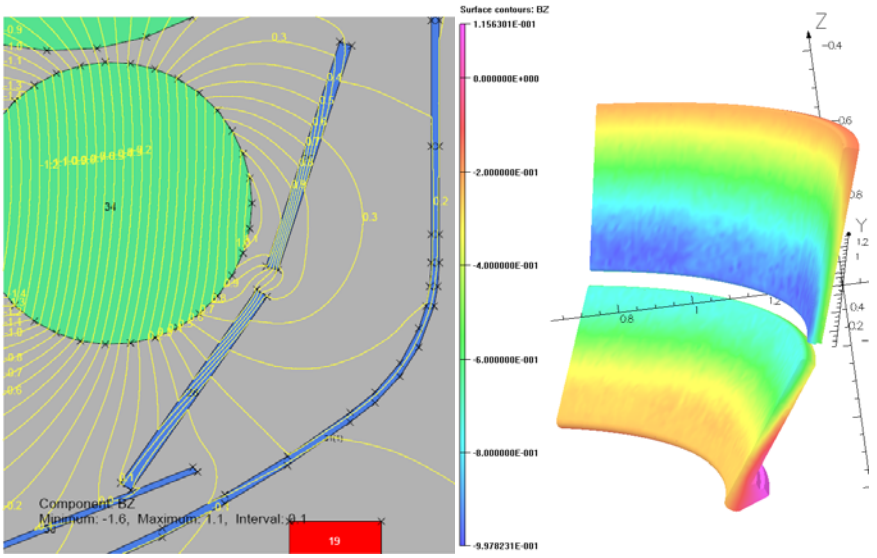

Figure 4 – Vertical field (in Tesla) from cyclic symmetric models (Left-Hatcher and Right-Zhai) during P1-P5 Slow VDE at 10 ms; very close agreement if same material property is used

Figure 5 presents the radial (left) and vertical (right) fields using copper conductivity from circular plasma for the cyclic symmetric model at 10 ms during P1-P5 slow VDEs. Very different from the above figures, the field penetrates into only a fraction of the plate thickness during disruption due to skin effect. Part of the plate in the back is shielded by eddy current flowing in front surface. Therefore, the net peak eddy current load is much smaller than that from the model using plate and bracket averaged conductivity during disruption.

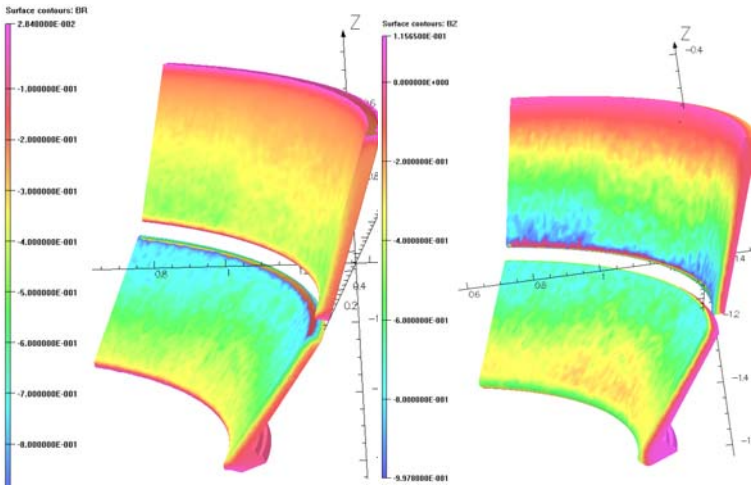

Figure 5 – Radial (left) and vertical (right) fields during P1-P5 slow VDE at 10 ms from cyclic symmetric models using CuCrZr conductivity – skin depth clearly seen through plate thickness

4. Match of Electrical Conductivity

Since Hatcher 2D cyclic symmetric OPERA model cannot model both copper plates and the SS support bracket, directly measured copper plate and SS bracket averaged electrical conductivity is used (see Table 2 – more than an order of magnitude smaller than CuCrZr). Therefore, skin depth effect is not captured in this 2D model as shown in above Figures – magnetic field penetrates through 1/2" copper plate which makes the disruption forces highly overestimated.

In the 3D OPERA model, due to the 3D meshing difficulty, the passive plates are connected with support bracket only through the long bolts without the steel plate behind the passive plate. Therefore, the electrical conductivity of SS bolts and bracket is adjusted to match exactly the measured conductivity for the eddy current loop consisting of passive plates, bracket and the vacuum vessel. To match the overall electrical conductivity used for cyclic symmetric model, TOSCA Current Flow solver in Vector Fields is used and 2 60 degree sector models are created as shown in Figure 2.2. In the first model, measured conductivity from Table 2 is used and net conductance for the 60 degree sector is obtained by applying 0 volt at one side and 1 volt at the other side to force current flow into the plate. In the second model, plate, bolt and bracket are included to form the conducting path from plate to bolt and bracket so eddy current flows to the vessel. The same voltage conditions are applied to obtain the net conductance for the 60 degree sector. The resistance or conductance is matched by adjusting conductivity in the bolt and the bracket. The results are in Table 3.

Table 3 – Electrical conductivity (S/m) matched with measurement for 3D disruption analysis

	Conductivity (S/m)
Passive Plate	5.07×10^7 (85% Cu)
Bracket	2.1×10^6
Bolts	5.0×10^7

The peak disruption force increased ~20% compare to previous results using steel conductivity (instead of the matched conductivity in connecting bolt and support bracket). The peak disruption moment on primary plate, however, is slightly reduced by a small fraction. Figure 6 presents the eddy current disruption in the lower plates during P1-P5 slow VDE from the OPERA 3D model. Figure 7 presents eddy current distribution in the plates during P1-P5 slow VDE at 10 ms.

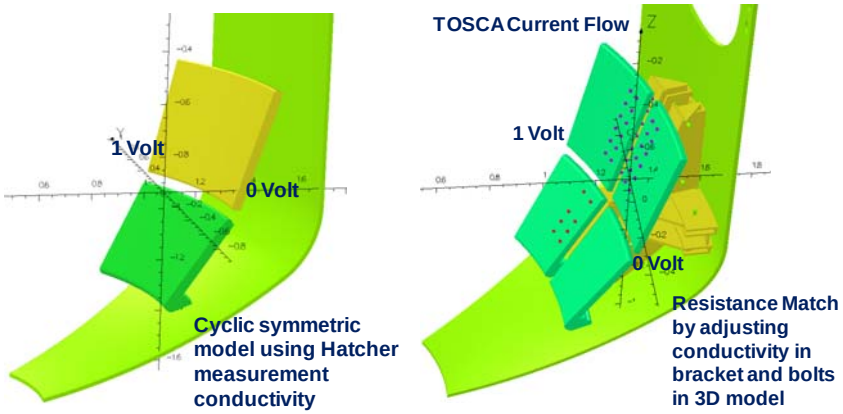

Figure 6 – Net current through cross section of lower PP, SP during P1-P5 slow VDE at 10 ms

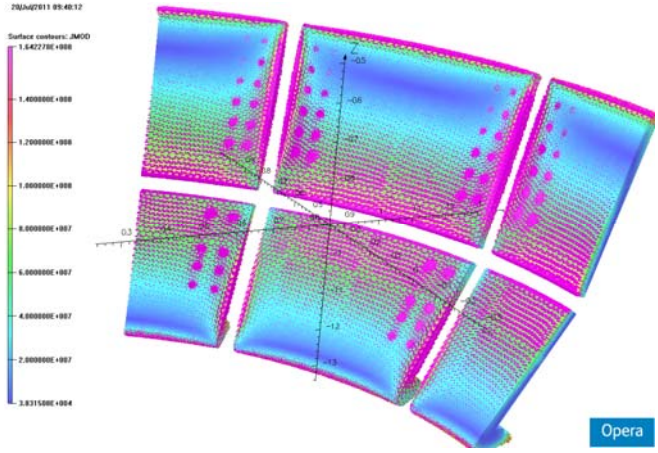

Figure 7 – Eddy current flowing in plates during P1-P5 slow VDE from 3D OPERA model

5. Disruption Loads

Disruption force and moment on the passive plate are extracted for stress analysis. Figure 8 presents the transient toroidal current flowing in the lower primary and secondary plates during disruption. Figure 9 and Figure 11 present the net disruption forces and moments on the primary and secondary plates respectively. Figure 10 presents the elemental force mapped onto the ANSYS structural model. The moment is given at the center of the passive plate.

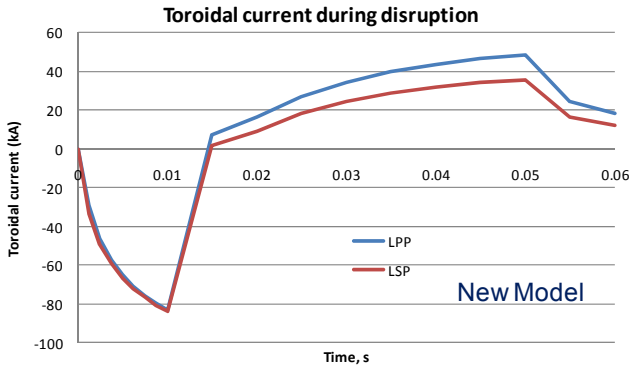

Figure 8 – Net current through cross section of lower PP, SP during P1-P5 slow VDE at 10 ms

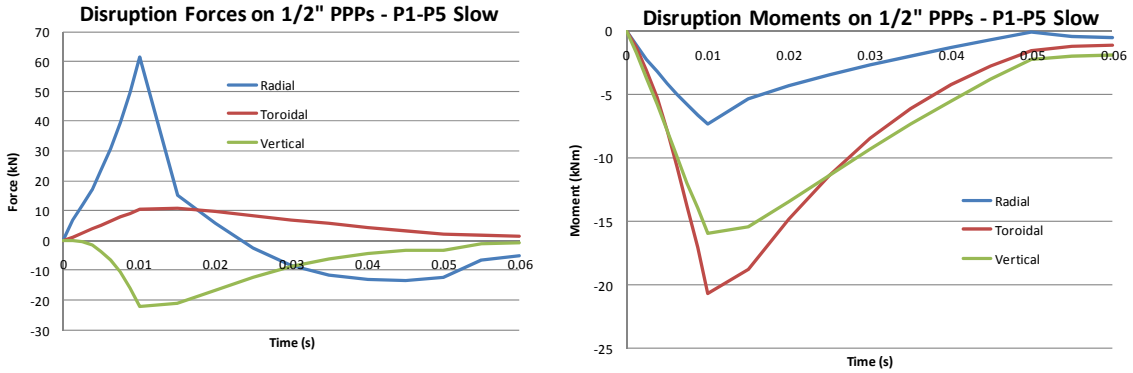

Figure 9 – Disruption force and moment on Primary PP during P1-P5 slow VDE at 10 ms – SS conductivity for bolts and bracket

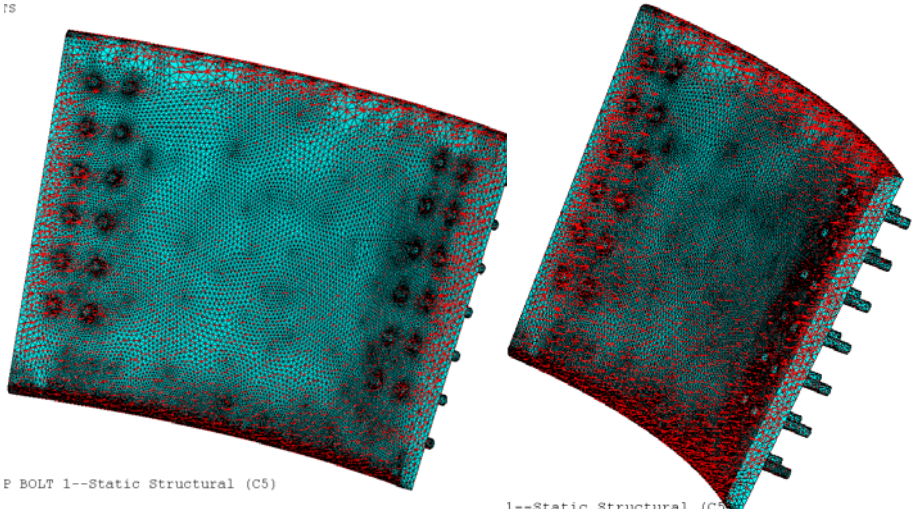

Figure 10 – Disruption forces on PPP during P1-P5 slow VDE at 10 ms from OPERA mapped onto ANSYS structural model

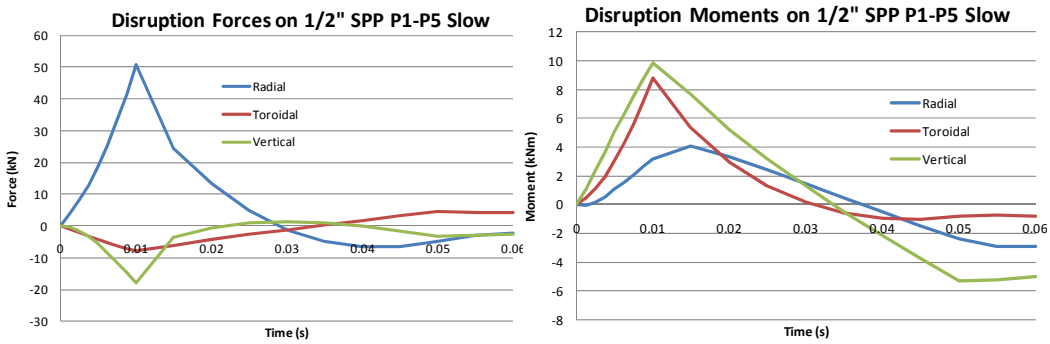

Figure 11 – Disruption loads on Secondary PP during P1-P5 slow VDE at 10 ms – SS conductivity for bolts and bracket

Figure 12 (P1-P5 VDE slow) and Figure 13 (P1-P5 VDE fast) present the net disruption forces and moments on the primary and secondary plates respectively using matched conductivities for bolt and bracket. The peak force increased ~20% but the peak moment is about the same compare to that from SS conductivity for bolt and bracket.

P1-P5 Slow Disruption Force and Moment on ½" Passive Plate

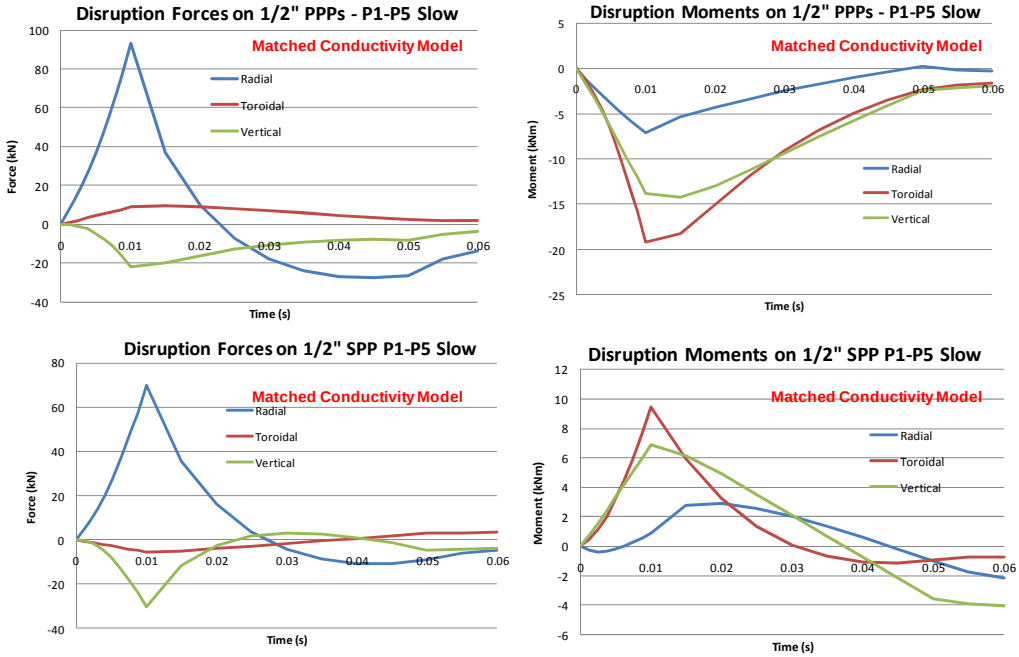

Figure 12 – Disruption loads on Secondary PP during P1-P5 slow VDE at 10 ms – matched conductivity for bolts and bracket (Table 3)

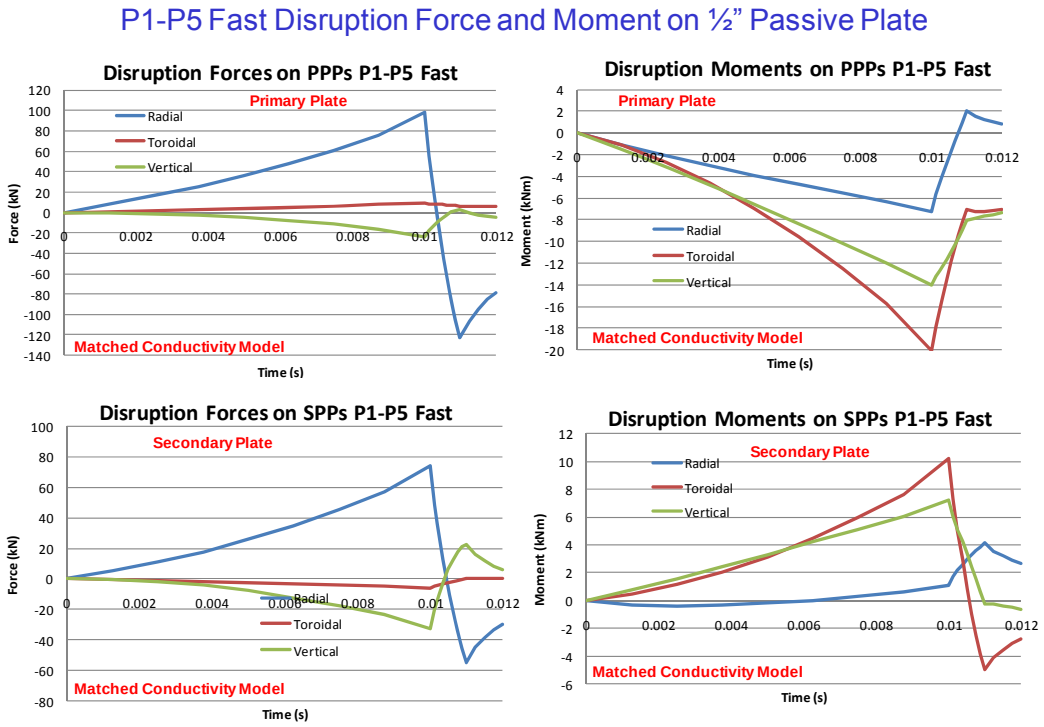

Figure 13 – Disruption loads on Secondary PP during P1-P5 fast VDE at 10 ms – matched conductivity for bolts and bracket (Table 3)

In both Figure 12 and 13, during the 10 ms P1-P5 translation, the disruption force is pushing the passive plate against the support bracket (positive radial force), but the force changes polarity during plasma disruption and it becomes pulling force to pull the plate off from the bracket. The peak pushing force is ~100 kN at the end of 10 ms plasma translation and the peak pulling force is ~120 kN at the end of the P1-P5 VDE fast quench as shown in Figure 13.

6. Static Structural Analysis

Static structural analysis is performed after mapping of the elemental forces onto the ANSYS structural model.
Figure 14 presents the deflection and Tresca stress distribution of the primary plate from static analysis under peak disruption force at 10 ms during P1-P5 slow VDE. The maximum deflection is ~1.2 mm.
Figure 14 also presents the stress intensity and the linearized stress from static analysis for P1-P5 slow VDE. The membrane stress and membrane plus bending stress are less than 100 MPa. The linearized stress on secondary plate is small because the peak disruption force on the secondary plate is smaller as shown in Figure 12.

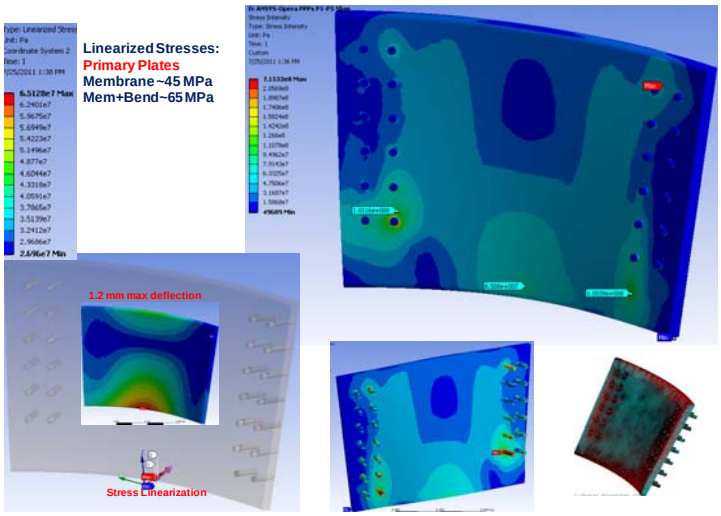

Figure 14 – Disruption force and moment on Secondary PP during P1-P5 slow VDE at 10 ms

7. Dynamic Stress Analysis

To understand the dynamic effect on passive plates during disruption, a full structural dynamic analysis of PP to obtain the Dynamic Amplification Factor (DLF) is performed. Basically, the time dependent elemental forces are mapped onto ANSYS structural model and the deflection and stress level are compared to results from static analysis. A damping ratio of 0.5% - mass to stiffness damping constant is used (the same as that used in Pete Titus calculation). Figure 15 presents the deflection on lower PP at 10 ms during P1-P5 VDE slow. Listed below is the ANSYS APDL commend to implement the dynamic analysis. Figure 17 presents the Tresca stress from the static and dynamic analysis.

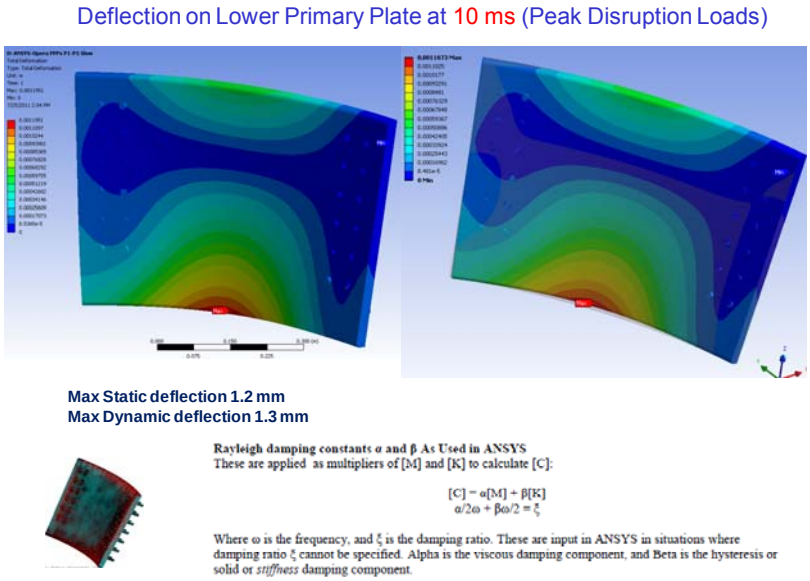

Figure 15 – PP deflection from static and dynamic analysis for P1-P5 slow VDEs; DLF is ~1.1.

```
/solu
antype,4  !use 4 for dynamic analysis
outres,all,1
!Output times:
```

```
t1=1e-5
t2=1.25E-3
t3=2.50E-3
t4=3.75E-3
t5=5.0E-3
t6=6.25E-3
t7=7.5E-3
t8=8.75E-3
t9=0.01
t10=0.015
t11=0.02
t12=0.025
t13=0.03
t14=0.035
t15=0.04
t16=0.045
t17=0.05
t18=0.055
t19=0.06
nsubst,5
betad,0.000008
alphd,12.56
kbc,0
fdele,all,all
time,t1
/input,C:\NSTX\lp_p1p5sw_1,fxyz
lswrite,1
time,t2
fdele,all,all
/input,C:\NSTX\lp_p1p5sw_2,fxyz
lswrite,2
….
time,t19
fdele,all,all
/input,C:\NSTX\lp_p1p5sw_19,fxyz
lswrite,19
lssolve,1,19,1
```

Deflection on Lower Primary Plate at 10 ms (Peak Disruption Loads)

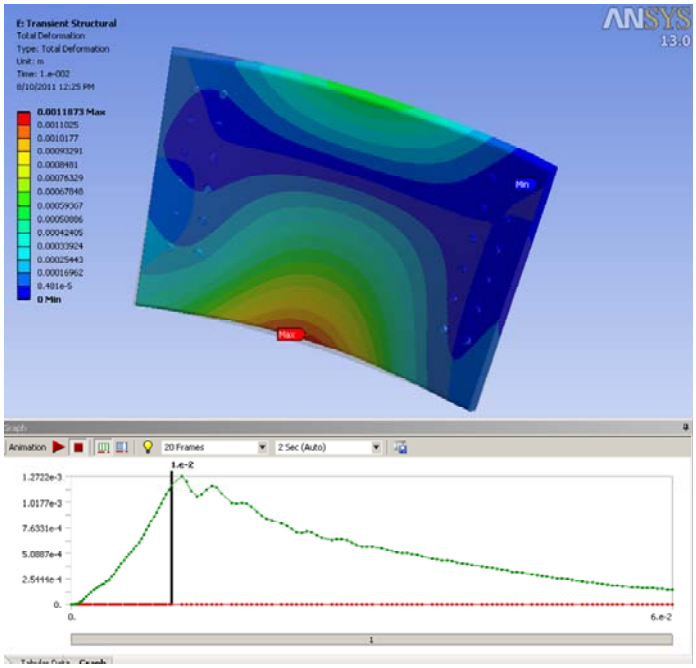

Figure 16 – Deflection of lower PP during P1-P5 slow VDE at 10 ms; bottom panel presents transient max deflection in the plate where dynamic effect is seen.

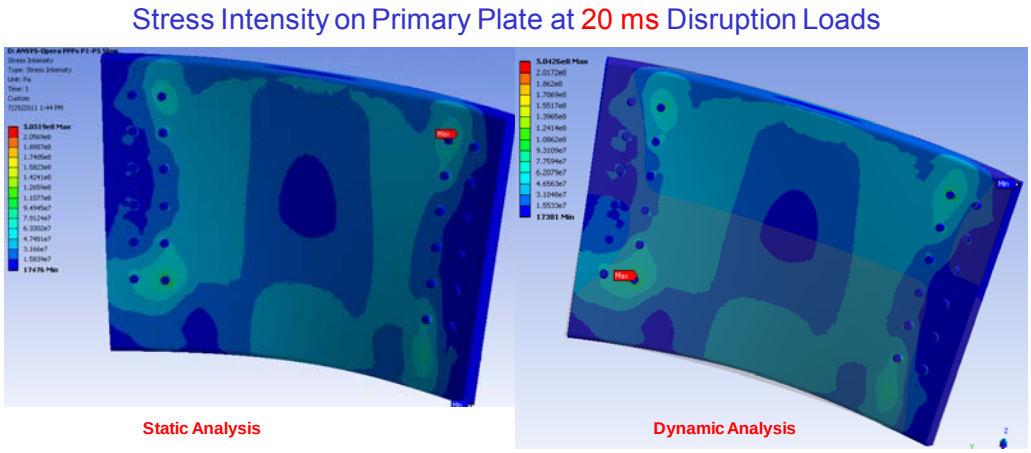

Figure 17 – Tresca stresses of lower primary PP during P1-P5 slow VDE at 10 ms;

8. Modal Analysis

Modal analysis has been performed to extract natural frequency of the plate and the mode shapes. Figures 18 and 19 present the first four mode shapes of the lower primary plate. The natural frequencies from ~380-480 Hz are bigger than that from Pete Titus calculation mainly because in Pete's model, not only the plate but also the bolt, bracket and part of the vessel also included into the modal analysis. Therefore, the stiffness is smaller in Pete's model.

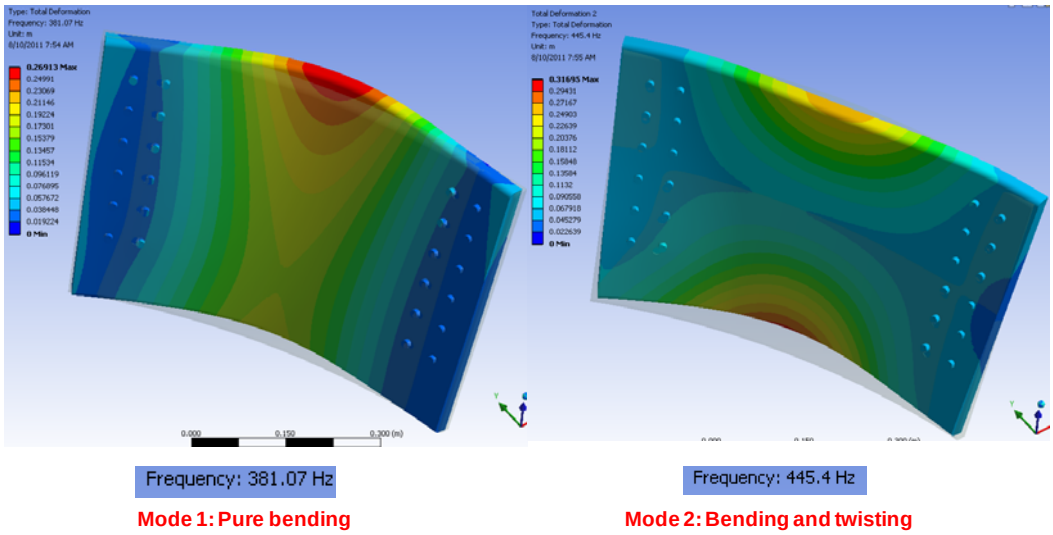

Figure 18 – Tresca stresses of lower primary PP during P1-P5 slow VDE at 10 ms;

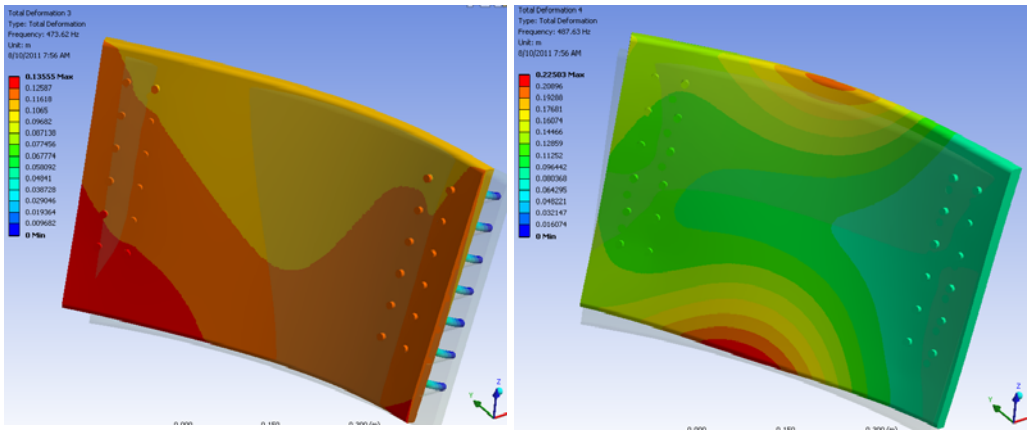

Figure 19 – Tresca stresses of lower primary PP during P1-P5 slow VDE at 10 ms;

9. Halo Current

Halo current impact on the passive plate during disruption is included in Pete's calculation report. Here I briefly review the results. Early study by Art Brooks showed that the time constant for establishing the halo current flow is fairly long relative to the disruption timescale (Brooks, 2010). Therefore, halo current will enter the vacuum vessel through the bracket behind the passive plate.

10. Structural Analysis with Better Layered Mesh and Corrected PP Thickness

An update on static structural analysis is performed with a finer and better layered mesh through the ½" plate thickness and with a corrected plate thickness – results from previous calculation are based on CAD model with a thicker plate. The new structural model also includes support bracket. The DC electrical conductivity match has also been rerun to reflect the change of actual plate thickness and inclusion of the support bracket. The LLD divertor is not included in the Opera model to be conservative. The max linearized membrane stress on the primary plate is smaller than 100 MPa but membrane plus bending stress is increased to about 200 MPa. The linearized stresses on the secondary plate should be smaller.
The following table presents the electrical conductivities of the PP components as conductivity of the integrated structure matches with the measured conductivity.

Electrical conductivity (S/m) - Matched

Passive Plate	5.07×10^7 (85% Cu)
LPP Bracket/bolt	5.2×10^5
LSP Bracket/bolt	1.0×10^6
VV	1.389×10^6 (SS)
CS Casing	0.7576×10^6 (Inconel)

Electrical conductivity - Measured

upper primary PP	**8.387×10^5**
upper secondary PP	**6.113×10^5**
lower primary PP	**8.207×10^5**
lower secondary PP	**6.668×10^5**

Figures 20-22 present eddy current, disruption loads and a new structural model with bracket, better layered mesh and corrected PP thickness during P1-P5 VDE fast. The maximum deflection is ~5 mm.

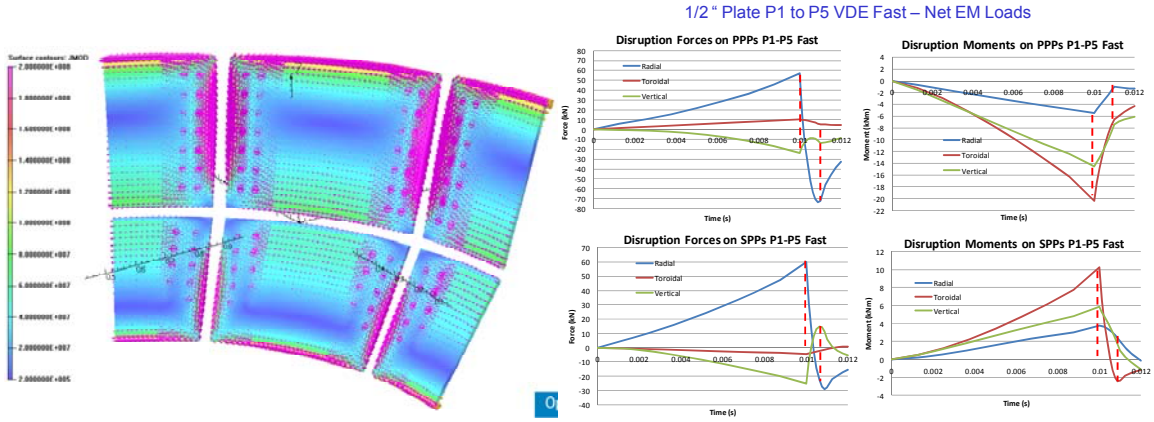

Figure 20 – Eddy current and disruption load on primary PP during P1-P5 VDE fast

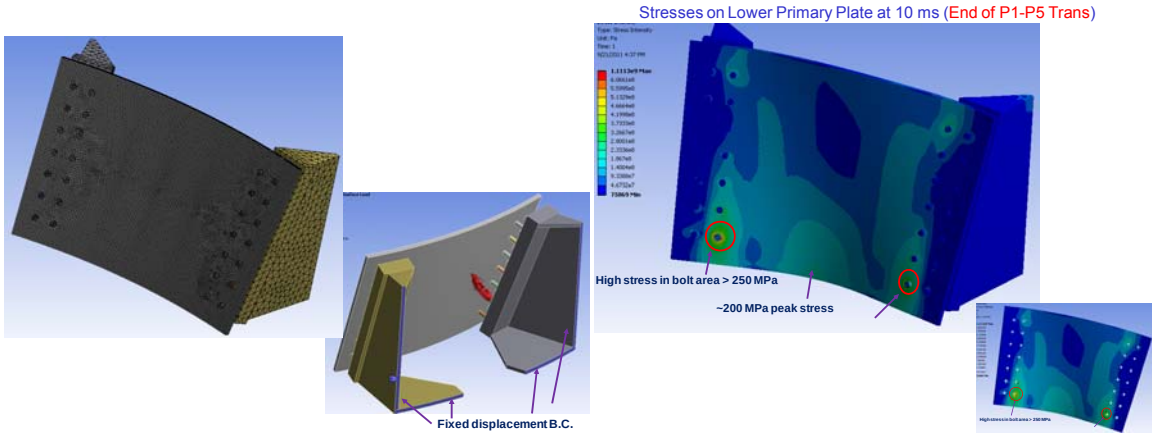

Figure 21 – Structural model with bracket, better layered mesh and stress distribution on primary PP during P1-P5 VDE fast

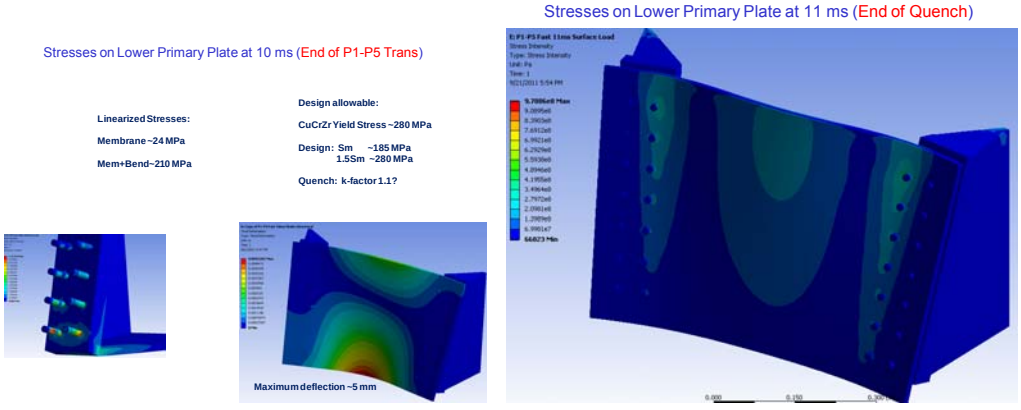

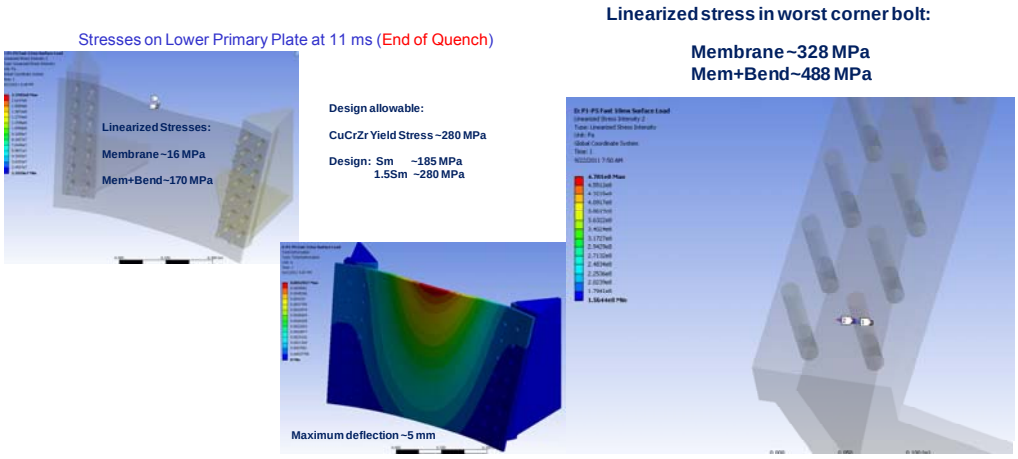

Figure 22 – Linearized stress from new structural model and stress distribution on primary PP at end of fast quench (left) and end of P1-P5 VDE translation (right)

11. Bolting Stress and Shear Stress in PP Counter-bore

The peak force during disruption on the primary plate is ~60 kN at the end of the P1-P5 slow VDE and the plasma current pushing the plate against its support bracket; the peak pulling force during disruption on the primary plate is ~75 kN at the end of 1ms fast plasma quench after a 10 ms P1-P5 VDE plasma translation.
The big pulling/pushing force plus bending of the plate due to non uniform distribution of eddy current flowing in the plate is a major concern for the 3/8" bolts, particularly for the close to corner bolts. The linearized stress in worst corner bolt at end of fast quench (pulling force) is ~200 MPa membrane stress and the linearized stress in worst corner bolt at end of P1-P5 translation (pushing force) is ~328 MPa membrane stress. The tensile force on the worst corner bolt during disruption due to pulling of the plate is 200e6*0.01187*0.0128*0.2248=~ 6,831 lbs. The pushing force on the worst corner bolt due to pushing force is ~11,263 lbs. The normal stress on the bolt hat will be 11263/(pi*(0.61^2-0.4^2)/4)=68 ksi=468 MPa. Inconel718 bolts of the same size (3/8") will be used to replace the existing steel bolts.

With the old washer design, the Tresca shear stress in passive plate counter-bore due to pulling force is ~132 MPa. 6,831/(1.01*pi*0.225)=9,568 psi and equivalent Tresca stress = 19,136 Psi ~132 MPa. If we consider dynamic rebound force at end of P1-P5 translation (rebound of pushing force – assuming 80%), the shear stress in passive plate counter bore is 11263*0.8/(1.01*pi*0.225)=12,621 psi ~ 87 MPa and equivalent Tresca stress is 174 MPa.

With the new washer and bushing design, the effective shear area is 1.125*pi*(0.0625+0.275+0.225)=1.988 sq in and the shear stress in counter bore due to pulling force is 6,831/1.988=3,436 psi and equivalent Tresca stress is 6.9 ksi. The shear stress due to dynamic rebound of pushing force is 11,263/1.988=5.66 ksi and equivalent Tresca stress is 11.33 ksi < 20 ksi

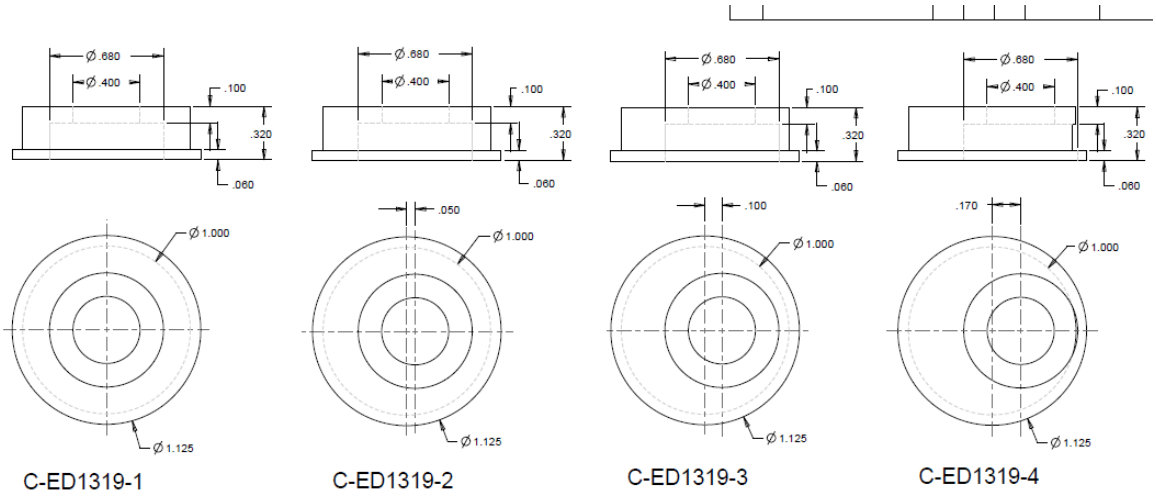

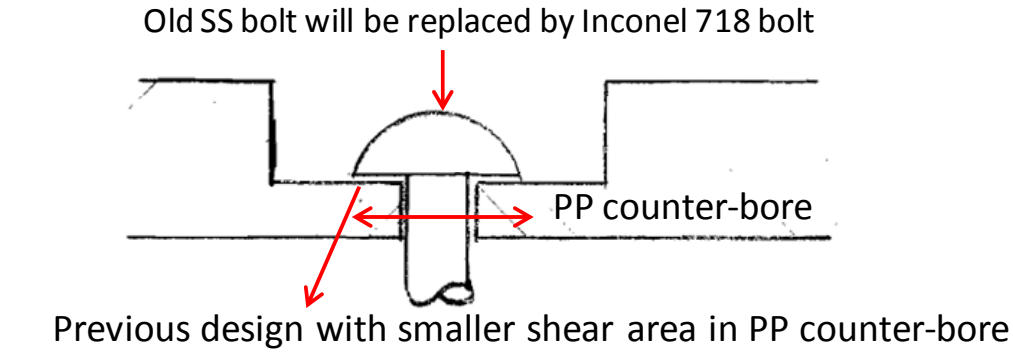

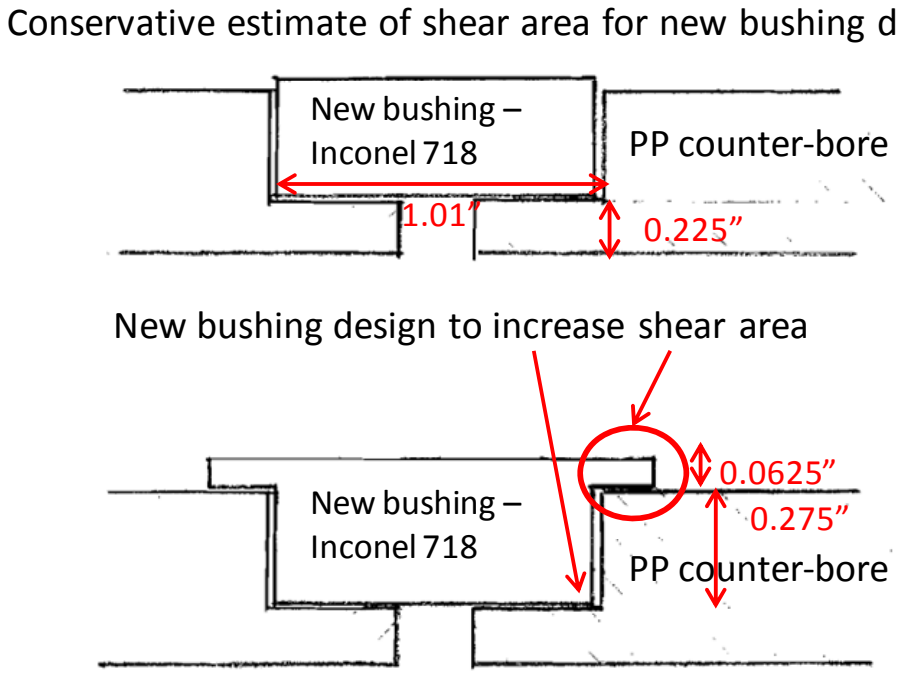

Figure 23 – New bushing design for the passive plate

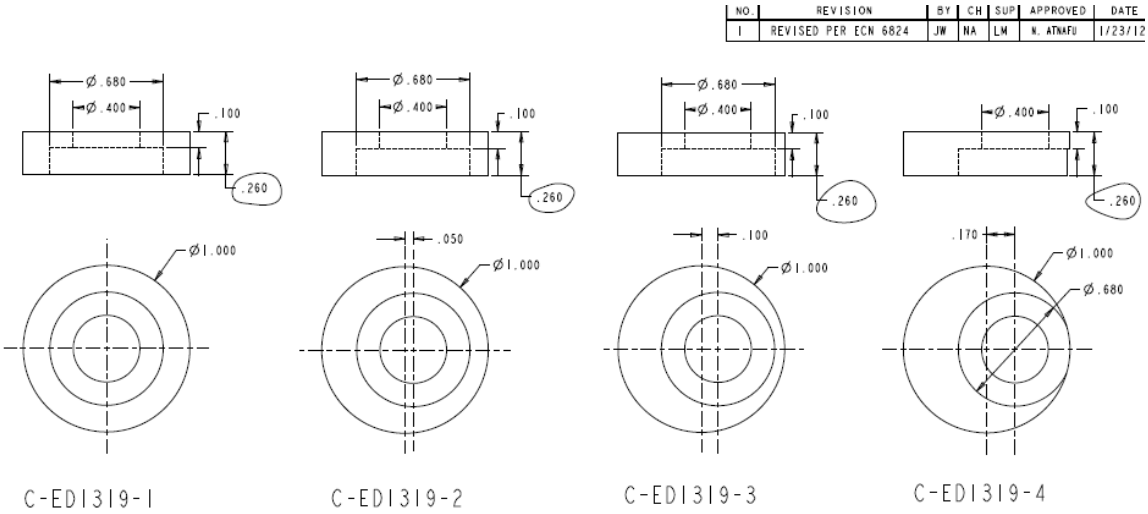

Figure 24 – Newly revised bushing design – washer without lips for the passive plate (from Neway Atnafu)

With the newly revised bushing – washer without lips shown in Figure 24, the PP counter-bore shear stress due to pulling force is rechecked during disruption – with the conservative calculation of washer/bushing shear area (remove the .06" lips).

With a total 75 kN pulling force per PP during P1-P5 fast disruption – no more than 20-30 kN pulling force on the worst bolt, the counter bore shear area is 1.01*pi*0.225=0.71393 sq inch, shear stress in PP counter bore at worst bolt = 30kN*0.2248/0.71393=9.45 ksi ~65 MPa and the equivalent Tresca stress is 18.9 ksi (~130 MPa)<20 ksi. This shows that remove the washer bushing lips should still be good even if we take shear strength as half of the ultimate strength 320*0.5=160 MPa.

12. Conclusions and Discussions

The 3D disruption analysis showed that current ½" primary and secondary passive plates should be adequate for the upgrade. The large disruption force on the worst corner bolt, however, showed that corner bolts should be replaced with at least ½" bolt with Fine Grade 2 bolt or bolt with higher strength such as Inconel bolts.

13. References

1. “NSTX turbo pump magnetic shielding analysis”, Y. Zhai, PPPL NSTX-CALC-24-04-00, 16 March 2011.

2. "NSTX Upgrade disruption analysis of passive plates, vacuum vessel and components", P. Titus et al, NSTXU-CALC-12-01-01 Rev 1, April 2011.

3. “NSTX CSU General Requirements Document”, C. L. Neumeyer, NSTX_CSU-RQMTS-GRD, Revision 3, December, 2010.

4. "NSTX halo current analysis of center stack", A. Brooks, NSTX-CALC-133-05-00, April 13, 2010.

Attachment I
3D Disruption Analysis of Passive Plates for NSTX Upgrade
Prepared by P. Titus

Errors were found in the original analysis using vector potential transfer of OPERA axisymmetric vector potential data to the 3D EM and structural models. These errors were found by Y Zhai when attempting to duplicate results from the vector potential transfer method. The adjustments in the resistivity of the segmented passive plates in the axisymmetric OPERA model caused an overestimate of the eddy currents and loads when the vector potential solution from the OPERA model was applied to the ANSYS analysis models. Y Zhai recalculated the response of the passive plates in 3D OPERA and this is forming the basis for the evaluation of the passive plate mounting hardware. A check of Y. Zhai's calculation is needed because it does not agree with the vector potential transfer method. An independent confirmation of Y Zhai's calculations is needed.

To provide the independent confirmation, a 3D electromagnetic model of the NSTX tokamak was developed, similar to those used to qualify Antennas in C-Mod [19]

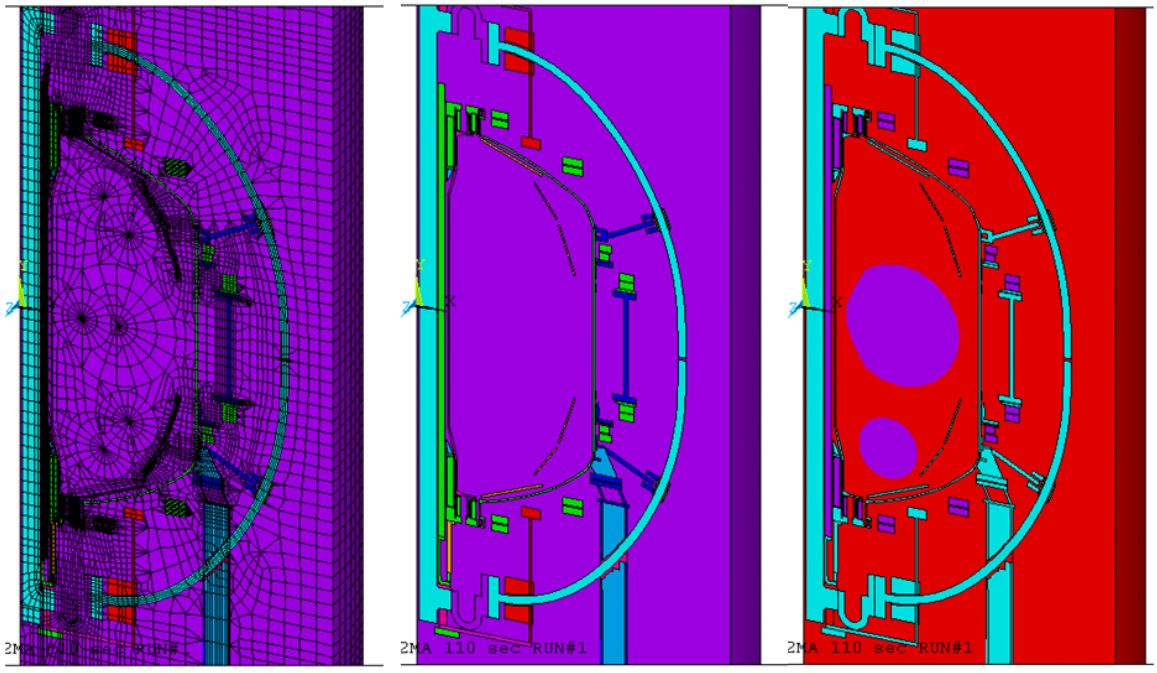

Mesh Materials Element Type

Figure I-1 ANSYS Electromagnetic Model, Mid slice of a 30 degree Cyclic Symmetry Model

The following plots are for the P1 to P4 10 ms VDE with a 2 ms quench

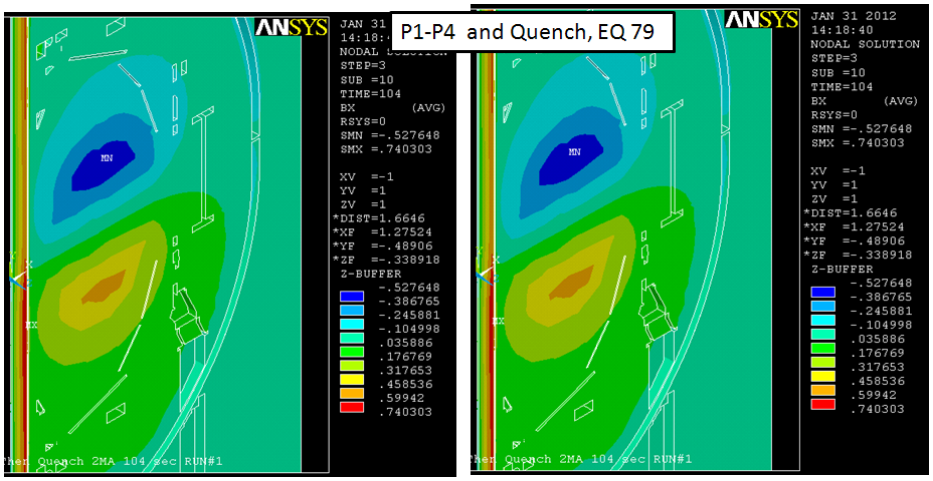

Figure I-2 Radial Field

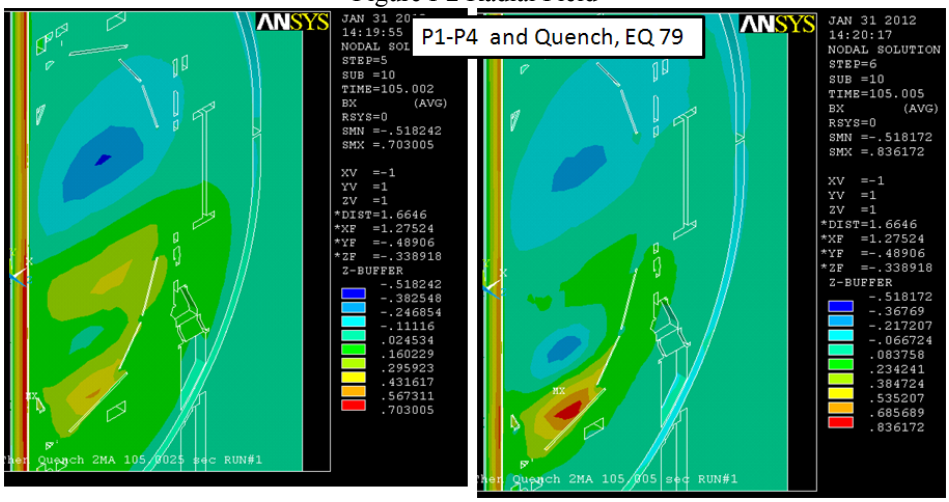

Figure I-3 Radial Field

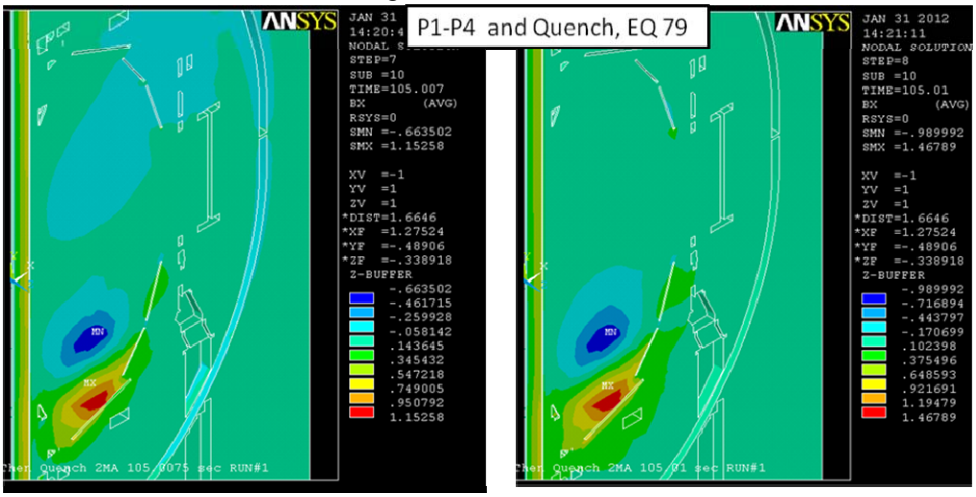

Figure I-4 Radial Field

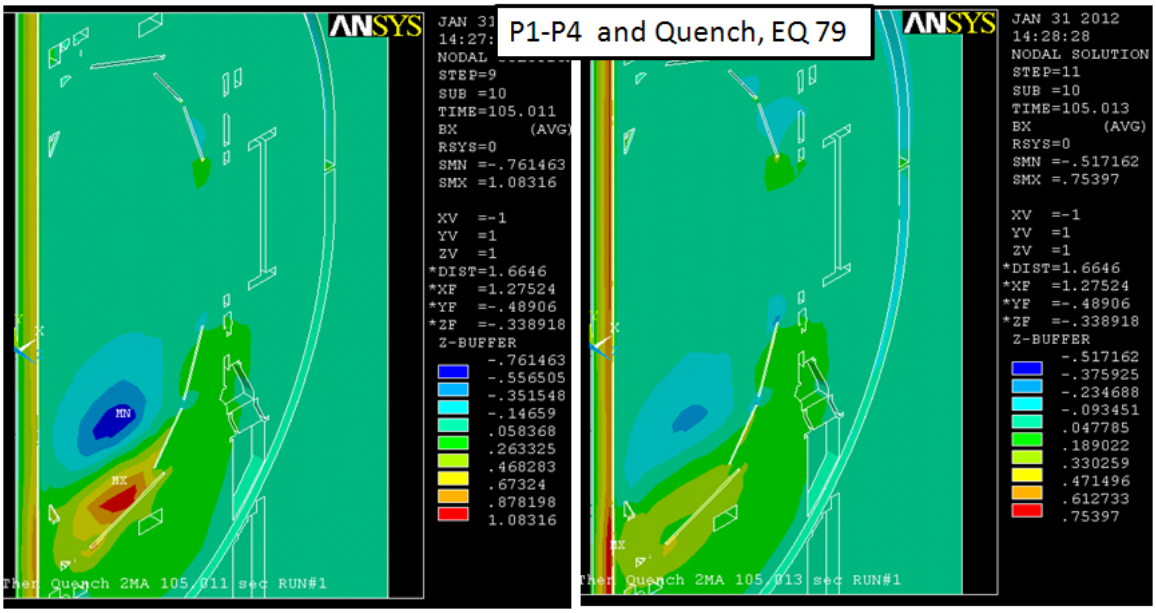

Figure I-4 Radial Field

The plots I-2 through 4 show the plasma movement and quench as they effect the radial field.

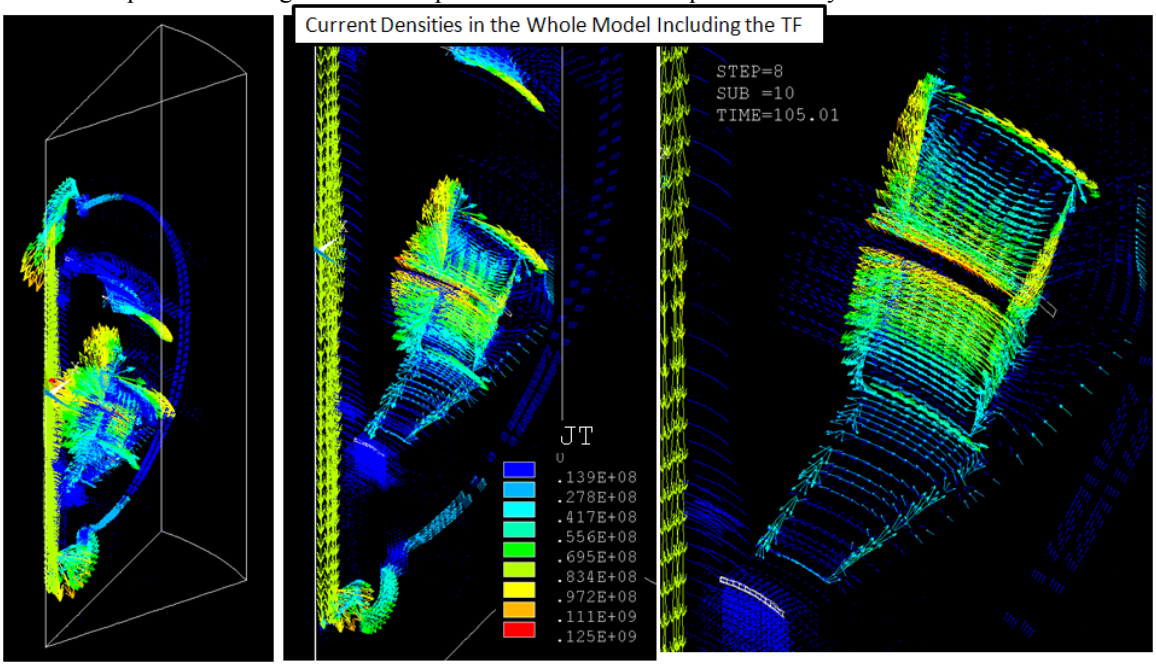

Figure I-5 Current Densities in the Whole Model Including the TF at Step 8 - P1-P5 End of 10ms VDE

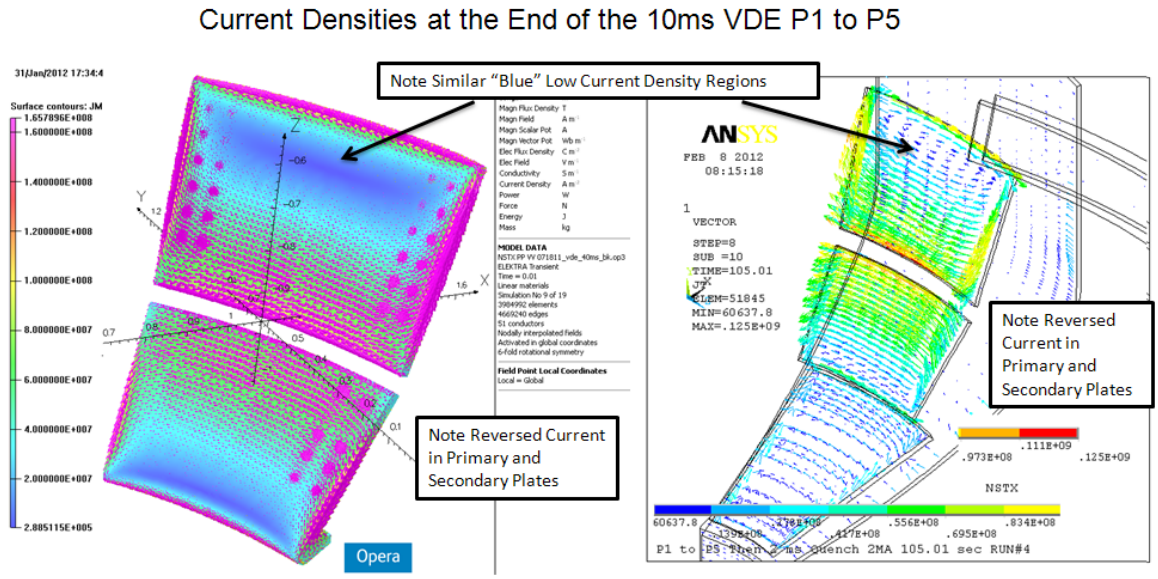

Figure I-6 Current Density Comparison

The plasma current is reversed in the two analyses, which accounts for the currents flowing in opposite directions in the two analyses.

Transient Analysis Results

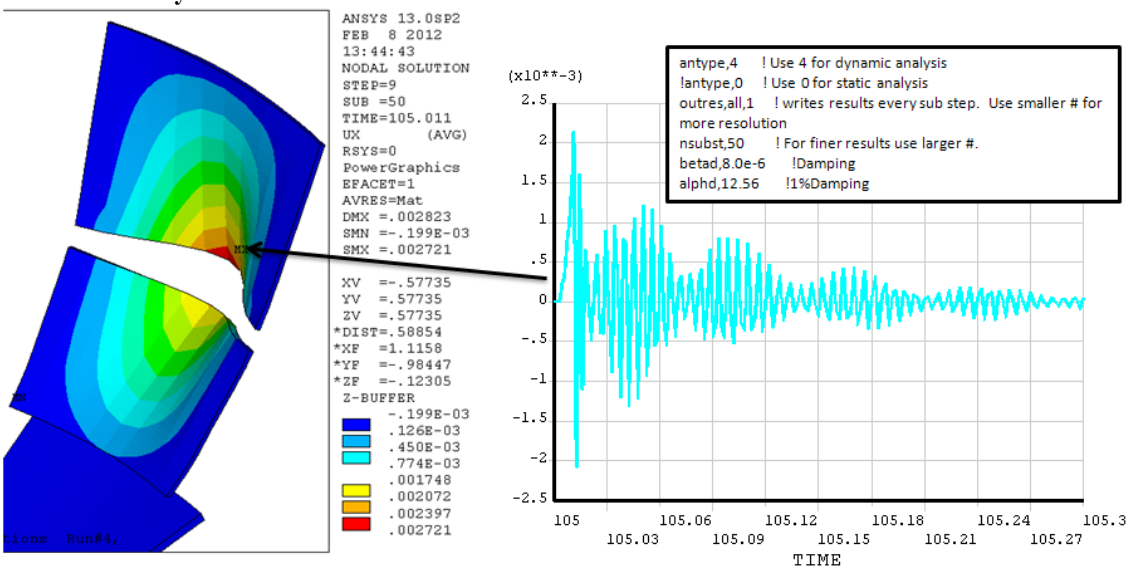

Figure I-7 Displacement Time History Showing Multiple oscillations of the Passive Plate

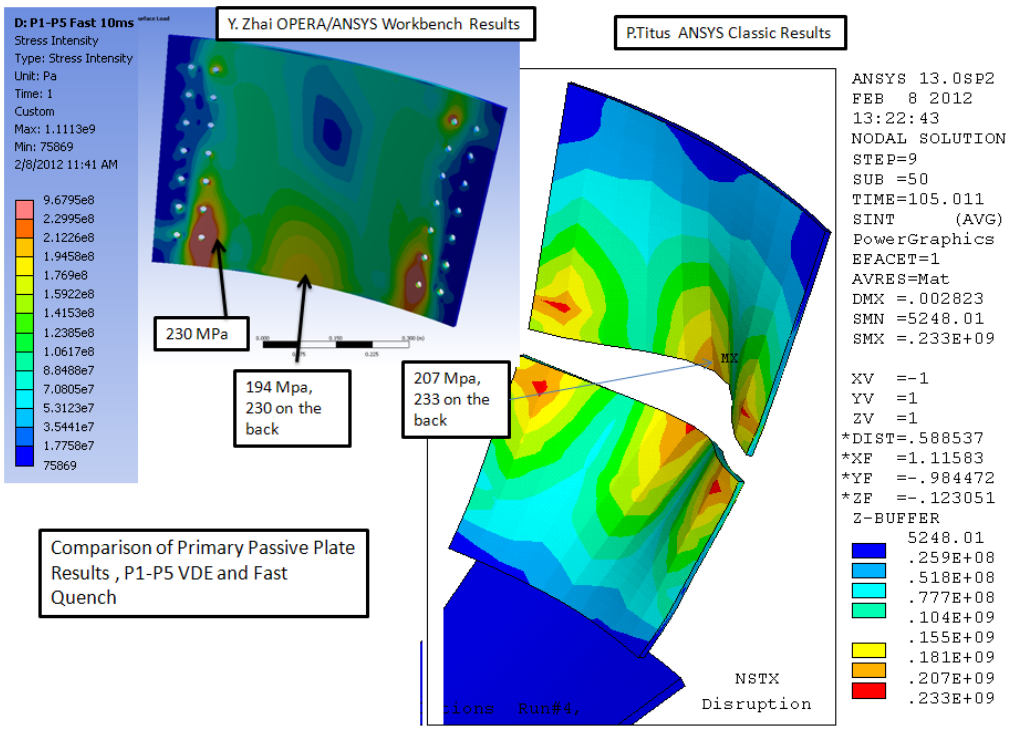

Figure I-8 Comparison of Primary Passive Plate Stress Intensity Results

The ANSYS Classic results are from the dynamic analysis and are the result of hunting around for the peak plate stress in the substeps of steps 8, 9 and 10

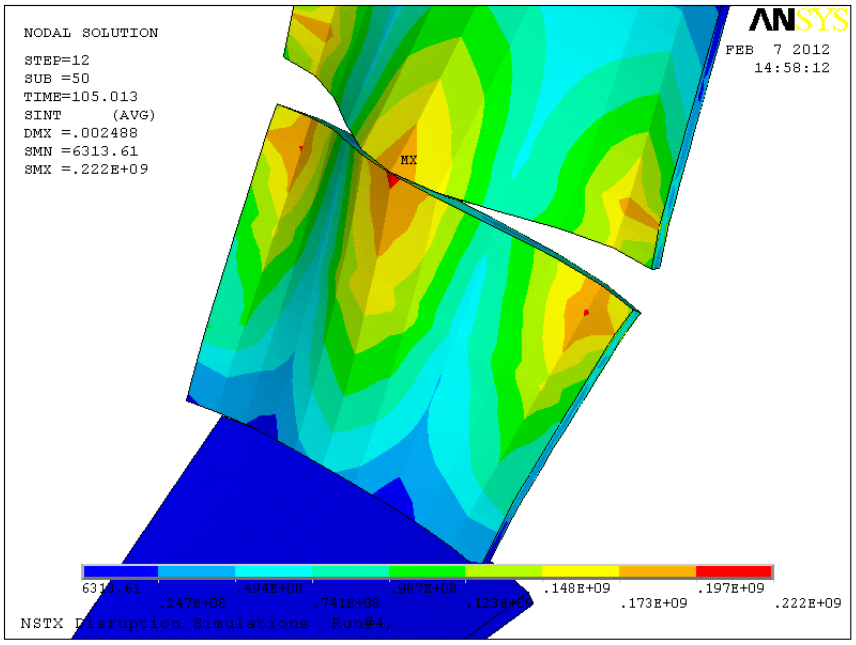

Figure I-8 Lower Passive Plates Stresses for the P1-P5 VDE and Quench Showing the Dynamic Rebound

Estimate of Bolt Stress

In the Titus/ANSYS Classic model, the bolt details are crudely modeled. However an important result to check is the attachment bolt load used to size the 718 inserts.

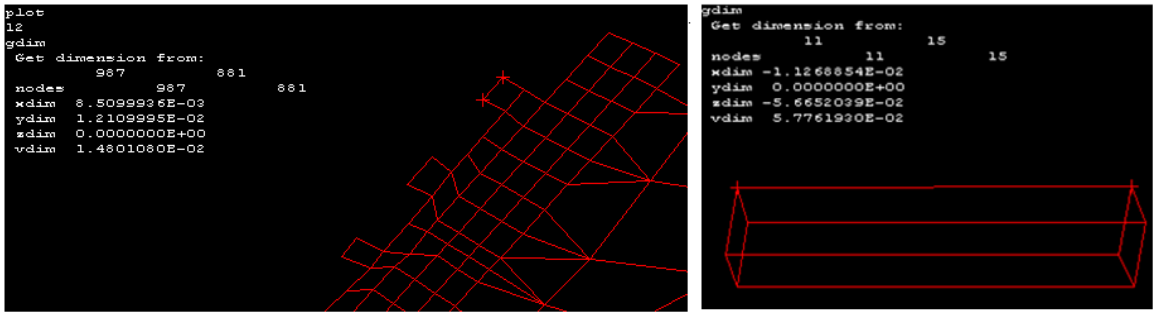

Figure I-9 Area of Rectangular FEA Block That Represents the Bolts

In Section H, the bolt load was calculated to be:

"no more than 20-30 kN pulling force on the worst bolt" or 6744lbs.

Estimates shown in the two following slides, produce 9442 lbs

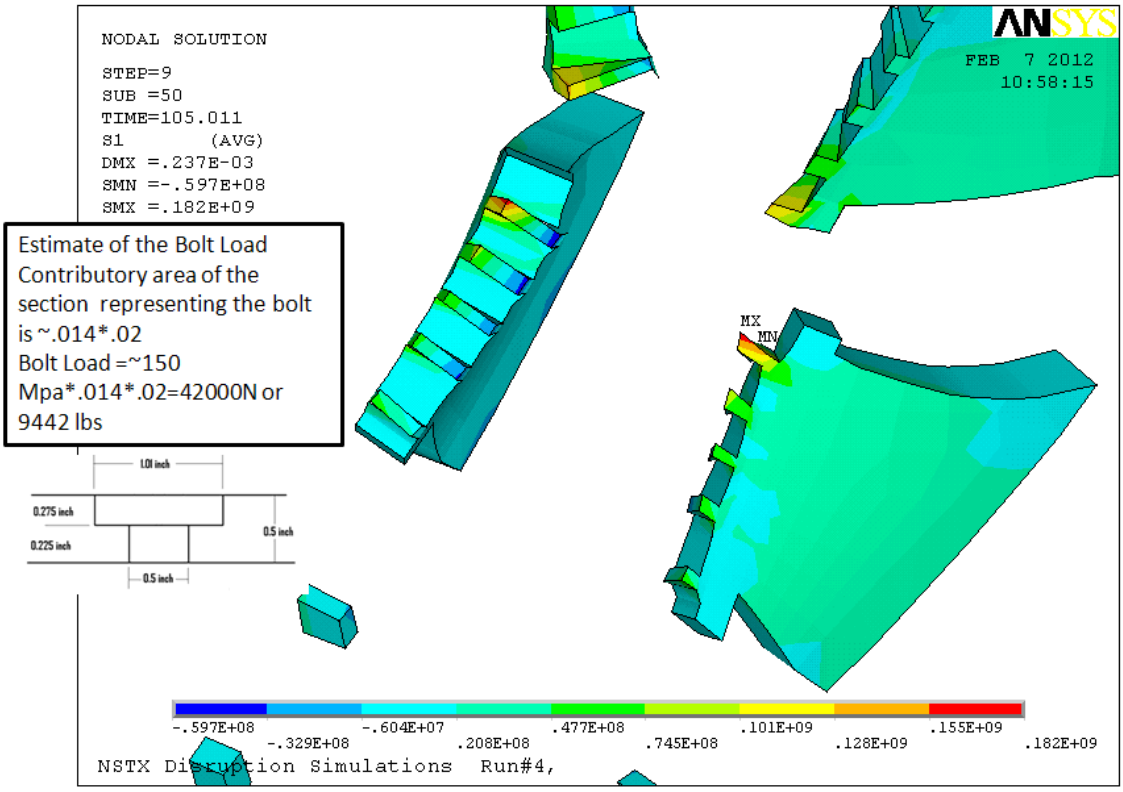

Figure I-10 Estimate of Bolt Load

The shear allowable is .6*Yield = .6*276 = 165.6 MPa or 24 ksi. The shear stress in the counterbore in the plates is 9442/pi/1/.225 = 13.3ksi

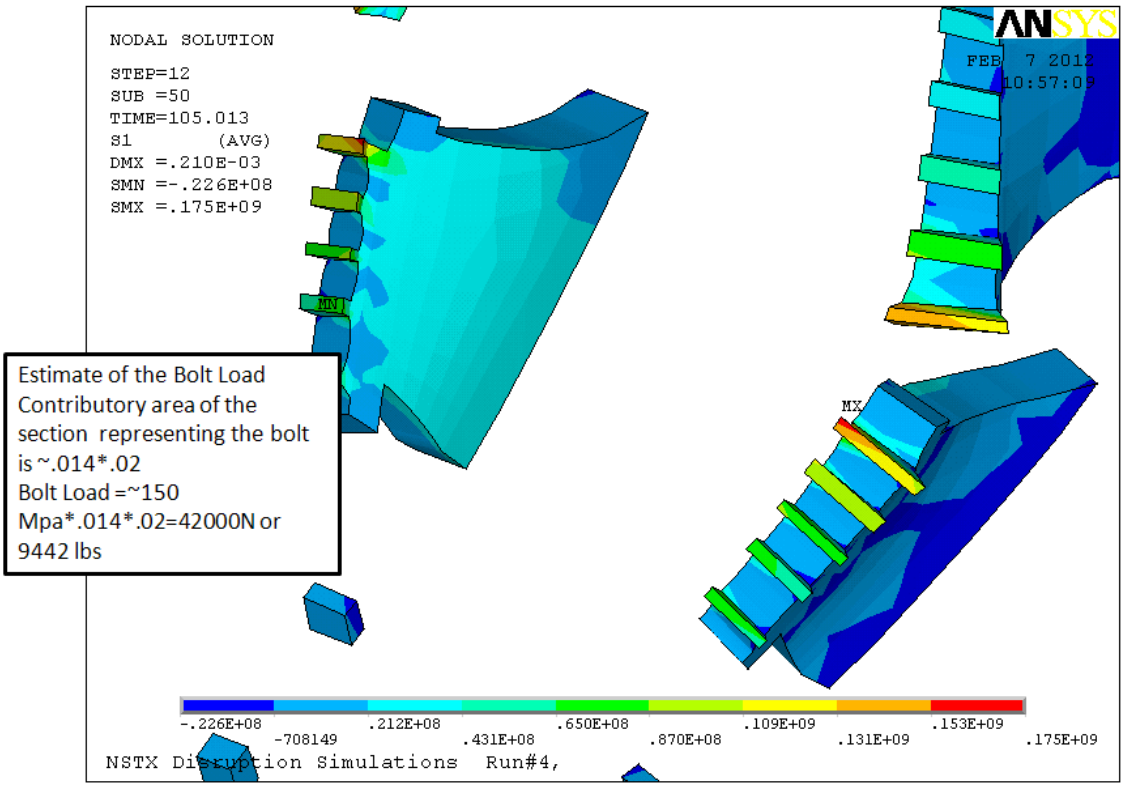

Figure I-1` Estimate of Bolt Load on the Dynamic Rebound